[redacted]

Coordinated Science Laboratory

UNIVERSITY OF ILLINOIS – URBANA, ILLINOIS

PROGRESS REPORT
FOR
JUNE, JULY, & AUGUST, 1965

October 11, 1965

The research reported in this document was made possible through support extended the Coordinated Science Laboratory, University of Illinois, by the Joint Services Electronics Program (U. S. Army Electronics Laboratories and U. S. Army Research Office, Office of Naval Research, and the Air Force Office of Scientific Research) under Contract DA 28 043 AMC 00073(E).

Portions of this work were also supported by

National Aeronautics and Space Administration

Research Grants NsG-376, NsG-443,
NsG-504, NGR-14-005-038

National Science Foundation

Grant NSF GK-36
Grant NSF GE-7809

Advanced Research Projects Agency

Through Office of Naval Research
Contract Nonr-3985(08)

Air Force Office of Scientific Research

Grant AFOSR 931.65

as acknowledged in footnotes in the text.

COORDINATED SCIENCE LABORATORY

SUMMARY OF

PROGRESS REPORT FOR JUNE, JULY, AUGUST, 1965

1. Aerospace Group

Work in data reduction for the ionospheric program is described. Analyses of spurious torques for the orbiting relativity gyro are presented. Variations in photographic observability are noted. The effect of micrometeorite cratering of the orbiting gyro has been studied.

2. Surface Physics

Some preliminary data obtained with the high-resolution secondary emission spectrometer are discussed. Additions and modifications to this apparatus and those for the study of the angular distributions of secondary particles and for the study of adsorption-desorption kinetics are described.

3. Computer Research Applications

A new measuring technique for bubble-chamber data processing, a new assembler for the CSX-1, and a new method of sequencing the control unit of a digital machine, tending to minimize the complexity of diagnostic procedures and of hardware, are described.

4. Control Systems

The project on optimization methods for time-lag systems was completed. Also completed was the project on pulse-width modulated control systems. The results for these two projects are described in R-254 and R-255. Several results were obtained in the continuing projects on the parameter variation problem, synthesis of interconnected linear time-varying systems, stability of nonlinear systems, suboptimal linear time-invariant control, and computer-oriented formulation and solution of the optimal control problem.

5. PLATO

Progress continues in circuitry development toward the goal of a 20 student station classroom. Plasma discharge display tube research this quarter has included experiments with tubes of varying widths and hole diameters, and trials with different gas additives. Modifications to the new PLATO Tutorial Logic were made to increase its flexibility and applicability to several courses; namely: 1) a revision of Electrical Engineering 322; 2) Library Science 195; and 3) FORTRAN Programming for Business Students. Revisions and modifications of TEXT-TESTER, ARITHDRILL, and PROOF have continued. Sixty students were used in the "retention of conceptual materials" experiment this quarter. A PLATO program, VERBOSE, using the CONNECT feature of the PLATO compiler was written as a starting point toward the development of more general PLATO programs useful in studying the structure of concepts.

6. Vacuum Instrumentation

The program of study of the pumping speed of ion-getter pumps at low pressures has continued. A pressure controller has been added to the system to improve the reproducibility of the data. This change and some recent data are discussed.

7. Plasma Physics

A careful evaluation of the errors in the Monte Carlo Method has been made for the hot side of the shock. Extensive measurements have been carried out in the Linear Plasma Betatron for various pressures and electric fields. It has been shown that the runaway current is associated with the buildup of ion-acoustic oscillations. A new experiment on electron-beam-plasma interactions has been started, in which the scattering of microwaves by instability-stimulated density fluctuation is used as the primary diagnostic tool. Theoretical studies of the influence of high-frequency turbulence can give rise to a parametric growth of the ion-acoustic mode.

8. Superconductivity Studies

Work is reported on a superconducting parametric amplifier (picovoltmeter), a study of the anisotropy of the energy gap in superconducting niobium, an attempt to observe microwave radiation from the ac Josephson effect in a superconducting bridge, studies of flux flow in type-II superconductors, a determination of the temperature dependence of the penetration depth using the ac Josephson effect, the thermal conductivity of a type-II superconductor in the mixed state, and the crystallization of Nb_3Sn from a solution of Nb in molten Sn.

9. High Voltage Breakdown

During gas conditioning, the electron-emitting protrusions on a tungsten cathode are blunted resulting in current suppression and breakdown voltage elevation, but the critical breakdown field at the emitter tips remains unchanged. Development of single-crystal emitter tips and high-resolution fluorescent screens is described.

10. Thin Films

Additional equipment is under construction for the work on size effects, and for that on Hall measurements on thin films. Results are reported for an ionization-gauge type of deposition rate monitor.

11. Computer Operations

Operation statistics for the CDC 1604 and CSX-1 systems are reported. The development of plotting routines for the cathode-ray output and a new assembler for the CDC 1604 are noted.

12. Switching Systems

The experimental study of self-diagnosis using the CSX-1 computer as a vehicle has been completed. New results are reported on the realization of sequential machines as linear and quasi-linear switching circuits. Further progress is reported on the computer compiler, state-model realizations, and computer diagnosis.

13. Networks and Communication Nets

The relationship of multiparameter sensitivity to synthesis procedures in networks has been studied, and the results of Kawakami relating to symmetric LC ladder networks have been extended. The problems of optimum flow in a communication net have received further attention. The concept of "relatively optimum flow" is introduced, and stochastic flow through a communication net is considered. Other studies relate to fundamentals of graph theory having application to the theory of communication nets.

14. Information Science

Work in information-theoretic methods for the design and optimalization of digital transmission and processing systems, particularly in algebraic coding theory, are described. Results are given in decoding cyclic codes, construction of codes for compound channels, and in the theory of linear residue codes for multiple-error correction. Applications of the coding theory are given for information-retrieval systems.

COORDINATED SCIENCE LABORATORY PERSONNEL

Faculty, Research Associates, and Research Engineers

Alpert, D., Director (on leave)
Anderson, R.
Ash, R.
Barrows, J.
Barthel, H. O.
Bitzer, D. L.
Bohmer, H.
Brown, R. M.
Chien, R.
Compton, W. D.*
Cooper, D. H.
Cruz, J. B. (on leave)
Dallos, A.
Fenves, S.
Franz, F. A.
Frauenfelder, H.
Associate Director
Gooch, J.
Hicks, B.
Huggins, R.
Ichikawa, Y.
Jackson, E. A.
Kirkwood, B. D.
Kishi, G.
Knoebel, H. W.
Kopplin, J. O.
Krone, H. V.
Lee, D. A.
Lichtenberger, W. W. (on leave)
Lyman, E. R.
Lyman, E. M.
Mayeda, W.
Metze, G.
Mueller, T.
Peacock, R. N.
Perkins, W.
Propst, F. M.
Prothe, W. C.
Asst. to Director
Raether, M.
Resh, J.
Rohrer, R. (on leave)
Satterthwaite, C. B.
Schuemann, W. C.
Seshu, S.
Simonelli, L.
Skaperdas, D. O.
Slottow, H. G.
Steinrisser, F.
Stifle, J.
Takagi, M.
Trogdon, R.
Van Valkenburg, M. E.
Acting Director
Voth, B.
Wax, N.
Yen, S.

Research Assistants

Agashe, S.
Aubuchon, K.
Barger, A. R.
Bleha, W.
Bouknight, J.
Brown, K.
Carlson, J.
Chan, S. K.
Chang, J.
Chang, S. C.
Chow, D.
Cooper, T.
Copple, J. D.
Craford, M.
Crockett, E. D.
Cummings, J.
Davies, M.
DeWan, E.
Eickert, D.
Frank, W.
Goodman, G.
Hosken, R.
Hsu, H. T.
Hyatt, W.
Jacobs, J. T.
Jenks, R.
Kamae, T.
Karr, G.R.
Killian, T.
Lie, T.
Lum, V.
Manning, E.
Marlett, R.
Martens, G.
Marzullo, E.
McKellar, A.
Mendel, C.
Meyer, J.
Moore, B. K.
Morgan, L.
Morrison, H.
Murata, T.
Myers, J. L.
Nash, B.
Nishijima, M.
Onaga, K.
Piper, T.
Rust, R. D.
Saul, K.
Schoenberger, M.
Schusterman, L.
Secrest, M.
Smith, M.
Tibbetts, G.
Toepke, I.
Walsh, F.
Willson, R. H.
Woodruff, R. A.

*Director effective September 1, 1965.

Fellows

Carr, W.
Kirk, D.
Numata, J.
Stumpff, G.
Tracey, R.

Secretary

Rudicil, J.

Photographer

Fillman, W.

Accounting Clerk

Potter, R. E.

Typists and Stenos

Gaudette, A.
Hanoka, N.
Harris, M.
Keel, D.
Lane, R.
McClerren, J.
McDonald, R.
Renn, J.
Shaw, C.

Storekeepers

Drews, C. E.
Lofton, C.

Electronics Engr. Asst.

Carter, E. N.
Gardner, O. E.
Hedges, L.
Neff, E. H.
Vassos, N.

Electronic Technicians

Casale, T. C.
Coad, D. E.
Crawford, G.
Deschene, D. R.
Holy, F. O.
Jordan, H.
Knoke, J. H.
Merrifield, F.
Roberts, G. R.
Schmidt, W.
Streff, L. W.
Turpin, F. G.

Laboratory Mechanics

Bales, R. B.
Burr, J. G.

Instrument Makers

Beaulin, W. E.
Bouck, G.
Merritt, K. E.
Zackery, R. L.

Draftsmen

Conway, E.
MacFarlane, R. F.

Glassblower

Lawrence, W.

Phys.Sci.Staff Asst.

Thrasher, W.

Res. Lab Shop Supr.

Bandy, L. E.

Student Assistants

Arnold, C.
Bailey, P.
Barkstrom, B.
Bernard, W.
Bloom, R.
Borris, J.
Danielson, D.
Dewell, E.
Ellison, J.
Hoffman, D.
Holland, L.
Hughes, J.
Johnson, M.
Metze, V.
O'Meara, T.
Panza, K.
Ries, R.
Robinett, D.
Samson, C.
Sandorfi, G.
Shallal, A.
Stragalas, G.
Streff, G.
Sutton, C.
Trombi, P.
Turner, R.
Walker, M.
Williams, R.

PUBLICATIONS AND REPORTS

1. Journal Articles Published or Accepted

D. L. Bitzer and J. A. Easley, Jr., "PLATO: A Computer-Controlled Teaching System" in Computer Augmentation of Human Reasoning, M. A. Sass and W. D. Wilkinson, ed., 89-103 (Washington: Spartan Books, Inc., 1965).

R. T. Chien, "A Simplification of the Coates-Desoer Formula for the Gain of a Flow Graph," Proc. of IEEE (to appear).

R. T. Chien and D. T. Tang, "What is a Burst?" IBM Journal (to appear).

E. S. Kuh and R. A. Rohrer, "The State-Variable Approach to Network Analysis," Proceedings of the IEEE 53, 672; July, 1965.

W. Mayeda and S. Seshu, "Generation of Trees without Duplication," IEEE Trans. on Circuit Theory CT-12, 181; June, 1965.

R. N. Peacock, "High-Current Feedthrough Assembly for UHV Systems," J. Vac. Sci. & Tech. 2, 161 (1965).

R. A. Rohrer, "The Scattering Matrix: Normalized to Complex n-Port Load Networks," IEEE Trans. on Circuit Theory CT-12, 223; June, 1965.

M. Sobral, Jr., "Sensitivity Considerations in the Synthesis of Doubly-Terminated Coupling Networks," IEEE Trans. on Circuit Theory CT-12, 272; June, 1965.

D. T. Tang and R. T. Chien, "Cyclic Product Codes and Their Implementation," Information and Control (to appear).

2. Meeting Papers

H. M. Barnard, "Tree Realizations of Probabilistic Communication Nets," Proceedings of the 8th Midwest Symposium on Circuit Theory, pp. 5-1 to 5-11; June, 1965.

L. O. Chua, "Equivalent Nonlinear Networks," Proceedings of the 8th Midwest Symposium on Circuit Theory, pp. 20-1 to 20-12; June, 1965.

K. Onaga, "Optimum Maximum Flows in Lossy Communication Nets," Proceedings of the 8th Midwest Symposium on Circuit Theory, pp. 4-1 to 4-8; June, 1965.

J. A. Resh, "On the Properties of Semi-cuts," Proceedings of the 8th Midwest Symposium on Circuit Theory," pp. 3-1 to 3-11; June, 1965.

H. G. Slottow, "Experiments with Crossed-Field Delay Lines," Conference on Electronic Devices (CEDR), Urbana, Illinois; June, 1965.

3. Technical Reports

R-186 A Descriptive List of PLATO Lesson Programs, 1960-1965; Elisabeth R. Lyman (July, 1965), Revised Report.

R-236 The Pseudo-Shock: A Non-linear Problem of Translational Relaxation; B. L. Hicks (June, 1965).

R-254 Optimal Control of Linear Systems with Time Lag; T. E. Mueller (June, 1965).

R-255 Optimization of Systems with Pulse-Width-Modulated Control; D. E. Kirk (June, 1965).

R-256 A Class of Flat Delay Filter Networks and Their Transient Responses; G. Kishi (June, 1965).

R-258 On the Generality of Switching Networks with Restricted Non-Linearity; A. C. McKellar (July, 1965).

R-259 Self-Diagnosis of Electronic Computers--An Experimental Study; E. G. Manning (July, 1965).

R-261 Modified Unistor Graphs and Signal Flow Graphs; J. Numata (July, 1965).

R-262 Network Synthesis to Minimize Multiparameter Sensitivity; S. C. Lee (August, 1965).

R-263 A Current Mode DA Converter; J. Stifle (August, 1965).

R-264 Computer Compiler. Part I: Preliminary Report; G. Metze and S. Seshu (August, 1965).

R-265 Ground State Occupation Probabilities for Optically Pumped Alkali Metal Atoms; F. A. Franz (August, 1965).

TABLE OF CONTENTS

1. AEROSPACE GROUP

H. W. Knoebel
D. O. Skaperdas
R. W. Anderson
H. O. Barthel
D. H. Cooper
J. D. Gooch
G. R. Karr
B. D. Kirkwood
H. V. Krone
E. Marzullo
H. C. Morrison
J. L. Myers, Jr.
W. C. Prothe
L. Schusterman

1.1 Ionosphere Program†

On June 14 and 15, 1965, two more Nike-Apache rockets were successfully launched at Wallops Island, Virginia, for measuring the differential absorption and Faraday rotation for the determination of electron density and collision frequency in the D-region. This brings the total number of rocket firings to 14, of which 13 were considered operationally successful. The single failure was attributed to malfunctioning of a commercial telemetry transmitter. These firings bring to a close CSL's participation in this phase of the project. The experimental equipment has been transferred to a group in the Electrical Engineering Department which will continue this type of experiment under the direction of Dr. Sidney Bowhill. A final report, describing in detail the complete system and operational procedure, is being prepared.

One of the novel features of this experimental system has been the high sampling rate of differential absorption and Faraday rotation. However, due to laborious methods of manual data analysis,

†Portions of this work were supported by the National Aeronautics and Space Administration under Grant NsG 504.

the total available data was never fully extracted from the recorded signals. The manual determination of Faraday rotation to resolutions of about one degree has been done at a limited number of altitudes for about five experiments (see, for example, Fig. 1.2, CSL Progress Report for June, July, August, 1964).

1.1.1 Automatic Data Processing System. During the previous quarter, a prototype automatic data processing system was put into operation, and the first differential absorption and Faraday rotation data was extracted from telemetry magnetic tape. To extract differential absorption, a magnetic tape containing the launch-range time signals and the extraordinary attenuator-monitor voltage is played back and fed to an analog-to-digital recorder at 1/16 real time. A synchronizer unit receives the launch-range time signals and changes them to a form suitable for punch-command signals to the analog-digital converter. The latter unit punches out the data points in binary form whenever commanded by the synchronizer. These command pulses can be set at rates of 1, 5, or 10 pps of real time. The punched paper tape is then fed to a digital computer which prints out the extraordinary attenuator setting versus Greenwich mean time. Data which formerly took one week to extract now takes about three hours and will be shortened to one-half hour, when fully automatized. A plot of automatically extracted differential absorption versus Greenwich mean time for rocket firing 14.149 is shown in Fig. 1.1.

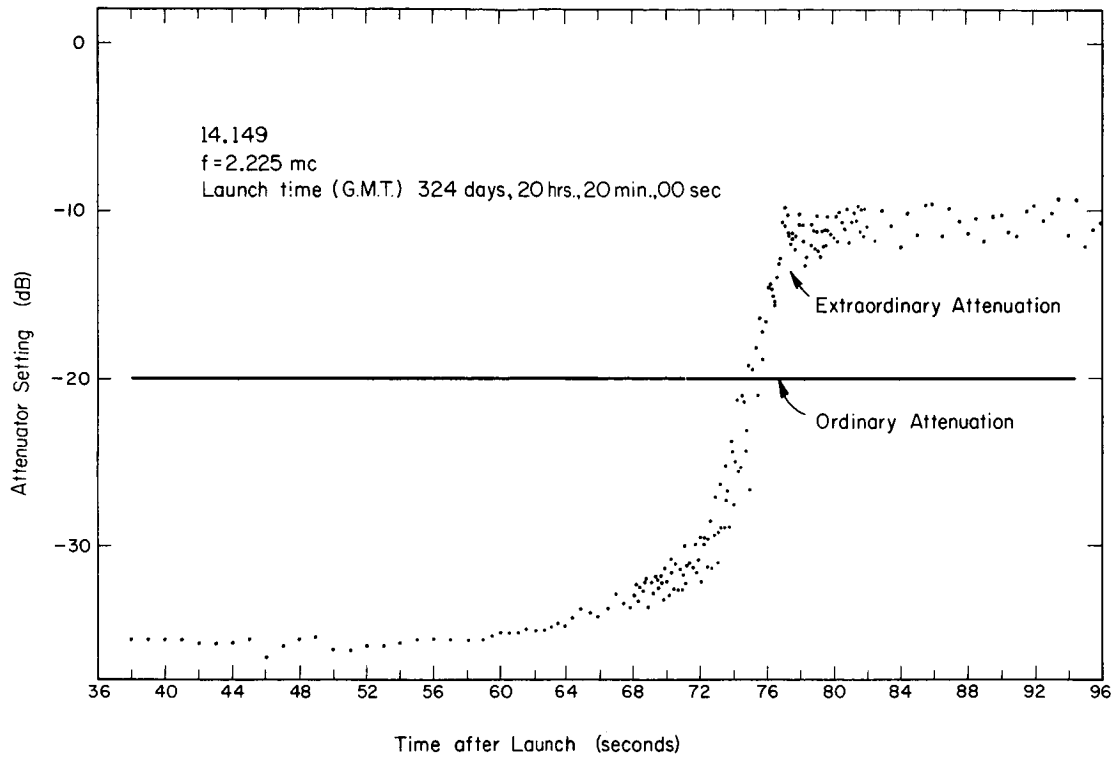

Fig. 1.1. Differential Absorption versus Time after Launch, Obtained by the Automatic Data Processor.

An even greater saving in time and labor has been accomplished with the automatic extraction of Faraday rotation. The prototype system block diagram is shown in Fig. 1.2 and described below. This system continuously measures the integrated phase shift between the ordinary and extraordinary transmitted waves. The analog-to-digital converter punches out the accumulated phase shift (Faraday rotation), upon command of the synchronizer, at a rate of 10 data points per second of real time. This punched tape is also fed to a digital computer which prints out the Faraday rotation versus Greenwich mean time. At the present time, phase corrections due to a filter component must be made to the Faraday rotation extracted by this method in regions where the rocket spin rate is varying--usually only near the start of the Faraday rotation. Fig. 1.3 shows a comparison of the Faraday rotation obtained by manual and by automatic methods, together with the rocket spin frequency versus Greenwich mean time for flight number 14.149, before phase corrections were made. The reason for the sudden drop in rocket spin rate at 50 seconds after launch is that the rocket moment of inertia was suddenly increased by the extension of two arms holding another organization's experimental (Sayers) probe. The discrepancy between the two methods is clearly seen only in the region of higher rocket spin velocity. Fig. 1.4 shows the same comparison after a simple phase correction. Both figures show only the lower region of Faraday rotation in order to demonstrate the high angular resolution possible with CSL's system. Further refinements of the prototype data reduction system are being investigated.

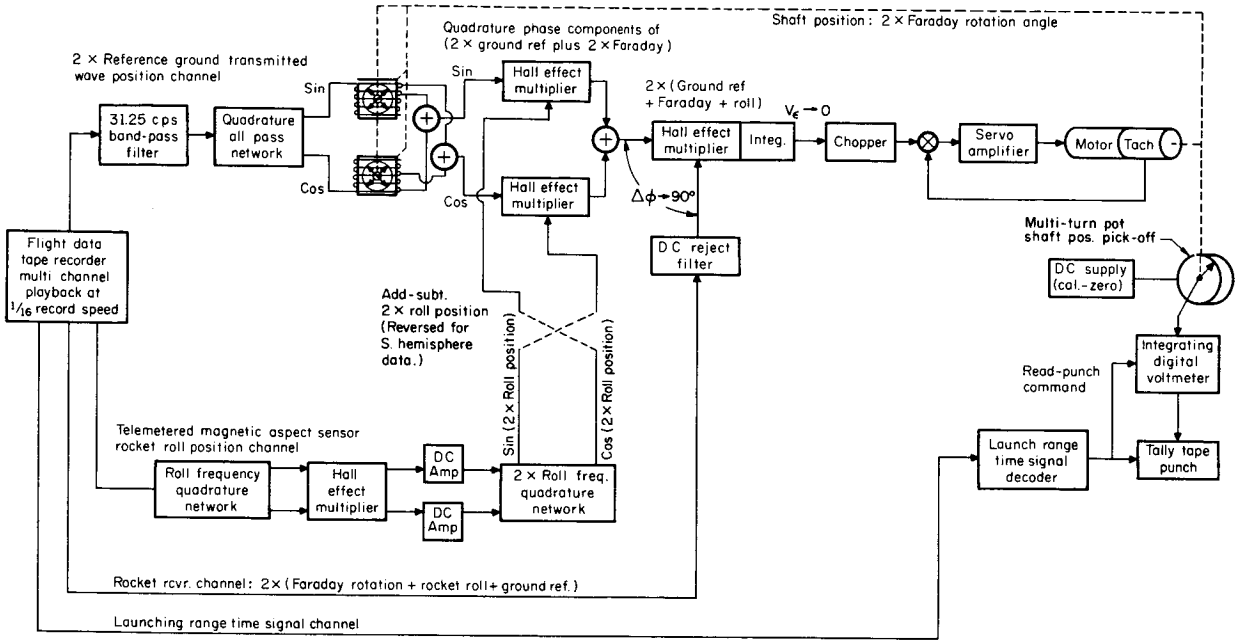

Fig. 1.2. Block Diagram of the Prototype Faraday Rotation Data Reduction System.

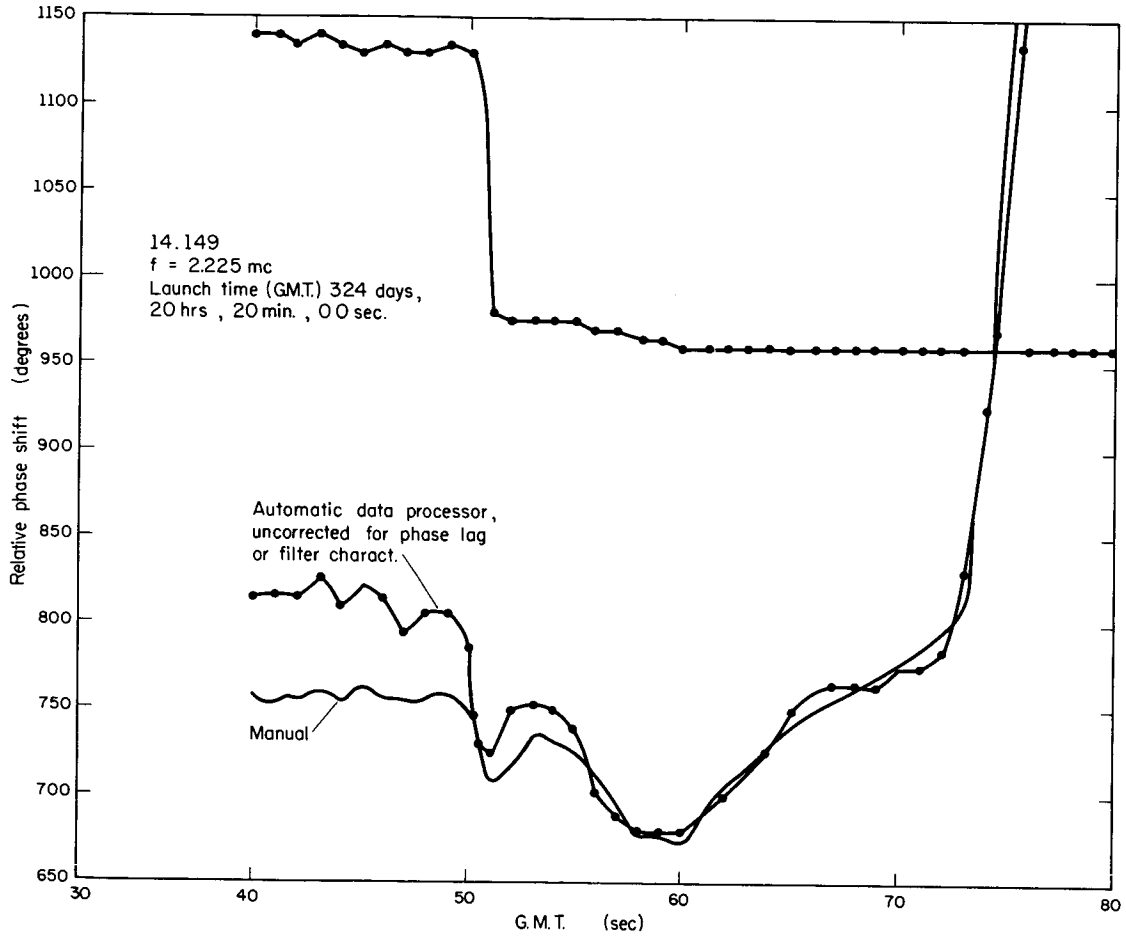

Fig. 1.3. Comparison of Faraday Rotation by Manual and Automatic Methods, before Phase Correction.

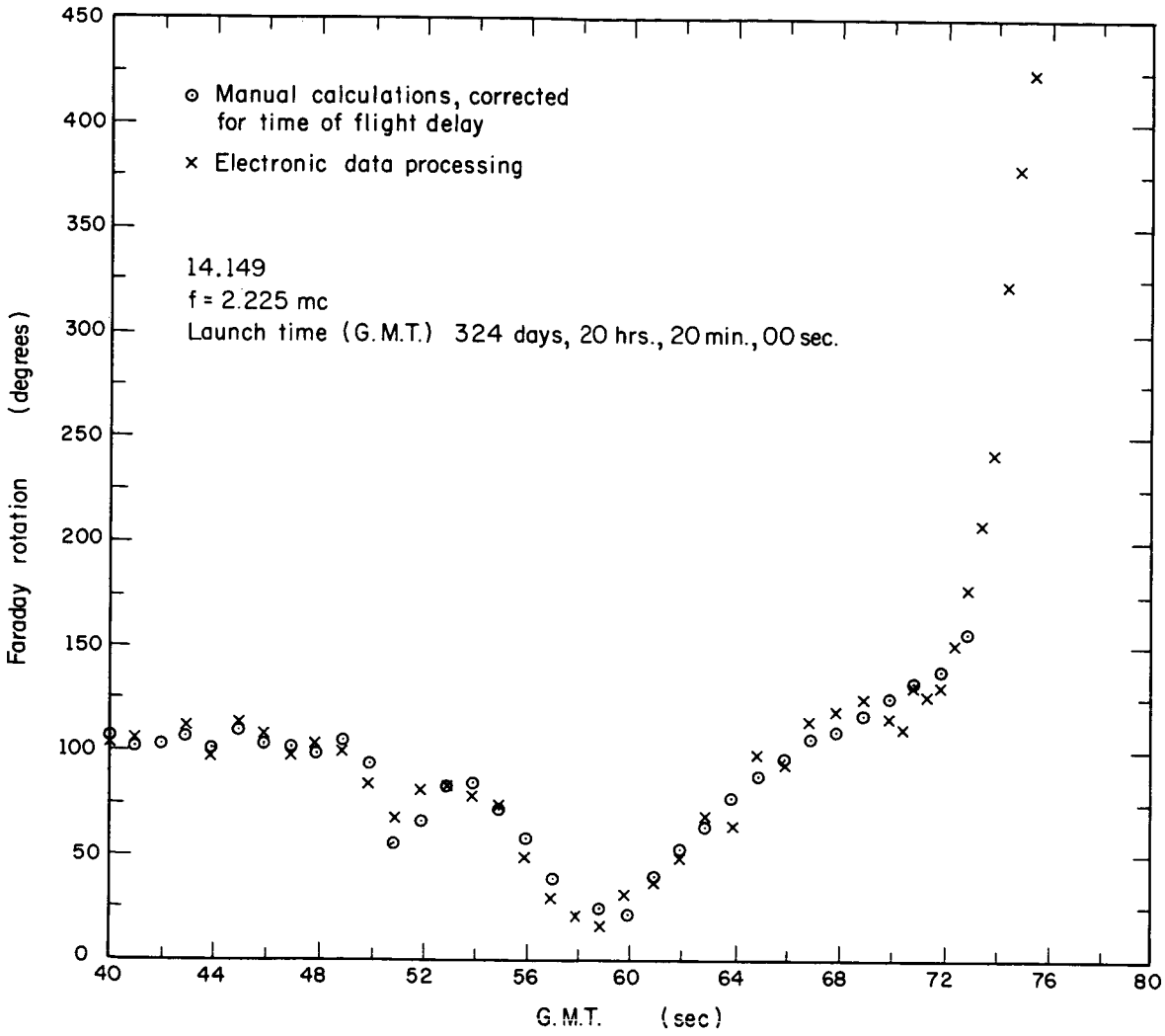

Fig. 1.4. Comparison of Faraday Rotation by Manual and Automatic Methods, after Phase Correction.

An alternate method of extracting high resolution Faraday rotation from the rocket data by digital computer only is being investigated and will be described if successful.

D. O. Skaperdas
H. C. Morrison

1.1.2 Analog Faraday Rotation Data Reduction System. An experimental assembly of the components of an analog data processor has been used in trial operation to extract the amount of Faraday rotation of the plane of polarization of vertically propagated, h.f. radio waves. The data to be reduced is obtained from magnetic tapes played back at 1/16 the speed used to record flight data from Nike-Apache rocket shots.

A block diagram of the data reduction system is shown in Fig. 1.2. It is a modified version of the system proposed previously.[1]

Four tape recorder outputs provide, in arc-cosine form,

1. the position of the ground-transmitted, circularly polarized, wave electric vector in double angle form,

2. the rocket roll position (not in double angle form) from a rocket-borne magnetic aspect sensor,

3. the rocket-received signal containing the sum of the above plus the Faraday rotation angle, all in double angle form,

4. the launching range timing signals, in binary form.

The second and third items above are obtained via telemetry from the rocket.

---

[1] CSL Progress Report for March, April, May, 1965, Section 1.1.3, p. 7.

The recorder output indicating ground-transmitted wave angle is fed to a mechanical phase shifter, whose servo-driven shaft position is twice the Faraday rotation angle. This shaft position is generated by a feedback loop whose components are described below.

The mechanical phase shifter output is added, in a polyphase heterodyne system, to twice the rocket roll position to form a synthesized reference to compare with the rocket received signal. (In the case of southern hemisphere launches where the Faraday rotation sense was opposite, and the ground-wave rotation was transmitted with opposite sense, but the rocket roll sense was unchanged, twice the rocket roll position is subtracted to synthesize the reference.) The synthesized reference signal differs from the rocket-receiver signal by twice the Faraday-rotation angle when the mechanical phase-shifter shaft is locked, but the servo shaft is caused to rotate at twice the Faraday angle by comparing the synthesized reference signal to the rocket-receiver signal in a phase detector. This produces a polarized servo-error signal, driving the mechanical phase shifter so that the synthesized reference is always at a constant phase-difference from the rocket-receiver signal.

This error signal tends to zero when the two compared signals are in phase quadrature. Using the error signal to excite a servo motor which is mechanically coupled to the phase shifter in the ground-reference channel operates to keep the two inputs to the cross-correlator-phase detector at a 90^{o} phase. The shaft rotation required to accomplish this is the desired Faraday-rotation indication. Synthesizing a reference signal at a relative high frequency near the

ground reference signal frequency, and doing the phase comparison at that frequency rather than at the lower rocket-roll frequency, has two advantages:

1. The ground-transmitted wave reference and the signal that indicates rocket roll are relatively noise-free and near sinusoidal. These are combined to form a synthesized sum reference that is noise-free and sinusoidal, and thus optimum for cross-correlating against the rocket receiver signal which is more noisy, especially at the time of rocket penetration of the ionospheric reflecting layer.

2. Also, by performing the phase-detector (multiple-integrator) operation of cross-correlation at the higher frequency of approximately ground reference, rather than at the lower frequency of near rocket roll (the alternate system choice), it is possible to obtain Faraday-rotation information at a higher data rate. This occurs because phase detection involves integration and requires a minimum of several half-cycles of input signal to operate.

Since the servomotor-to-phase-shifter coupling-shaft position indicates twice Faraday rotation, it is geared to a multi-turn potentiometer to obtain data output. With a voltage across the pot which causes the wiper arm to output 1.80 volts per shaft revolution, 0.01 volts per degree of Faraday rotation is obtained. An adjustment allows the initial voltage output to be set to zero at low rocket altitude, where Faraday rotation is zero. The potentiometer-arm voltage is fed

to an integrating digital voltmeter which outputs to a tally-tape punch, on repetitive commands that are derived from, and synchronized with, the launching-range timing marks.

J. D. Gooch

1.2 Orbiting Relativity-Gyro Torques†

In order to measure the general relativistic precession of an unshielded orbiting gyro, the drifts due to spurious torques must either be kept much lower than the relativistic precession or the spurious drift must be accurately known to account for them in the data. The former alternative is currently favored in establishing the gyro and orbital parameter tolerances.

1.2.1 Gravity-Gradient Torque. The most troublesome spurious torque presently analyzed is that due to gravity gradient. If C and A are the moments of inertia about the symmetrical and transverse axes, respectively, the gravity gradient arises from the gyro's finite ratio, $\gamma = (C-A)/C$, and inclination of its spin axis with its orbital plane. The "preferred" moment of inertia C is a requirement of the readout system. The resultant gyro motion is a precession of its spin axis about a normal to the orbital plane according to the relation (for circular orbits)

$$\Delta\psi/\Delta t = -(3/2\Omega)(2\pi/T)^2\gamma\cos\theta \ , \qquad (1)$$

†Portions of this work were supported by the National Aeronautics and Space Administration under Grant NsG 443.

where $\Delta\psi/\Delta t$ is the gyro precession rate about the orbital plane normal, Ω is the gyro spin rate, T is the orbital period, and θ is the gyro spin-axis inclination with respect to the orbital plane normal. A plot of the gyro spin-axis precession rate about the normal to its orbital plane versus the γ ratio for various orbital heights above the earth's surface for constant inclination θ is shown in Fig. 1.5. The ordinate is expressed as $f(\Delta\psi/\Delta t)$ divided by $\cos\theta$ where f is the gyro-spin rate in hundreds of cycles and $\Delta\psi/\Delta t$ is in arc seconds per year. It is seen that the precession rate is not significantly reduced by higher orbits. As an example, for f = 100 cps, γ = 0.001 and an orbital height of 600 miles, θ would have to be greater than 86.3 degrees in order to keep the resultant drift rate less than one arc second per year. This means that the gyro-spin axis would have to lie in its orbital plane to better than 3.7 degrees. A plot of the maximum relativistic precession versus orbital height is shown in Fig. 1.6. This shows that the use of orbits higher than 1000 miles is disadvantageous, because the maximum relativistic precession rate decreases to less than five arc seconds per year at that height. The use of smaller γ ratios is difficult because centrifugal deformations or inhomogeneous materials could change the design "preferred" moment-of-inertia axis. The above results have not included the effect of orbital plane regressions due to the earth's oblateness. These are presently being studied.

1.2.2 Gas-Drag Torque. The atmospheric-drag torque arises from momentum transferred to the spinning gyro during diffusely deflected collisions with the rarified gas molecules. The fraction of such

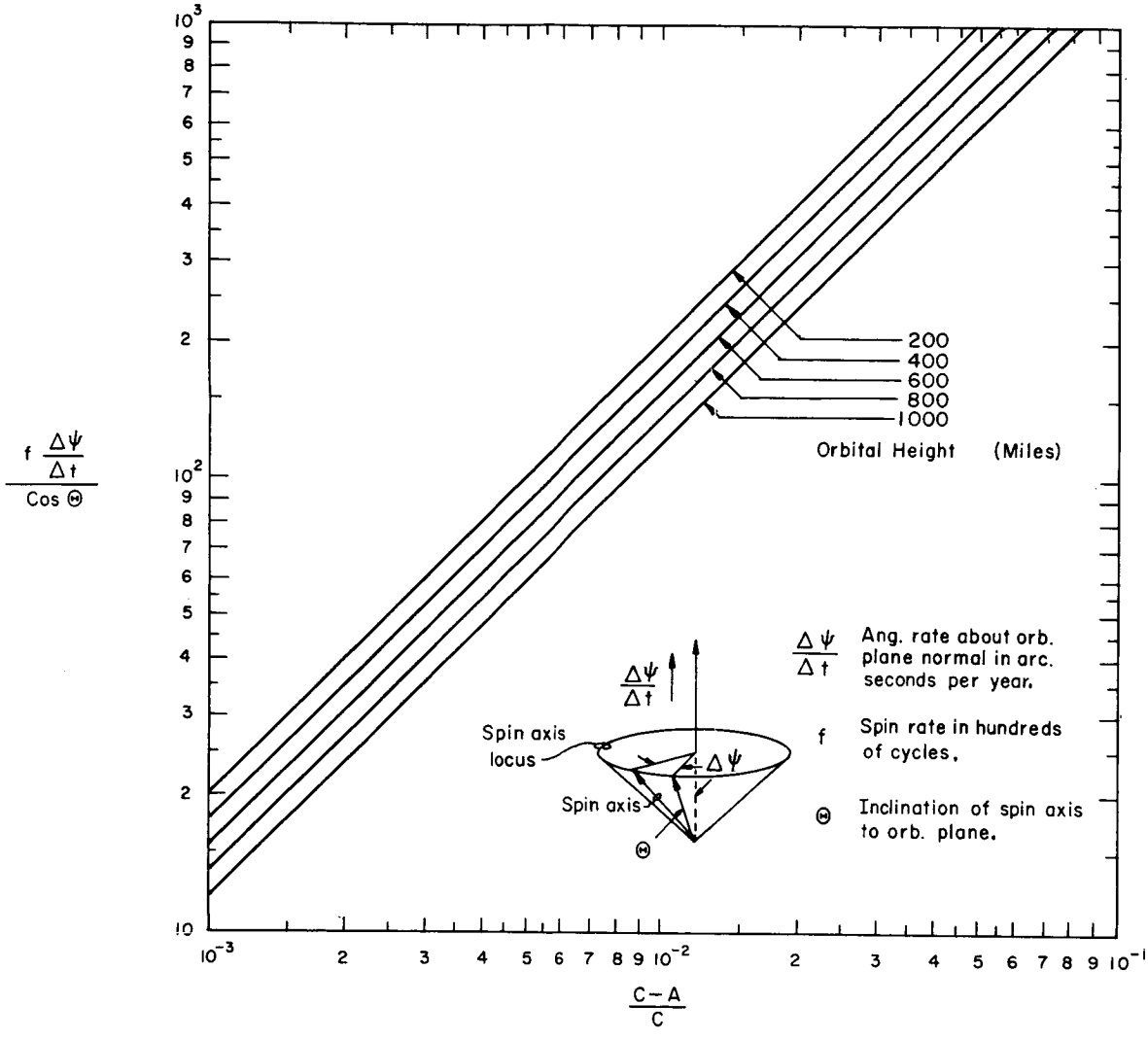

Fig. 1.5. Gyro Drift due to Gravity Gradient for a Circular, Non-Regressing Orbit.

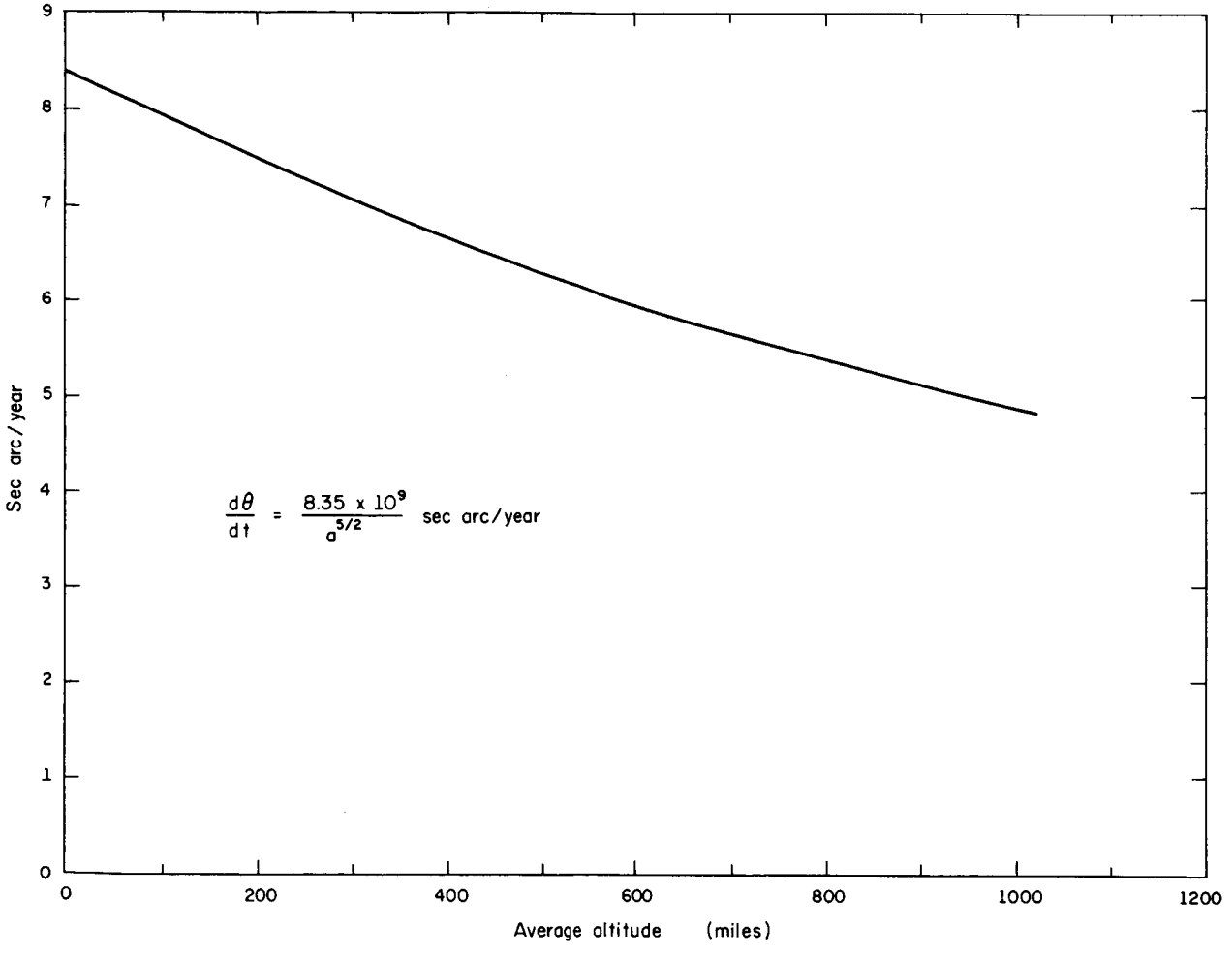

Fig. 1.6. Relativistic Precession versus Orbital Height.

diffuse reflections can be regarded as the accommodation coefficient α_d, and is a function of the gyro surface, temperature, surface smoothness, gas ionization level, and gyro material properties. It ranges from zero to unity and at present can only be measured experimentally. The gyro-spin axis drift rate arising from the atmospheric drag, for circular, nonregressing orbits, is given by

$$\Delta\theta_s/\Delta t = (15/128)\alpha_d(\rho/\rho_s)(R_e/R)(g/R_o)\sin 2\theta \ , \qquad (2)$$

where α_d is the accommodation coefficient, ρ is the atmospheric density, ρ_s is the satellite density, R_e is the earth's radius, R is the satellite radius, g is the acceleration due to gravity, R_o is the satellite distance from the earth's center, and θ is the gyro spin-axis inclination with respect to the orbital plane normal. The direction of this drift rate is such as to align the spin axis with its orbital plane. The drift rate $\Delta\theta/\Delta t$ in arc seconds per year divided by the accommodation coefficient α_d and by $\sin 2\theta$ is shown in Fig. 1.7 plotted versus orbital altitude above the earth's surface in miles. The drift rate due to this torque can be greatly reduced by larger orbital heights. For a height of 600 miles and a most pessimistic value of $\alpha_d = 1$, it is seen that $\Delta\theta/\Delta t = 0.25$ seconds of arc per year if θ is restricted to inclinations larger than 86.3 degrees as required by the gravity gradient restrictions.

At the lower altitudes, the gas drag torque is the most dominant torque. For example, at an orbital altitude of 140 miles and $\theta = 45^o$, the drift rate could be a maximum of about 2.8 degrees per year, a

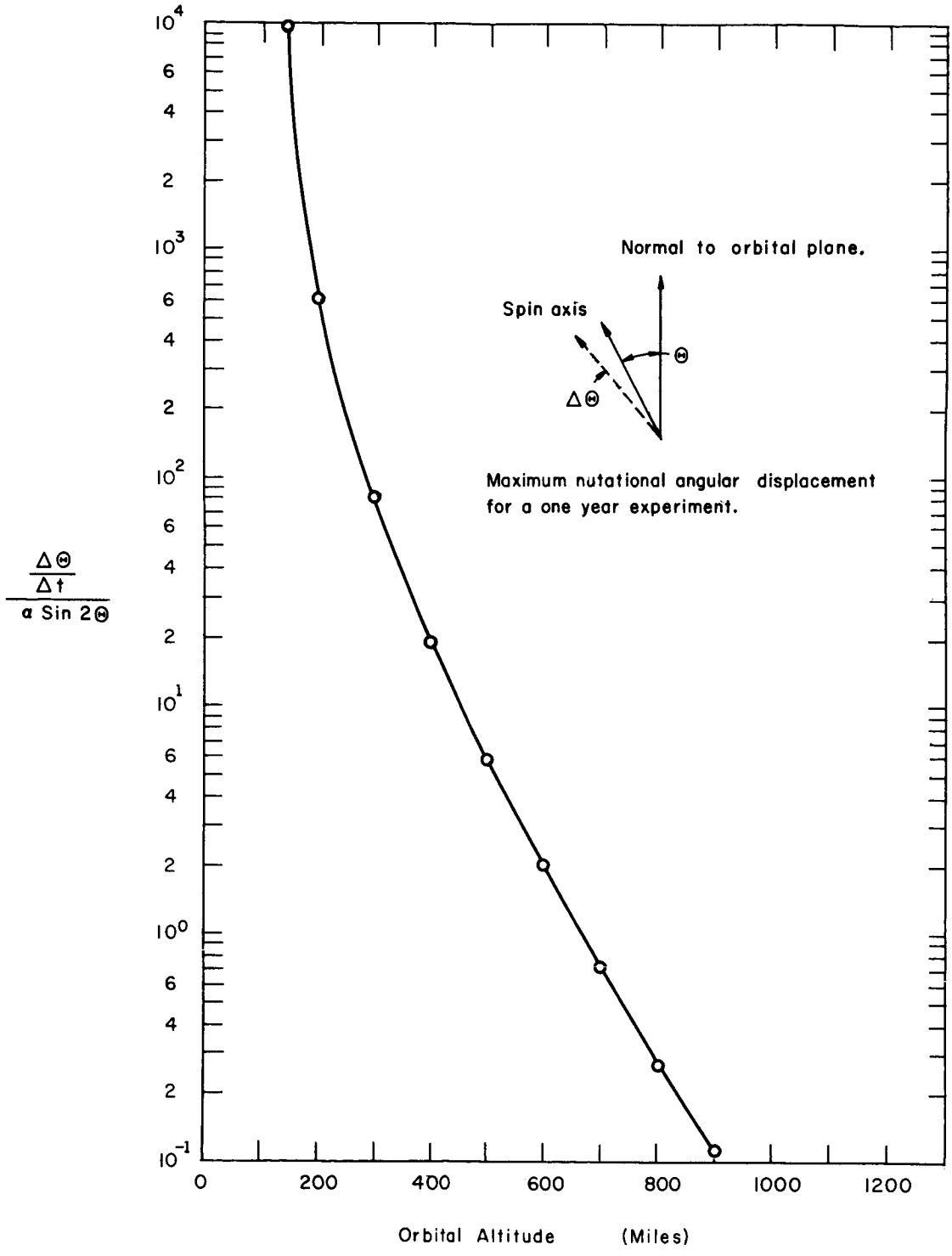

Fig. 1.7. Gyro Drift due to Gas Drag for a Circular, Non-Regressing Orbit.

value easily measured by the proposed readout methods. This experiment could therefore be used for measuring the accommodation coefficient under orbital conditions.

If the required orbital tolerances established by the gravity-gradient torque are too demanding, then the associated spurious drift rate must be known to an accuracy of about 0.1 seconds of arc per year in order to remove it from the total drift rate. This requires knowing the quantities $\gamma = (C-A)/A$, Ω, T, and θ to great precision, as seen from equation (1). Methods for measuring γ for the polyhedral satellite are being investigated. The quantities Ω and θ can be obtained from the proposed readout scheme and the period T would have to be computed from satellite tracking data.

H. W. Knoebel
D. O. Skaperdas
G. R. Karr
J. L. Myers, Jr.

1.2.3 Radiation Pressure Torque. For an incident flux $w = 1.34 \times 10^{3}$ Watts per square meter, representative of the solar constant, the incident pressure is w/c, or 4.46×10^{-6} Newton per square meter, where c is the speed of light. This, multiplied by the area of a gyro facet, would be the normal force on a perfectly reflecting facet oriented at 45° to the direction of incident flux. If the facet absorbed a fraction α of the incident flux, this normal force should be multiplied by the factor $1-\alpha$, and there would also be a force $\alpha/\sqrt{2}$ as large as the above, but in the direction of the flux. For a facet

normal to the flux, the two components would be proportional to $2(1-\alpha)$ and α, respectively, and both would be normal to the facet, etc.

For a body of the symmetry assumed (see Fig. 1.1 of the Progress Report for Dec. 1954, Jan., Feb., 1965), the facet normals are all directed at the center of mass, so that the reflected component should cause no torque. Similarly, an assumption of equality in absorptivity α for all of the facets would imply the sum of absorptive components also to be directed at the center of mass, so that this component also should cause no torque. Any inexactness in these assumptions would account for the presence of a torque due to radiation pressure.

Some fraction of this torque would be aligned with the spin axis and would produce no precession. Also, some fraction of this torque would be periodic with the rotation of the body and would produce no observable cumulative effect, either in alteration of the magnitude of the spin, or in precession. Again, the torque would not be "on" all the time by reason of the satellite's passing through the earth's shadow.

The result of these considerations is that a net precessional torque can arise only becuase of an optical asymmetry tending to favor either the northern or the southern hemispheres on the gyro. The torque then must be normal to both the spin axis and the direction to the sun. Since the direction to the sun changes by 360^{o} during the course of the year, so does the direction of the torque, i.e., the torque is periodic with that same period. The locus, then, of the

spin axis, plotted on the celestial sphere, will be a small ellipse of eccentricity dependent upon the angle between the spin axis and the ecliptic plane. This figure will close in the course of a year unless the optical symmetry changes during that time, then the figure for the axis trajectory would be a spiral. The resolution of the trajectory into such a periodic, or growing periodic, component along with the steady relativistic component will not, of course, require as fast a data rate as the detection of perturbing motions having a shorter period, although the availability of many points on the curve would be helpful from the point of view of accuracy.

To estimate the magnitude of this precession, it is useful to consider a numerical example. For this, 10 per cent of the radiation intercepted by the body is assumed to produce a steady force which is applied at a constant distance of 1 millimeter from the center of mass. This would be equivalent, of course, to assuming 1/k as much force, applied through a constant moment arm of k millimeters, etc. This calculation may be taken as a base upon which one may estimate the effect of the various mitigating factors, cited above, once their magnitudes have been estimated.

For the area of the body presented to the radiation, take the cross-section of a sphere of radius 0.15 meter (approx. a 12-inch diameter). This area is $7.07 \times 10^{-2} m^2$. The radiation force assumed, then, is $0.1 \times 4.46 \times 10^{-6} \times 7.07 \times 10^{-2} = 3.15 \times 10^{-8}$ Newton, and the torque is 3.15×10^{-11} Newton-meter.

The moment of inertia is taken to be that of a solid sphere, $2Mr^2/5$, of the same radius r. The mass is $M = 4\pi\rho r^3/3$, for which take ρ to be about the density of glass, i.e., 2.5×10^3 kg/m^3, so that the moment of inertia is $8\pi\rho r^5/15$, or 0.318 kgm^2. Spinning at 100 cps, the spin angular momentum is $0.636\pi\times10^2$ kgm^2/sec, or 200 kgm^2/sec.

The above torque gives a rate of change in angular momentum of 3.15×10^{-11} kgm^2/sec^2, or 3.15/2 parts in 10^{13} per second. Since, in a year's time, there are 3.16×10^7 seconds, this is an angular momentum change of 5.0 parts in 10^6 per year, a precession of 5.0×10^{-6} radian. There being 4.85×10^{-6} radian per second of arc, this precession is 1.03 seconds of arc per year. This is down one order of magnitude from the relativistic effect to be observed, so that the operation of the mitigating factors, cited above, should permit the observation with satisfactory precision.

D. H. Cooper

1.3 Variability of Factors Affecting Gyro Photographic Brightness†

As in calculating the effect of radiation pressure, the calculation of photographic brightness in the previous progress report may be interpreted as a base calculation using specific numerical parameters. One may then consider variations in these parameters to determine the variability in photographic brightness.

†Portions of this work were supported by the National Aeronautics and Space Administration under Grant NsG 443.

1.3.1 Variability of Slant Range. The slant range figure used in the base calculations was 500 km, a nominal value for the orbital height. Actually, orbital heights ranging from 10 per cent to 25 per cent of the earth's radius, i.e., from 637 km to 1590 km are under construction. The horizon distance from such heights corresponds to positions from 24.6^{o} to 36.9^{o} from the ground track, i.e., to slant ranges of from 2920 km to 4780 km. On the other hand, if it be required that the satellite trajectory be above about 30^{o} from the horizon, the slant ranges would be 1500 km to 3000 km, at most. These ranges involve a loss factor falling between 9 and 36.

1.3.2 Variability in Photographic Equipment. The aperture of the telescope assumed was 100 cm^2, producing, with a 1 meter focal length, a diffraction image measuring 5 microns. One would be likely to be using a camera whose parameters were like those of the Baker-Nunn camera, however. The aperture is 20 inches, with an area nearly 2000 cm^2 producing a focal spot measuring 30 microns. The gain of a factor 20 in aperture is offset by the loss in image spreading by the factor 36 to yield a net loss factor of nearly 2.

The use of a higher film speed can offset this factor. An order of magnitude improvement, moving from ASA 400 to ASA 4000, is possible, yielding a net gain by the factor 5. Combining this with the factors in the preceding section leaves a net loss factor ranging from nearly 2 up to about 7, for the greater slant ranges. Observers nearer the ground track will not be troubled by such factors, however.

It is probably reasonable to assume that most of the observations may be made with the accuracy estimated in the previous report, but with useful contributions to the store of data also deriving from observing stations farther from the ground track.

D. H. Cooper

1.4 Micrometeorite Cratering of Gyro†

A study of the effects of micrometeorite cratering on the direction of the gyro maximum-moment-of-inertia axis has been made by Professor H. O. Barthel of the Department of Aeronautical and Astronautical Engineering and will be presented in the next quarterly progress report.

†Portions of this work were supported by the National Aeronautics and Space Administration under Grant NsG 443.

2. SURFACE PHYSICS

F. Propst
F. Steinrisser
T. Cooper
M. Nishijima
T. Piper
G. Tibbetts

2.1 High Resolution Study of Secondary Emission†

More preliminary data on the energy distribution of secondary electrons have been obtained with the monochromator-analyzer system described in previous progress reports. An unusual structure has been observed in the low energy region of the distribution of electrons ejected from the 111 surface of partially cleaned tungsten. This structure and several modifications of the instrument which have been made during the last quarter will be discussed below.

2.1.1 Preliminary Data. Fig. 2.1 shows two distributions which were presented in the previous progress report. Curve a is the distribution obtained by Harrower[1] for 20 eV electrons incident on a clean polycrystalline tungsten surface. Curve b was obtained in the present work for 20 eV electrons incident on highly contaminated 111 surface of tungsten. These curves are typical of the results which have been obtained for low primary energies.

---

†Portions of this work were supported by the National Aeronautics and Space Administration under Grant NsG 376.

[1]Harrower, G. A., Phys. Rev. 104, 52 (1956).

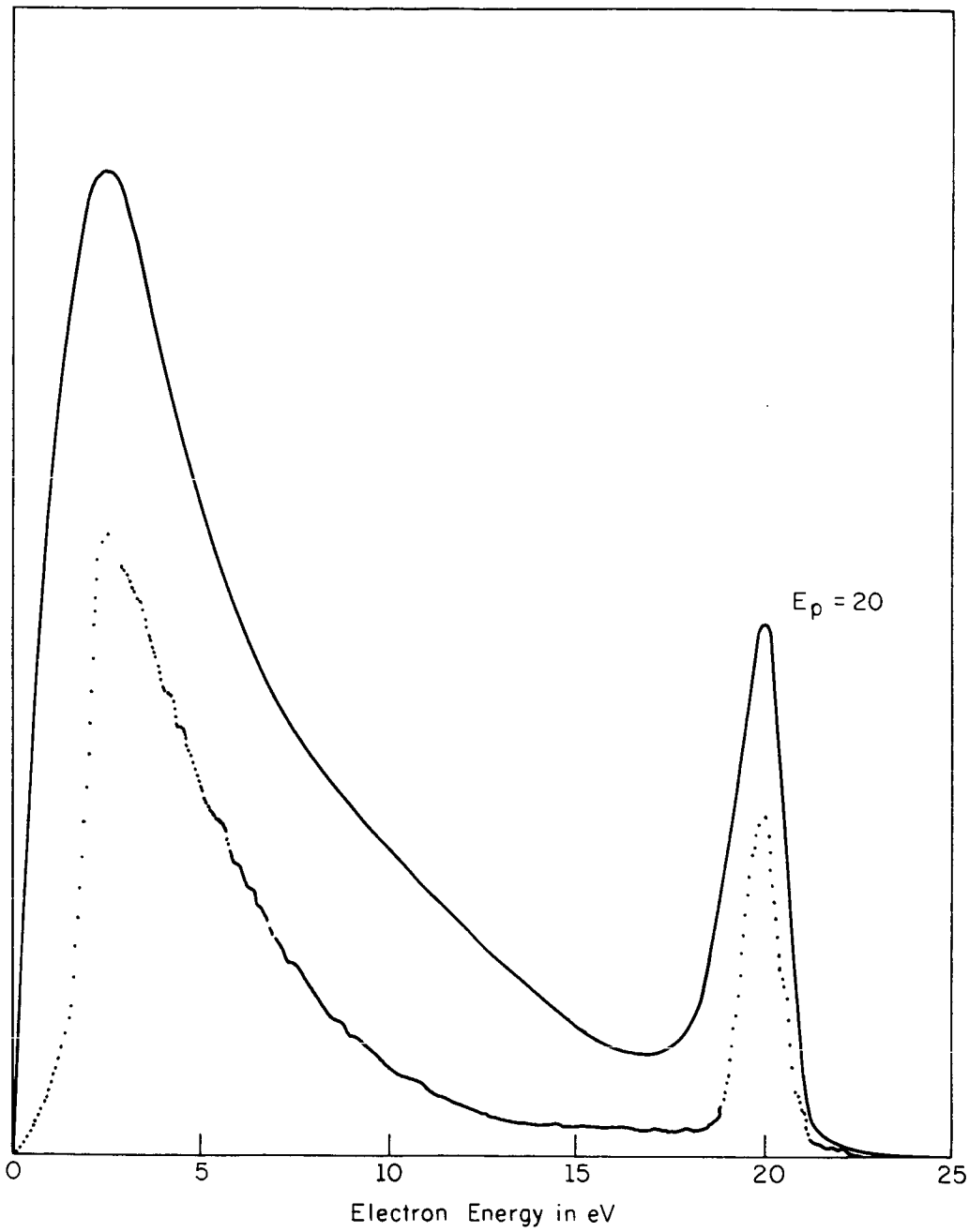

Fig. 2.1.

Fig. 2.2 shows four distributions taken after high-energy electron-bombardment cleaning of our previously-dirty single-crystal tungsten target. The four curves (their zero line being displaced vertically from one another) are quite different from the curves of Fig. 2.1. The most striking difference is in the low energy region. Here, curve a of Fig. 2.2, for 20 eV primaries incident on the relatively clean single crystal, exhibits a low-height double peak in the secondary region. The lower energy peak remains fixed at about 1.2 volts above the target vacuum level for each of the four primary energies shown in Fig. 2.2. This peak might possibly be associated with a high density of states immediately above the vacuum level. In this case, there should also be a resonance effect in the scattering, when the primary energy is reduced to 1.2 eV. This effect may have been observed, also. Preliminary checks have been made in an effort to confirm the reality of this structure. Each of these tests gave positive results; however, more work is necessary to definitely confirm the effect and to understand the mechanism responsible for it.

2.1.2 Apparatus Modifications. Several modifications have been made in an effort to improve the performance of the apparatus. These are primarily associated with increasing the amount of current injected into the monochromator.

"Deflection-focusing" plates have been installed beside the cathode to enable one to make some adjustment of the flow of electrons from the cathode through the monochromator entrance slit. These, after proper adjustment, will increase the current through the system

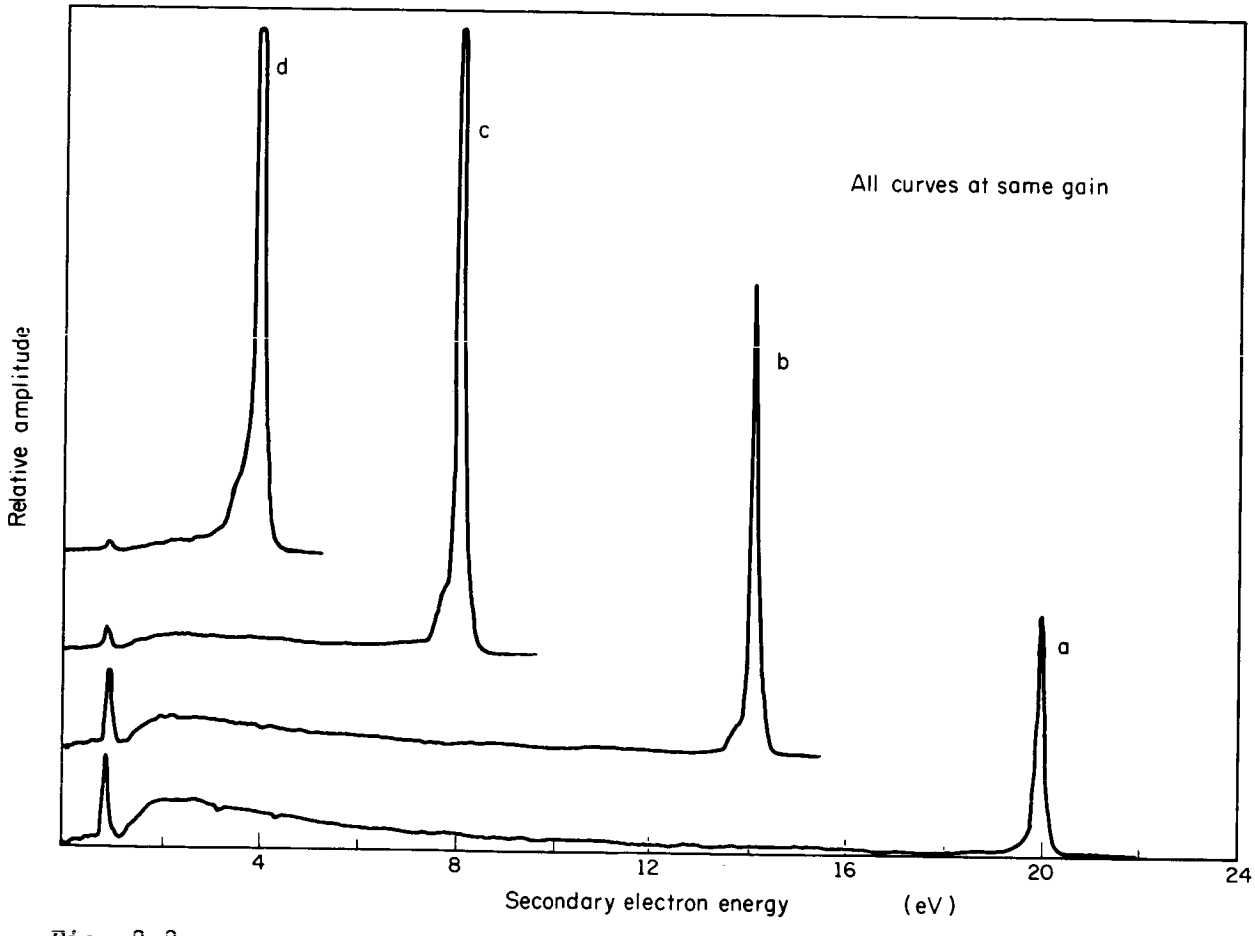
d
c
b
a
All curves at same gain
Relative amplitude
4
8
12
16
20
24
Secondary electron energy (eV)

Fig. 2.2.

somewhat, and thus allow operation of the analyzers at a lower energy than before. Previously, the pass energy of both the monochromator and the analyzer had been 3.0 volts (~60 mV resolution) for primary energies above about 10 volts. Below 10 volts primary energy, there was sufficient current for a good output signal with the selectors set at 1.8 volts pass energy (approx. 35 mV resolution).

The apparatus previously used a 25L6 cathode sleeve and heater, but this has been found to radiate too much heat. Subsequent outgassing of parts near the cathode caused the system pressure to rise slowly from 5×10^{-10} to 5×10^{-9} mm Hg. A smaller cathode and heater have been checked out and will be installed.

In order to put the data obtained for different primary energies in their proper relative scale, the lead to the target is being "guarded," and the cathode enclosed, so that the current striking the target via the monochromator can be accurately measured. Also, being able to measure the target current will permit another check on the energy of the electrons coming from the monochromator. This energy is uncertain due to the various contact potentials involved.

All green-fire stainless-steel screws have been removed from the apparatus because they have been found to be "moderately" magnetic. Dry H_2-fired stainless steel screws and washers are now used throughout the critical regions of the system. These are found to be completely free of magnetization (as low as can be measured by us--about 0.2×10^{-3} Gauss at 5 mm distance).

New grids have been installed in the monochromator and the target chamber. The grids of the monochromator were found to be contaminated (and thus the contact potential changed) due to the outgassing during the activation of the cathodes used earlier.

2.2 Angular Distribution of Secondary Electrons†

Assembly, testing, and modification of components for the angular distribution apparatus[2] are underway.

A new-type output shaft and bearing assembly (Fig. 2.3) for the rotary-motion feedthrough[3] has been constructed. Provided the slot in the slotted disc is made sufficiently long to allow for radial motion of the drive shaft relative to the slot, it is unnecessary for the axes of the output shaft and driving assembly to be colinear. Thus, the output shaft can be moved in a plane perpendicular to its rotation axis independent of the driving assembly. This arrangement makes possible accurate alignment of the rotation axes of the target and collector.

The ability to focus a high intensity (approx.10^{-8} Ampere) ion beam onto the target is of primary importance. The image diameter

†Portions of this work were supported by the National Aeronautics and Space Administration under Grant NsG 376.

[2]Coordinated Science Laboratory Progress Report for March, April, May, 1964.

[3]Coordinated Science Laboratory Progress Report for March, April, May, 1965.

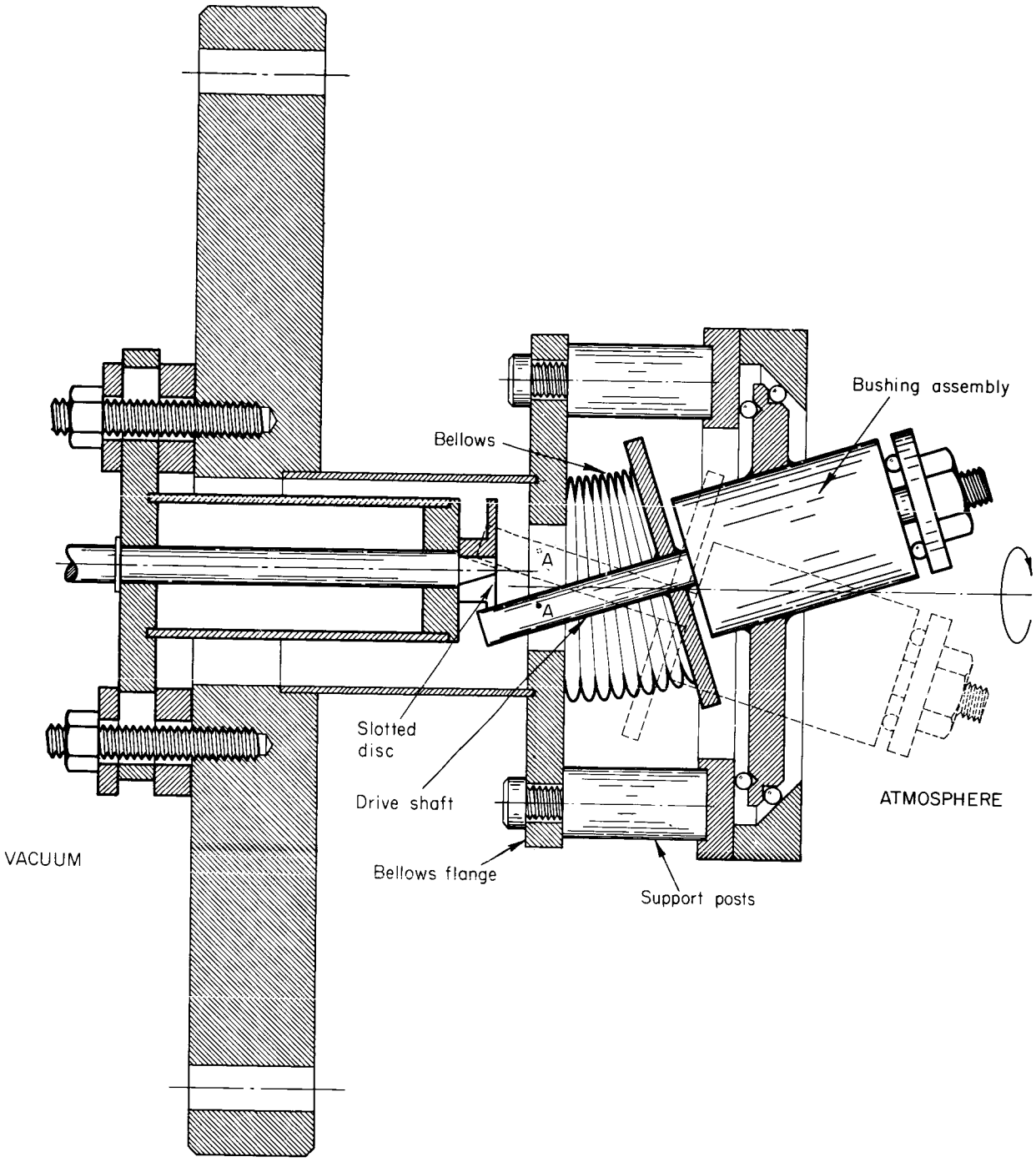
Bushing assembly
Bellows
A
A
Slotted
disc
Drive shaft
ATMOSPHERE
VACUUM
Bellows flange
Support posts

Fig. 2.3.

must be small enough to insure good angular resolution, and the beam must be intense enough to insure good sensitivity. Experiments are underway using different ion gun designs to attempt to satisfy these conditions.

Partial pressure measurements have been made on the vacuum system[3] using a quadrupole mass analyzer. A typical spectrum (before bakeout, but after outgassing the analyzer and the Bayard-Alpert gauge) is shown in Fig. 2.4 and Fig. 2.5. The absence of a mercury (200 amu) peak is to be noted (the system is evacuated by mercury diffusion pumps). The analyzer also presents a convenient method for leak-checking large vacuum systems.

2.3 Adsorption-Desorption Studies†

The experiment for the study of gas-surface interactions by Auger ejection of metallic electrons by ions is continuing.

Repeated study and alteration of the ion optics has produced a beam of diameter much smaller than the target width, a condition for successful operation of the apparatus. Several test runs have been made indicating the feasibility of measuring sticking coefficients by this method.

Results of this experiment are analyzed in terms of

$$\gamma = \frac{\text{Auger electron current}}{\text{Incident ion current}} .$$

†Portions of this work were supported by the National Aeronautics and Space Administration under Grant NsG 376.

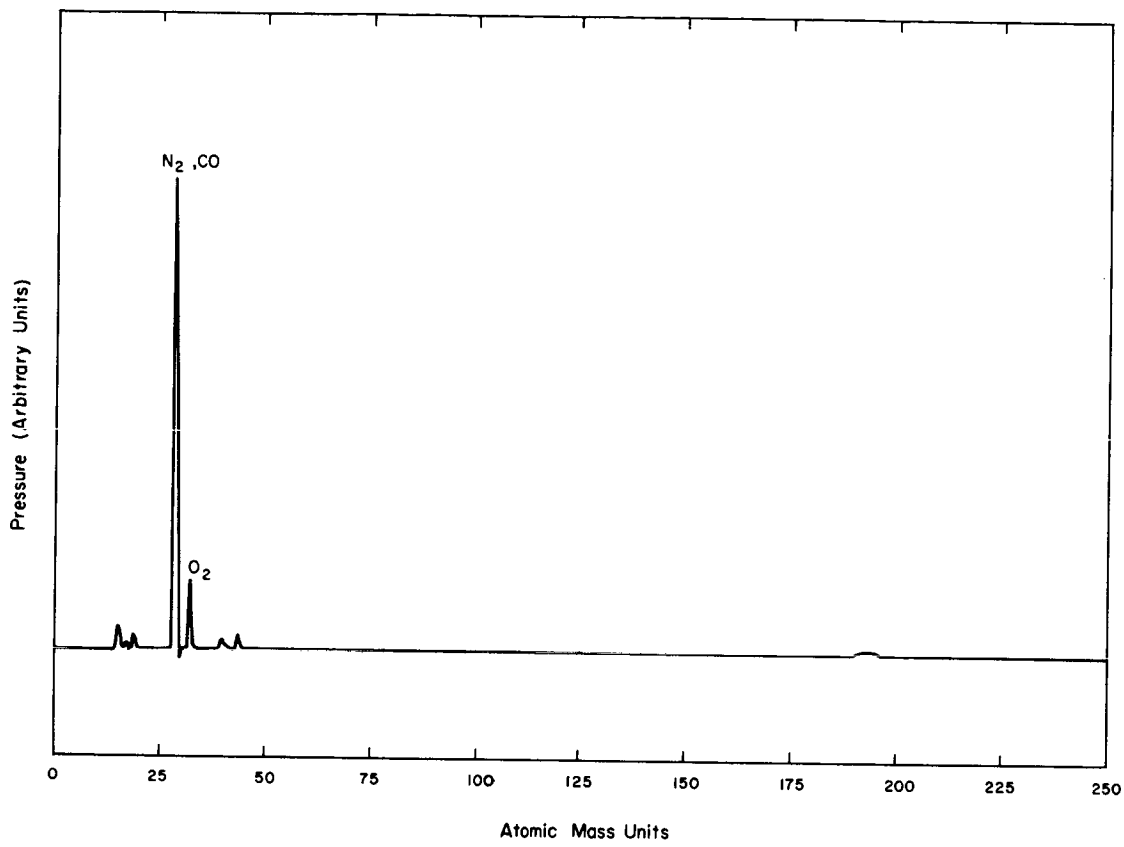
N_2 ,CO
O_2
Pressure (Arbitrary Units)
0
25
50
75
100
125
150
175
200
225
250
Atomic Mass Units

Fig. 2.4.

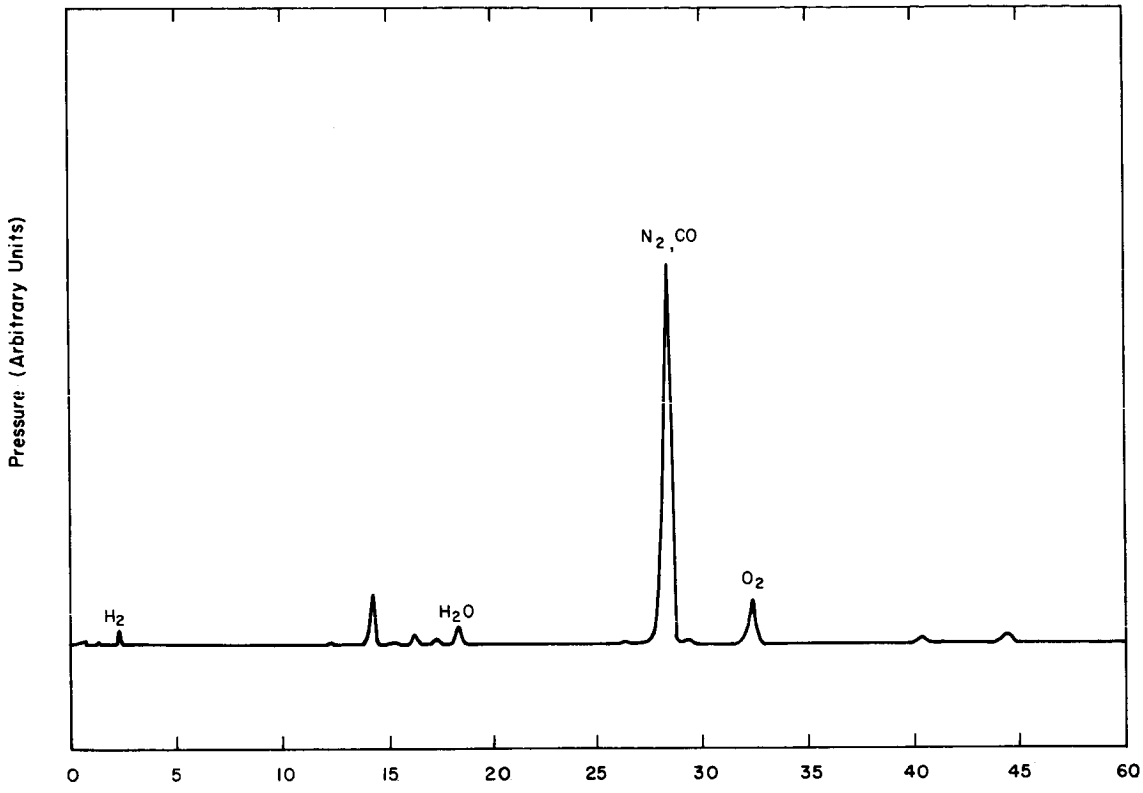
Pressure (Arbitrary Units)
N_2, CO
O_2
H_2
H_2O
0
5
10
15
20
25
30
35
40
45
60
Atomic Mass Units

Fig. 2.5.

Since we intend to measure solely the Auger electron current, the accuracy of the experiment depends upon how closely the incident ion current is held to its initial value. A negative feedback system, to hold the ion current constant, is being constructed.

3. COMPUTER RESEARCH APPLICATIONS

R. M. Brown
S. Fenves
R. Trogdon
J. Stifle
R. Jenks
W. Stoltey

3.1 Introduction

The work of this group concerns applications of digital computers in the fields of artificial intelligence and non-numerical data processing, primarily towards the applications for computer structure and programming techniques.

3.2 Bubble Chamber Data Processing

The new point measuring technique has been incorporated into the SMC-CSX-1 system. Analysis of sample data shows greatly improved results particularly for short track events. These events are now represented by several points along the line, an improvement over the earlier two-point straight-line representation. The technique has also increased the accuracy and rapidity with which previously difficult vertices can be measured.

3.3 CSX-1 Programming

A new CSX-1 machine language assembler, SACRE, designed to facilitate coding, editing, and debugging of large programs is now available. A by-product of a SACRE assembly is a relocatable BCD-version of the program which may itself be edited and separately loaded into core.

3.4 New Equipment

A method of sequencing the control unit of a digital device that involves storing the desired operations in flip-flops prior to the execution of the operations is believed to have several desirable characteristics. A control so designed has small cut-sets and thus lends itself well to diagnosis of malfunction and is also amenable to modification. Being an iterative structure, such a control requires only small circuit fan-out and short interconnections between circuits. The latter characteristics are particularly desirable when high-speed circuit operation is required.

The group is engaged in the design and fabrication of a device that uses this principle of control sequencing and employs digital circuits with transition times of less than ten nanoseconds. The equipment is to be used in gathering data from plasma-physics experiments and consists of three registers which share a common adder. During any input cycle, the two data registers may be either incremented, incremented and decremented, or not modified, depending upon inputs from the experiment. The third register serves as a clock and is incremented by one count for each data sample. For the immediate application, the function of this device could be achieved by five counters. However, the equipment being constructed is to have special features of operating convenience and maintainability and is believed to require fewer components than counters built to ordinary computer standards.

R. Trogdon

4. CONTROL SYSTEMS

J. B. Cruz, Jr.
W. R. Perkins
S. D. Agashe
M. S. Davies
H. Hoyt
T. J. Killian
T. E. Mueller
M. Schoenberger
R. Werner

4.1 Parameter Variations in Control Systems†

A proof was developed for a necessary and sufficient condition for non-increase of finite-time energy of signals mapped by a linear time-invariant causal operator. This work was carried out in collaboration with I. W. Sandberg of Bell Telephone Laboratories. The condition was derived earlier as a sufficient condition for a linear time-invariant multivariable feedback control system to be less sensitive than an equivalent open loop system with the same nominal transfer-function matrix.

Digital computer programs will be developed for incorporating the criterion in synthesis procedures. Preliminary programming has been carried out by T. E. Mueller and M. Schoenberger.

W. R. Perkins
J. B. Cruz, Jr.

4.2 Optimal Control and Sensitivity Considerations†

Investigation continues into the problem of minimizing a performance index averaged over a range of plant parameters, under the

†Portions of this work were supported by the Air Force Office of Scientific Research under Grant No. AFOSR 931.65.

restriction that the controller does not know the values of these parameters, but only a statistical estimate of them. The restriction that the control law may not depend explicitly on some variable parameter in the dynamic equations is a principal stumbling block in the development of an analytical theory. This is because, while the desired control law will likely have an implicit dependence on the variable parameters through feedback, there is no general theory for determining optimal control in feedback form. Many conventional techniques for determining a feedback control law depend on the idea that the feedback is merely another way of producing the optimal open-loop control function u(t). This concept does not extend, however, to problems where the controller does not have complete information about all parameters in the system. The optimal open-loop control is a function u(t) which optimizes the performance based on a priori estimates of the trajectories at each instant of time. However, by the addition of feedback, the controller can utilize actual observations of the trajectories, as well as a priori estimates, and the resulting performance index will usually be lower than that obtained without observation of the trajectories.

Because the optimal controller will require feedback and there is no analytic theory for solving such problems in feedback form, one is led to seek approximate solutions.

One such approach is to assume the control law has a specified form with undetermined constants; for example, a polynomial in the feedback variables with coefficients to be determined. This approach

was tried on a linear system with quadratic loss function. This example was chosen because an optimal control law could be obtained analytically and could be used for comparison. The optimal control law, however, is determined for particular values of plant parameters. In general, performance will not remain optimal as parameters vary.

This example was studied on a computer by assuming a polynomial in the feedback variables and determining the coefficients so that the average value of the performance index is minimized. The minimization was achieved by means of a gradient technique. Of course, use of a higher-order polynomial would usually obtain an improvement in performance, but at the cost of increased computing time. The question of how many terms to include cannot be answered in advance, and this is a drawback of this approach. In the example studied, a greatest lower bound could be obtained to be used as a standard to determine when to terminate the approximation process.

The most interesting result of this study is that, for the example considered, a nonlinear control law was better than a linear system in dealing with parameter uncertainty, even though a linear feedback system would have been optimal for fixed parameters.

The greatest deficiencies in this method are the lack of any guide to choosing the approximating functions and the absence of a theory about the degradation in performance from choosing a small number of terms in the approximating sequence.

Work continues on the development of more general procedures to attack the problem.

T. J. Killian

4.3 Synthesis of Interconnected Linear Time-Varying Systems†

A simple method for the description of interconnected linear time-varying differential systems in composite state-vector form has been developed. A synthesis method utilizing these composite-state equations has been found. The method requires neither the solution of time-varying differential equations nor the complicated manipulation of time-varying operators. Application of the method to the design of feedback control systems has been made. The details of the technique will be described elsewhere.

W. R. Perkins

4.4 Time-Lag Systems†

During this quarter, computer programs were written to solve the equations for the optimal linear regulator problem on the CDC 1604. A paper was prepared from CSL report R-254 for submission to a technical journal. Also, an interesting relation was derived for the optimal regulator problem where the constraints are linear differential-difference equations. This relation provides a new means of deriving the Riccati equation. The derivation is given below.

The necessary and sufficient conditions for minimizing

$$J = \int_{t}^{t_1} \{\tfrac{1}{2}\underset{\sim}{x}^T(\sigma)Q\underset{\sim}{x}(\sigma) + \tfrac{1}{2}\underset{\sim}{u}^T(\sigma)R\underset{\sim}{u}(\sigma)\}d\sigma \ ,$$

†Portions of this work were supported by the Air Force Office of Scientific Research under Grant No. AFOSR 931.65.

with

$$\dot{\underset{\sim}{x}}(\sigma) = A\underset{\sim}{x}(\sigma) + B\underset{\sim}{x}(\sigma-\tau) + C\underset{\sim}{u}(\sigma), \quad t \le \sigma \le t_1 ,$$

and x(s) given for $t - \tau \le s \le t$, and $\underset{\sim}{x}(t_1)$ free, are the following:[1]

$$\dot{\underset{\sim}{x}}(\sigma) = A\underset{\sim}{x}(\sigma) + B\underset{\sim}{x}(\sigma-\tau) + CR^{-1}C^T\underset{\sim}{\lambda}(\sigma), \quad t \le \sigma \le t_1, \tag{1}$$

$$\dot{\underset{\sim}{\lambda}}(\sigma) = -A^T\underset{\sim}{\lambda}(\sigma) - B^T\underset{\sim}{\lambda}(\sigma+\tau) + Q\underset{\sim}{x}(\sigma), \quad t \le \sigma \le t_1-\tau, \tag{2}$$

$$\dot{\underset{\sim}{\lambda}}(\sigma) = -A^T\underset{\sim}{\lambda}(\sigma) + Q\underset{\sim}{x}(\sigma), \quad t_1-\tau \le \sigma \le t_1, \tag{3}$$

$$\underset{\sim}{\lambda}(t_1) = \underset{\sim}{0}, \tag{4}$$

$$\underset{\sim}{u}(\sigma) = R^{-1}C^T\underset{\sim}{\lambda}(\sigma), \quad t \le \sigma \le t_1, \tag{5}$$

$$x(s) \text{ given } t-\tau \le s \le t . \tag{6}$$

Consider the following identity with (1) through (6) satisfied:

$$\underset{\sim}{\lambda}^T(t_1)\underset{\sim}{x}(t_1) - \underset{\sim}{\lambda}^T(t)\underset{\sim}{x}(t) = -\underset{\sim}{\lambda}^T(t)\underset{\sim}{x}(t) =$$

$$\int_t^{t_1} \frac{d}{d\sigma}\{\underset{\sim}{\lambda}^T(\sigma)\underset{\sim}{x}(\sigma)\}d\sigma = \int_t^{t_1} \{\dot{\underset{\sim}{\lambda}}^T(\sigma)\underset{\sim}{x}(\sigma) + \underset{\sim}{\lambda}^T(\sigma)\dot{\underset{\sim}{x}}(\sigma)\}d\sigma =$$

$$\int_t^{t_1} \{\underset{\sim}{x}^T(\sigma)Q\underset{\sim}{x}(\sigma) + \underset{\sim}{\lambda}^T(\sigma)CR^{-1}C^T\underset{\sim}{\lambda}(\sigma)\}d\sigma + \int_t^{t_1} \underset{\sim}{\lambda}^T(\sigma)B\underset{\sim}{x}(\sigma-\tau)d\sigma$$

$$- \int_t^{t_1} \underset{\sim}{\lambda}^T(\sigma+\tau)B\underset{\sim}{x}(\sigma)d\sigma . \tag{7}$$

---

[1] Mueller, T. E., "Optimal Control of Linear Systems with Time Lag," Technical Report No. R-254, Coordinated Science Laboratory, University of Illinois, Urbana, Illinois.

The last two integrals in (7) combine to yield $\int_{t-\tau}^{t} \underset{\sim}{\lambda}^T(\sigma+\tau)B\underset{\sim}{x}(\sigma)d\sigma$. Therefore (7) becomes

$$-\underset{\sim}{\lambda}^T(t)\underset{\sim}{x}(t)-\int_{t-\tau}^{t} \underset{\sim}{\lambda}^T(s+\tau)B\underset{\sim}{x}(s)ds = \int_{t}^{t_1} \{\underset{\sim}{x}^T(\sigma)Q\underset{\sim}{x}(\sigma) + \underset{\sim}{\lambda}^T(\sigma)CR^{-1}C^T\underset{\sim}{\lambda}(\sigma)\}d\sigma \ . \tag{8}$$

The right-hand side of (8) is identified as twice the minimum of J starting with the given initial conditions (6). Therefore (8) gives the minimum of the performance index in terms of the initial conditions and the multipliers. It is

$$-\tfrac{1}{2}\underset{\sim}{\lambda}^T(t)\underset{\sim}{x}(t)-\tfrac{1}{2}\int_{t-\tau}^{t} \underset{\sim}{\lambda}^T(s+\tau)B\underset{\sim}{x}(s)ds = J^*(\underset{\sim}{x}(s),t) \ , \tag{9}$$

where J^* is the minimum of the performance index for given $\underset{\sim}{x}(s)$, with $t-\tau \le s \le t$. Equation (8) can be used for deriving the Riccati equation when B is a matrix of zeros. Let $\underset{\sim}{\lambda}(\sigma) = P(\sigma)\underset{\sim}{x}(\sigma)$ for $t \le \sigma \le t_1$ where P is symmetric, then (8) becomes

$$\underset{\sim}{x}^T(t)P(t)\underset{\sim}{x}(t)+\int_{t}^{t_1} \underset{\sim}{x}^T(\sigma)[Q+P(\sigma)CR^{-1}C^TP(\sigma)]\underset{\sim}{x}(\sigma)d\sigma = 0 \ . \tag{10}$$

Let $\Phi(\sigma,t)$ be the transition matrix of

$$\dot{\underset{\sim}{x}}(\sigma) = [A+CR^{-1}C^TP(\sigma)]\underset{\sim}{x}(\sigma) \ , \tag{11}$$

with $\underset{\sim}{x}(t)$ given. Then (10) becomes

$$\underset{\sim}{x}^T(t)[P(t)+\int_{t}^{t_1} \Phi^T(\sigma,t)[Q+P(\sigma)CR^{-1}C^TP(\sigma)]\Phi(\sigma,t)d\sigma]\underset{\sim}{x}(t) = 0 \ , \tag{12}$$

for all $\underset{\sim}{x}(t)$. The bracketed matrix is symmetric, therefore

$$P(t)+\int_t^{t_1} \Phi^T(\sigma,t)[Q+P(\sigma)CR^{-1}C^TP(\sigma)]\Phi(\sigma,t)d\sigma = 0 \ . \tag{13}$$

Differentiating (13), there results

$$\dot{P}(t)-Q-P(t)CR^{-1}C^TP(t) +$$

$$\int_t^{t_1} \frac{\partial \Phi^T(\sigma,t)}{\partial t}[Q+P(\sigma)CR^{-1}C^TP(\sigma)]\Phi(\sigma,t)d\sigma +$$

$$\int_t^{t_1} \Phi^T(\sigma,t)[Q+P(\sigma)CR^{-1}C^TP(\sigma)]\frac{\partial \Phi(\sigma,t)}{\partial t}d\sigma. \tag{14}$$

But one has

$$\frac{\partial \Phi(\sigma,t)}{\partial t} = -\Phi(\sigma,t)[A+CR^{-1}C^TP(t)] \ . \tag{15}$$

Using (13) and (15) in (14), there results

$$\dot{P}(t)-Q-P(t)CR^{-1}C^TP(t)+[A^T+P(t)CR^{-1}C^T]P(t)$$

$$+P(t)[A+CR^{-1}C^TP(t)] \ , \tag{16}$$

or

$$-\dot{P}(t) = A^TP+P(t)A+P(t)CR^{-1}C^TP(t)-Q \ . \tag{17}$$

Equation (17) is the Riccati equation for this problem, and (13) yields $P(t_1) = 0$.

T. E. Mueller

4.5 Stability of Nonlinear Systems†

Investigation has been continued on sufficient conditions for the stability of a nonlinear system containing several nonlinear elements. A Liapunov function of the form "quadratic of the states plus integral of the nonlinearity" leads to a frequency-domain criterion reducible to that of Popov in the case of a single nonlinearity. Work at present is concentrated on showing that this criterion is a sufficient condition for the existence of certain quantities used in establishing the negative definiteness of the time derivative of the Liapunov function.

M. S. Davies

4.6 Sub-optimal Control†

The solution to the optimal control problem involving a linear time-invariant system and quadratic performance index with fixed-terminal time is time-varying linear feedback. The sub-optimal solution, in which the feedback is constrained to be linear and time-invariant, is presently being investigated. The results for 1^{st} and 2^{nd} order examples indicate that there is little to be gained by using the time-varying feedback, which is difficult to implement. Numerical procedures for higher-order systems will also be investigated.

Analytic solutions to the optimal control problem involving a linear system and quartic performance index with infinite terminal

†Portions of this work were supported by the Air Force Office of Scientific Research under Grant No. AFOSR 931.65.

time have not been found. Rekasius has developed a sub-optimal procedure, but, as my results show, much better results can be obtained. A computer program is almost completed for determining the best linear, time-invariant control for an arbitrary linear system and arbitrary quartic performance index.

M. Schoenberger

4.7 Computer-Oriented Formulation and Solution of the Optimal Control Problem†

Consider the usual fixed-end-point optimal control problem. In a given class of control functions, to each of which corresponds a solution of the differential equation system

$$\dot{\underset{\sim}{x}}(t) = \underset{\sim}{f}(\underset{\sim}{x}(t),\underset{\sim}{u}(t),t) \ , \tag{1}$$

such that

$$\underset{\sim}{x}(t_o) = \underset{\sim}{x}_o, \quad \underset{\sim}{x}(t_f) = \underset{\sim}{x}_f \ ,$$

where t_o, t_f, $\underset{\sim}{x}_o$, $\underset{\sim}{x}_f$ are given, find a control function which minimizes the performance index

$$J = \int_{t_o}^{t_f} f_o(\underset{\sim}{x}(\xi),\underset{\sim}{u}(\xi),\xi)d\xi \ . \tag{2}$$

In very few cases, a closed-form expression for such an optimal control can be obtained, either explicitly as a function of time only, in terms of familiar functions such as the algebraic and

†Portions of this work were supported by the Air Force Office of Scientific Research under Grant No. AFOSR 931.65.

exponential functions, or in feedback form, i.e., as familiar functions of the state vector $\underset{\sim}{x}$.

The maximum principle reduced the above problem to a two-point boundary-value problem with a non-differential inequality constraint on the state, control, and adjoint vectors, and system (1) and the system of adjoint differential equations as differential constraints. Every solution of the two-point boundary-value problem so far obtained has required an integration, and most often, iterated integration of the state and adjoint equations, necessitating recourse to the digital computer.

To solve a differential equation system on a digital computer, a discrete multistep analog of it is set up, either explicitly, before programming the problem, or implicitly, via the program itself. These considerations lead to the following question: Can one take account of the fact that a digital computer has to be used at one stage or the other?

Attempts are being made to answer this question, resulting in a computer-oriented formulation and solution of the optimal control problem. Efforts are being made to improve on dynamic programming and other discretization techniques.

S. D. Agashé

5. PLATO

D. L. Bitzer
J. A. Adams*
M. Axeen*
S. K. Chan
J. Easley*
L. Fillman
H. Gelder*
W. Golden*
J. Gilpin
B. Hicks
L. M. Holland, Jr.
J. M. Kraatz*
E. R. Lyman
W. E. Montague*
M. Secrest
T. L. Smith*
M. Uretsky*
B. Voth
M. Walker
C. E. Webber*
R. Willson
B. Wilson*

5.1 Introduction†

The purpose of the PLATO project has been to develop an automatic computer-controlled teaching system of sufficient flexibility to permit experimental evaluation of a large variety of ideas in automatic instruction including simultaneous tutoring of a large number of students in a variety of subjects. The PLATO system differs from most teaching systems in that the power of a large digital computer is available to teach each student since one such computer controls all student stations. The project work has fallen into three categories, no two of which are wholly separate from each other: (1) development of the tools for research; (2) learning and teaching research; (3) provision of a prototype for multi-student teaching machines. An ever-increasing amount of the time of the PLATO staff is also spent demonstrating the PLATO system to technical visitors and colleagues. In

---

*CSL consultants.

†Portions of this work were supported by the Advanced Research Projects Agency through the Office of Naval Research under Contract Nonr-3985(08).

all the categories of its research, the PLATO group has interacted frequently with various other groups at the University of Illinois that are concerned with curriculum studies, college teaching, and behavioral science research.

5.2 PLATO III System Equipment

During this quarter, work continued in the development and construction of circuitry required for the realization of a 20-student station teaching system.

Student-station circuitry constructed to date includes that required for the full operation of 10 student stations. Construction of the remaining to complete the 20-student-station system continues and is expected to be completed after November, 1965.

Developmental work required to update present system circuitry or to provide new system facilities continues to be under study. Included are transistor deflection-circuits that will replace existing vacuum-tube types operating in storage-tube and flying-spot scanner equipments, and audio-storage circuits to provide for random-access audio-readout capability for all student stations in the PLATO teaching system.

B. Voth

5.3 Plasma-Discharge Display-Tube Research

The purpose of the plasma display-device is to develop an inexpensive replacement for the present student storage-tube system.

This quarter, tubes were constructed with different widths and hole diameters. Preliminary analysis of the data indicates that the minimum permissible operation voltages occur when the hole radius and the cell thickness are equal. Work is continuing on the investigation of the memory mechanism. Various gas additives have been tried, and in some cases separation between the firing and sustaining voltages of 100 per cent have been observed. Cells as small as .01 inch by .02 inch have been investigated.

R. W. Willson

5.4 PLATO Learning and Teaching Research

5.4.1 A New PLATO Tutorial Teaching Logic. Major changes have been made in the teaching logic developed during the spring semester, 1965, for the section of the course in circuit analysis, EE 322, given using the PLATO teaching logic (see 5.4.2). The logic provided the students with the ability to read material, answer questions with constructed responses, ask for help, plot graphical results that were dependent upon their own parameter inputs, and make comments. The logic with its modifications has proved general enough to teach lesson material in other areas than circuit analysis so it is now known as the new PLATO Tutorial Logic. It has been used for both the course in FORTRAN Programming for Commerce Students and the course in How to Use the Library (see 5.4.6 and 5.4.7).

The major changes in the logic program include the following:

(1) The maximum length of an answer has been extended from 14 characters to 69 characters. Answers longer than 69 characters may be plotted on the screen, but will not be stored in the student bank.

(2) A spelling judger in addition to other judges has been added. For a misspelled answer, "SP" will be plotted next to the answer when judged, instead of "NO."

(3) Lesson parameters can now be stacked up on one magnetic tape instead of requiring one tape for each set of parameters.

(4) There is now a second way to introduce lesson parameters into the program. Instead of putting parameters on-line from the keyset, a paper parameter-tape can be prepared on the flexowriter and then read into the computer along with the master program.

M. Walker

5.4.2 Electrical Engineering 322 - Circuit Analysis. A new set of PLATO lesson materials for the electrical engineering course, EE 322, is being written with half the course having been completed during this quarter. The new set of lessons will teach the complete course using the PLATO system in contrast to last semester's procedure of one-half the course with PLATO, one-half in the classroom. The students will meet four hours a week. Three hours will be spent using PLATO with the remaining hour being used for hour exams and problem-discussion sessions. No complete class section will be taught using the PLATO system until the second semester of 1965-66, at which time the

additional ten PLATO stations will be operative. Experimental groups of students will be tested this fall, however, using various portions of the EE 322 course materials (see also 5.4.1).

S. K. Chan

5.4.3 TEXT-TESTER. As a result of preliminary reports during the spring, the generalized, student-controlled, PLATO teaching logic called TEXT-TESTER has been completed, except for annotations and minor modifications. As only one of its multiple uses, TEXT-TESTER is now being adapted for use with a Braillewriter (braille typewriter) in order to experiment with training sighted volunteers to transcribe printed materials, exams, etc., for blind students.

An adapter has been built to sense braille characters and transmit them to the computer, and special subroutines for plotting braille characters have been prepared. Although eventually it seems likely that the difficulties of automatizing the transcription process will be overcome, the training of sighted volunteer braillists meanwhile is an active concern of the University Rehabilitation Center and appears to provide an opportunity for experimentation with PLATO in the training of a technical skill.

An inquiry-type program, TEXT DOPE, to permit authors to examine student responses to TEXT-TESTER is being coded.

A. Easley
J. Easley
W. Golden
J. Hicks
J. Kraatz
B. Wilson

5.4.4 PROOF. The program called PROOF, which is a generalized version of an old ILLIAC-language program, is nearing completion. It is hoped that it may be ready for use with University High School UICSM mathematics classes this winter.

H. Gelder
W. Golden
T. Smith

5.4.5 ARITHDRILL. The new teaching logic that provides timed drill in arithmetic with repetitions controlled individually by pupil success has been revised. This program, called ARITHDRILL, is expected to be used in connection with UICSM classes this fall.

J. Gilpin
B. Wilson

5.4.6 FORTRAN Programming for Business Students. The purpose of this experiment is to investigate programmed methods for teaching computer programming using the FORTRAN language. Particular emphasis is being placed upon an investigation of the types of difficulties faced by business students while learning to program computers.

During the past semester a major portion of the teaching material was developed. Using the new PLATO Tutorial Logic, the parameters were put on tape and tested. Two groups of elementary accounting students worked through the first ten units. The data derived as a by-product of student actions are currently being analyzed in preparation for additional trials during the fall of 1965.

M. Uretsky

5.4.7 Library Science 195. A course, "Introduction to the Use of the Library," (known as the LIBUSE program)has been written for the PLATO system this summer and will be ready to test during the fall semester. The course consists of fourteen units and covers the content of Library Science 195, a course on how to use the library.

During the months of July and August, eight test runs were made on various units. As a result of these test runs the needs were evident for a spelling judger and the inclusion of the selective-erase, in addition to the total-erase, facility. Subroutines for these effects were subsequently added to the new PLATO Tutorial Logic.

The library-science course will be the first credit course at the University of Illinois to be completely taught using the PLATO system.

M. Axeen

5.4.8 Learning and Retention of Verbal Materials. During June and July, 60 subjects participated in an experiment on retention of conceptual material, begun during the previous quarter. The flexibility of the PLATO system allowed individualized subject treatment and complete automatic recording of the data. Except for one power failure, data was accumulated smoothly. Data analysis is in progress.

W. E. Montague
C. E. Webber
J. A. Adams

5.4.9 VERBOSE Program. The PLATO program, VERBOSE, was developed as an exercise in the use of the CONNECT feature of the PLATO compiler, CATO, and as a first step toward more general PLATO programs that would be useful in studying the structure of concepts.

The VERBOSE program records the keyset activities of two subjects, A and S. Subject S generates a string of (stimulus and response) words by partially free association, after A gives him the first word. The screen for S displays the last word that has been added to the string of words and a new word as he types it. The screen for A displays the last two words in the string of words and the link word that he types. The link word is supposed to indicate in some way the relationship that A sees between these last two words. Each types a "period" to indicate "end of word." Each is guided by instructions on PLATO slides.

Design of the VERBOSE program suggested a method of analysis of mode states and mode transitions in PLATO programs that use CONNECT. The VERBOSE program and a few simple results of this analysis are described in CSL Report I-129.

B. Hicks

6. VACUUM INSTRUMENTATION

F. Propst F. Steinrisser

6.1 Pumping Speed of Getter-Ion Pumps†

Experiments under better controlled conditions were continued. In this quarter we aimed at two goals: 1) reproducibility of pumping speed vs. time curves, and 2) measurement of electric pump currents down to the lowest pressures obtainable.

To reproduce pumping-speed measurements it is necessary to keep the parameters constant both during the measurements and from one measurement to another. One of these parameters is the pressure at the pump side of the system which should stay constant within about 10 per cent. It has been found that Granville-Phillips Automatic Pressure Controller maintains the pressure constant within a few per cent for many days at pressures above 1×10^{-10} Torr even with strongly changing pumping speeds. It has been found that the initial pumping speed of the same pump with the same gas (N_2 was used only) changes considerably, depending upon the previous treatment of the pump. After every pumping-speed measurement, the pump is bombarded for several hours with N_2 at such a pressure that the power input is 50 to 100 Watts. This procedure serves to erase the "memory" of the pump. When the whole system is then brought to a very low pressure in the

†Portions of this work were supported by the National Aeronautics and Space Administration under Grant NsG 376.

usual way (see preceding progress report, "Bakeout Procedures for Small Ultrahigh Vacuum Systems"), the initial pumping speed of the pump (and of the clean system!) is high. It decreases with time to a fraction of its initial value. When the system is exposed to air, after erasing the pump memory, the initial pumping speed is quite low, increases with time, and decreases again. The "long term" pumping speed approaches the same value for different treatments and different pressures. More measurements are necessary to understand the mechanism leading to the observed time dependence of the pumping speed.

The electric pump current I, together with pressure p and pumping speed s, gives the ratio of molecules pumped per charge transported, ps/I. To measure I with a regular Keithley micro-microammeter, a shielded battery-power supply was built. The leakage current is less than 1×10^{-10} A at 7 kV. This corresponds to 1×10^{-12} Torr pressure if the sensitivity of the pump is constant over the whole pressure range. Leakage currents in the previously used battery-power supply were two orders of magnitude higher.

Work with experimental pumps, i.e., getter-ion pumps with hot-filament electron sources, was discontinued. These pumps were primarily built for very low-pressure operation. Even low-temperature filaments caused so much additional outgassing due to an elevated temperature of the surroundings that the net pumping speed decreased. At higher pressures (10^{-7} to 10^{-8} Torr), the pump models showed their optimum pumping

speed at very low anode voltage. The resulting speed was very small (a few per cent) compared to regular pumps of the same size, and the addition of electrons increased it by a factor of two in the best case.

7. PLASMA PHYSICS

M. Raether
H. Bohmer
W. Carr
J. Chang
B. Hicks
R. Hosken
Y. Ichikawa
T. Lie
C. Mendel
K. Saul
H. G. Slottow
M. A. Smith

7.1 Boltzmann Equation

The translational relaxation (or "pseudo-shock") problem, that was solved numerically during the previous several quarters, has now been described in CSL Report R-236. This report has been revised for submittal to Arnold Nordsieck as co-author with Bruce L. Hicks before it is submitted to The Physics of Fluids. This research will also be described at the October meeting of the American Physical Society.

Understanding of the sources and magnitudes of the errors in the Monte Carlo method is essential to the success of our future Boltzmann studies. We have therefore made a careful evaluation of these errors during the past quarter for the "hot" side of a shock wave. It has been possible to resolve the total error into its random and systematic parts. A similar, but shorter, analysis of errors on the cold side is being made which should show how these two errors depend upon Monte Carlo sample size and upon interval size.

Professor G. A. Bird (who is Chairman of the Department of Aeronautics, The University of Sydney) visited Hicks and Yen on August 25 to discuss our Monte Carlo techniques. We plan to compare our Monte

Carlo (pseudo-shock) results directly with Bird's results, which will be obtained by an entirely different Monte Carlo method that is faster but less accurate than ours.

B. Hicks

7.2 Linear Plasma Betatron[1,2]

A new tube has been installed in the L.P.B. The main differences between it and the previous tube[2] are heavier B_z windings (1650 Gauss available with new firing circuit), heavier shielding of shim brass around tube, and a movable B_φ probe (Fig. 7.1).

7.2.1 Runaway Current. In this experiment, a collector picks up electrons which have passed through a small orifice in the anode. . . . . This experiment has been done throughout the pressure range of 29 to 96 microns for condensor bank voltages of 6 and 8 kV. At both voltages there is a marked reduction in runaway current above 50 microns.

7.2.2 B_φ. By looking at the integrated output of the B_φ coil the magnetic field in the φ direction can be obtained. This can give both the current distribution and the variation of the electric field with radius. Fig. 7.2 shows one set of results of this experiment. In this particular case the electric field varies about 40 Volts/cm from the surface to the axis of the discharge, which is reasonably small compared to the 325 V/cm at the surface.

---

[1] Progress Report for March, April, May, 1964.

[2] Progress Report for September, October, November, 1964.

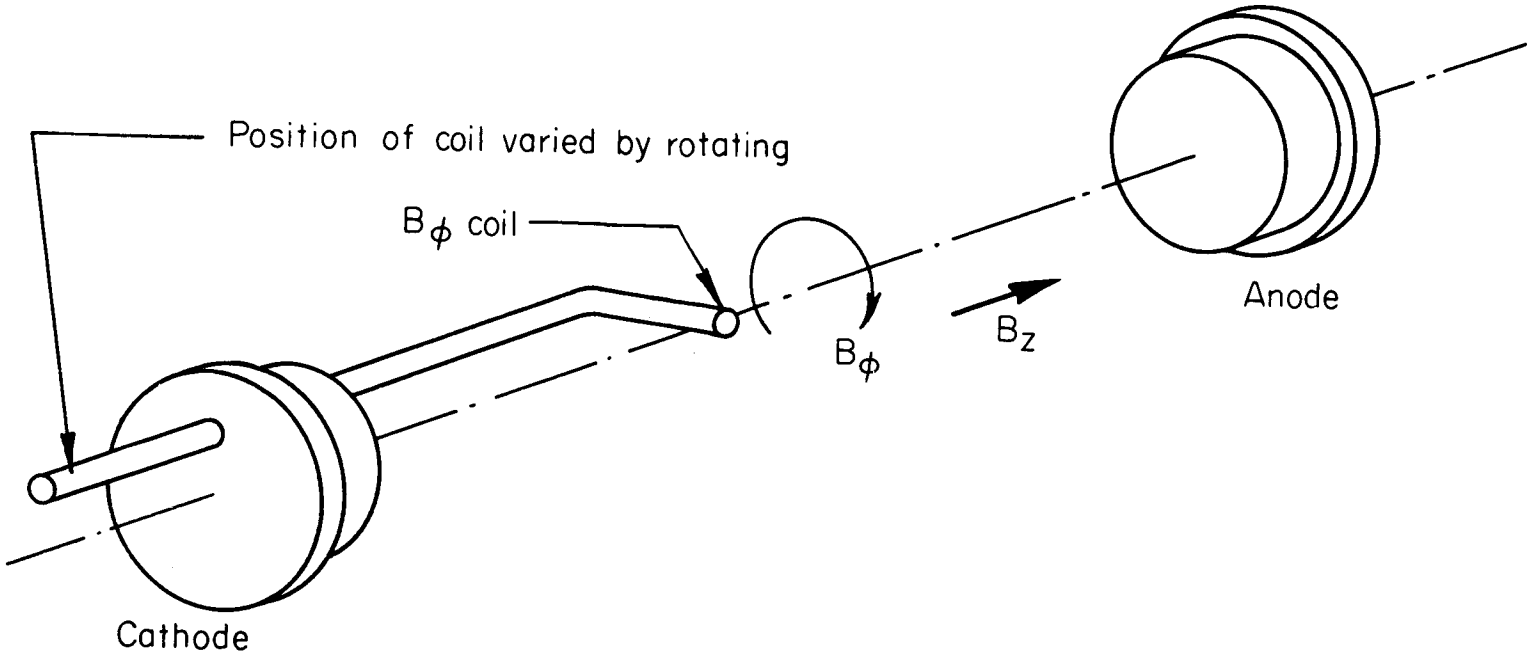

Fig. 7.1. B_φ Probe.

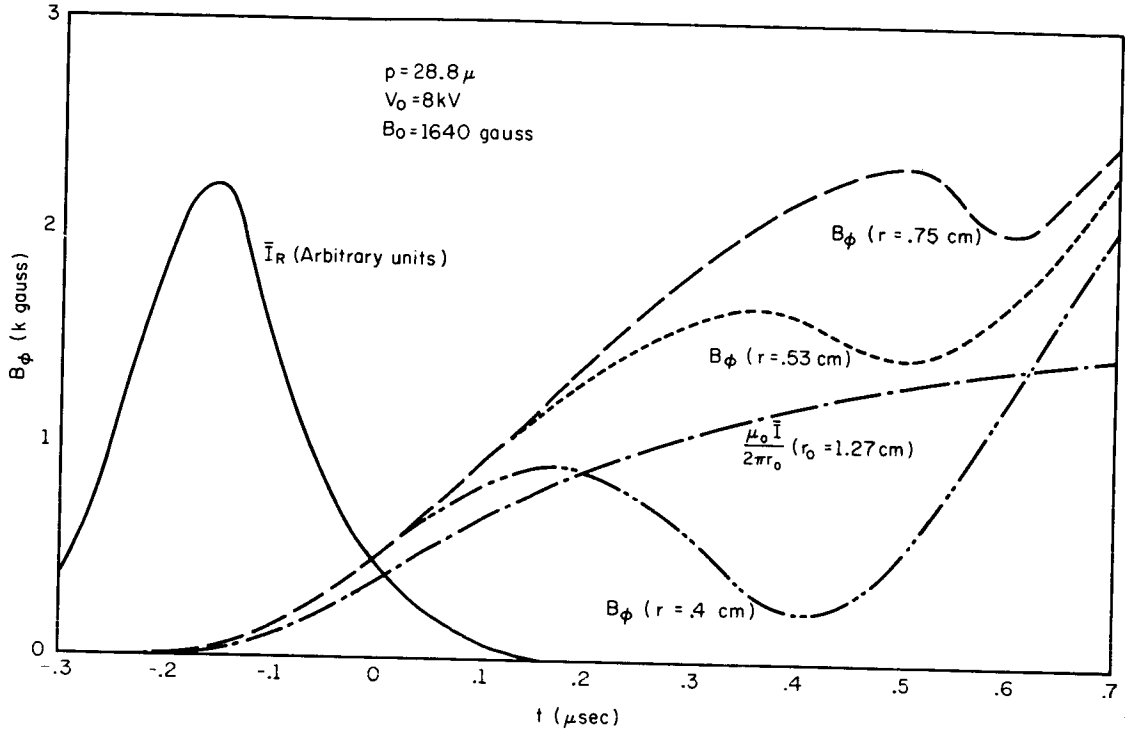

Fig. 7.2. Runaway Current and Axial Magnetic Field.

7.2.3 Ion-Acoustic Oscillations. It has been proposed that ion-acoustic oscillations have a very strong effect on the conductivity of a plasma.[3] It also appears that they may give the electrons a double-humped distribution whereupon electron-plasma oscillations would be able to build up and stop runaway. For this reason oscillations in the conduction current are being investigated. The approximate response of the system can be seen in Fig. 7.3. Fig. 7.4 shows typical results. At low condensor-bank voltages, oscillations do not build up and the current rises to a higher value as in I_1 in Fig. 7.4. If the condensor voltage is raised slightly, the oscillations do build up, giving the output shown in the upper drawing of Fig. 7.4 (for two different values of f_o) and there is a drastic change in the rate of rise of conduction current I_2. These measurements indicate the oscillations are in the 50 to 100 megacycle range. We tentatively attribute them to ion-acoustic oscillations.

7.2.4 Electron Energy. As stated previously,[2] the electron energy will be observed by detecting X-rays from a tungsten target upon which they impinge. This has just begun, but an early result indicates that they have voltages as high as 10 kev. which would mean that they had traversed the whole length of the tube.

In the following months the experiments mentioned will be continued and an effort to measure the electron density will be made.

C. Mendel

---

[3] Field and Fried, Phys. of Fluids 7, 1937 (1964).

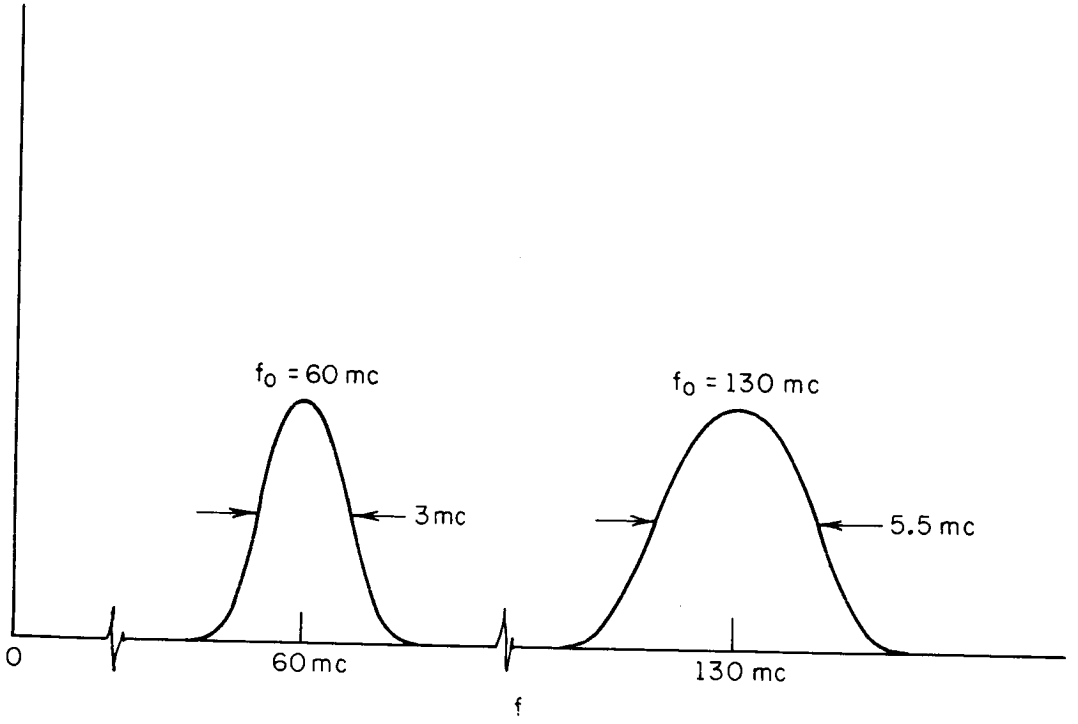

Fig. 7.3. Oscillation Pickup Response.

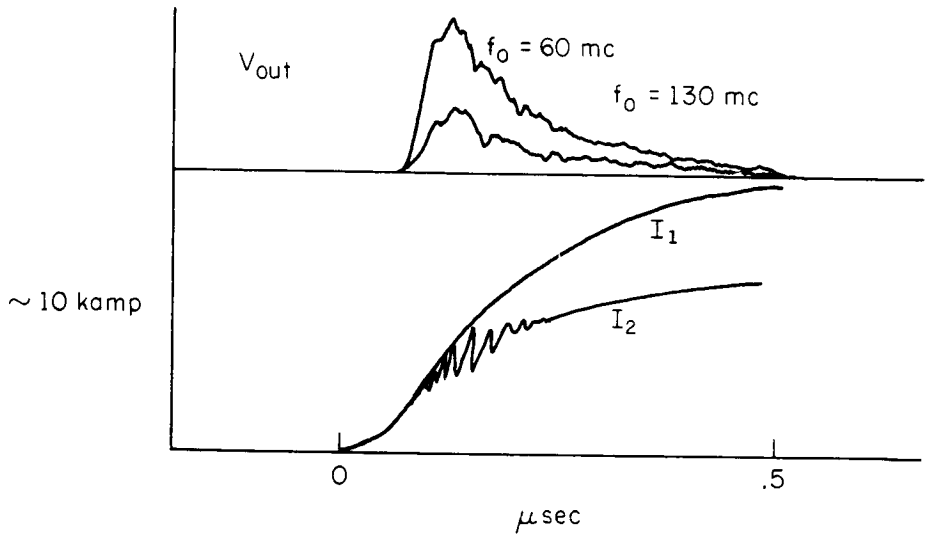

Fig. 7.4. Current Oscillations and Conduction Current.

7.3 Electron Beam-Plasma Interaction

The excitation of plasma oscillations due to electron beam-plasma interaction has gained considerable interest during the past years. These instabilities are of practical interest for the amplification or excitation of microwaves, for the injection of charged particles into magnetic traps and for the heating of a plasma. Besides, this instability is important for all experiments with "run-away electrons." Apart from these applications, beam-plasma interactions serve as an important tool for the understanding of the plasma behavior.

From the large number of theoretical papers dealing with beam-plasma interactions only a few basic publications shall be mentioned here. Bohm and Gross,[4] also Akhiezer and Fainberg[5] developed the first useful theories using linear equations for small signals. A new version of this linear theory was given by Imshennik and Morozov.[6] At large oscillation amplitudes the linear theory fails and one has to use a quasilinear approach (Drummond and Pines[7]) or even a nonlinear theory (Shapiro[8]). While all theories consider either an infinite

---

[4] D. Bohm and E. Gross, Phys. Rev. 75, 1851 (1949).

[5] A. I. Akhiezer and Ya. B. Fainberg, Sov. Phys., JETP 21, 1262 (1951).

[6] V. S. Imshennik and Yu. I. Morozov, Sov. Phys. Tech. Phys. 6, 464 (1961).

[7] W. E. Drummond and D. Pines, Report No. 134, Conference on Plasma Physics, Salzburg (1961).

[8] V. D. Shapiro, Sov. Phys., JETP 17, 416 (1963).

beam-plasma system with one-dimensional variations in all quantities, or a finite beam and plasma in a finite, axial magnetic field, Fainberg and Shapiro[9] recently published a quasilinear theory for a semi-infinite plasma. It can be said that, due to the theoretical effort, the beam-plasma instability is a reasonable well understood phenomenon.

Unfortunately, the experimental confirmation of these theories is far from being satisfactory. It is shown experimentally that the electron beam in passing a plasma and exciting oscillations loses energy (Berezin, Fainberg et al.[10]), and that the beam becomes disrupted when the oscillations become violent (Getty[11]). High frequency oscillations are also detected by means of probes or antennas,[12,13] but there is no confirmation if and how the oscillation amplitude depends on the ratio of beam to plasma density as predicted by the theories, no exact measurements of the energy distribution of the electron beam after it has interacted with the plasma, and no experimental clue as to how the interaction depends on the plasma temperature and the thermal spread of the beam. Also, all experiments so far are

---

[9] Ya. B. Fainberg and V. D. Shapiro, Sov. Phys., JETP 20, 937 (1965).

[10] A. K. Berezin, Ya. B. Fainberg, et al., Plasma Phys. Accel. Thermonucl. Res. 4, 291 (1962).

[11] W. D. Getty, Thesis, MIT (1963).

[12] G. D. Boyd, R. W. Gould, and L. M. Field, Phys. Rev. 109, 1393 (1958); Proc. IRE 49, 12, 204 (1961).

[13] I. F. Kharchenko, Ya. B. Fainberg, et al., Sov. Phys.-Tech. Phys. 9, 798 (1964).

done with a beam-generated plasma. The plasma density therefore is not constant during the time the beam is switched on. Finally, in most experiments the beam is confined by a longitudinal magnetic field, which makes the interpretation of the experimental results more complex because of the coupling between longitudinal and transversal modes in a magnetic field.

In the present experiment, we intend to study the frequency distribution of the electron density fluctuations after the instability has developed into a steady turbulent state. To this end we measure the scattering of microwaves by electron density fluctuations resulting from these instabilities and the frequency distribution of the noise radiated by the beam enhanced plasma oscillations. Our long-range plans are to time-resolve the instability and to study the transition between the stable and the unstable state. Further plans call for the use of higher frequency microwave equipment in order to be able to measure the angular distribution of the scattered radiation. This would give us information about the wave-number dependence of the fluctuation spectrum.

Microwave-scattering experiments are not used as a diagnostic technique for laboratory plasmas for the following reason: In a stable plasma the scattering of electromagnetic waves is due to the thermal

density fluctuations of the plasma[14,15,16,17,18]. The total scattering cross section per electron is half of that calculated for scattering from a free electron, namely $\frac{1}{2}r_o^2$, with r_o being the classical electron radius. The scattered signal contains a doppler-broadened peak around the incident frequency and two peaks at the incident frequency plus or minus the plasma frequency which contain a small fraction of the total scattered power. In a typical laboratory experiment, where one is mainly concerned with the scattering at the plasma frequency, the scattered power is of the order of 10^{-24} watts per cycle, so that sophisticated means of detection are necessary.

In an unstable plasma, like the one generated by an electron beam, the oscillation amplitude will exceed the amplitude of the thermal fluctuations. Therefore, the scattering cross section can be expected to be several orders of magnitude bigger than in the equilibrium case, and we should be able to detect the scattered power with a conventional microwave receiver.

---

[14] J. P. Dougherty and D. T. Farley, Proc. Roy. Soc. A259, 79 (1960).

[15] E. E. Salpeter, Phys. Rev. 120, 1528 (1960).

[16] J. A. Fejer, Can. J. Phys. 38, 1114 (1960).

[17] M. N. Rosenbluth and N. Rostocker, Phys. Fluids 5, 776 (1962).

[18] D. C. Montgomery and D. A. Tidman, Plasma Kinetic Theory, New York (1964).

In our experiment, we want the plasma density to be independent of the beam current. This can be done by injecting the beam into an externally created plasma and choosing the gas pressure, the beam current, and beam energy in such a way that the additional ionization due to the beam remains small compared with the primary electron density. We decided to use a pulsed plasma and to perform the experiment in the afterglow because, in this way, the plasma density can be made high enough (up to 10^{13} electrons/cm^3) and the density can be varied conveniently by changing the delay time between discharge pulse and beam pulse.

X-band microwave equipment and receiver are being used; that means that if we want to detect plasma oscillations and set the receiver frequency at 9 kmc, the plasma density is 10^{12} el./cm^3. We want the beam-plasma system to be reasonably unstable so that we can detect the oscillations, but the amplitude should stay in the limits of the quasilinear theory. To fulfill these conditions, the beam electron density should be a factor 10^3 to 10^4 smaller than the plasma electron density. Therefore, assuming a beam diameter of 1 cm and a beam energy of 20 kV, the beam current should be of the order of amperes.

Fig. 7.5 shows schematically the experimental setup. The vacuum system contains the electron-gun section, magnetic focusing, plasma, and analyzer section. It can be evacuated to a pressure better than 10^{-6} Torr. Between the gun and the focusing section a tube 0.31" inner diameter 2-1/2" long, and between the plasma and the analyzer section a tube 3/4" inner diameter 5" long are located to allow

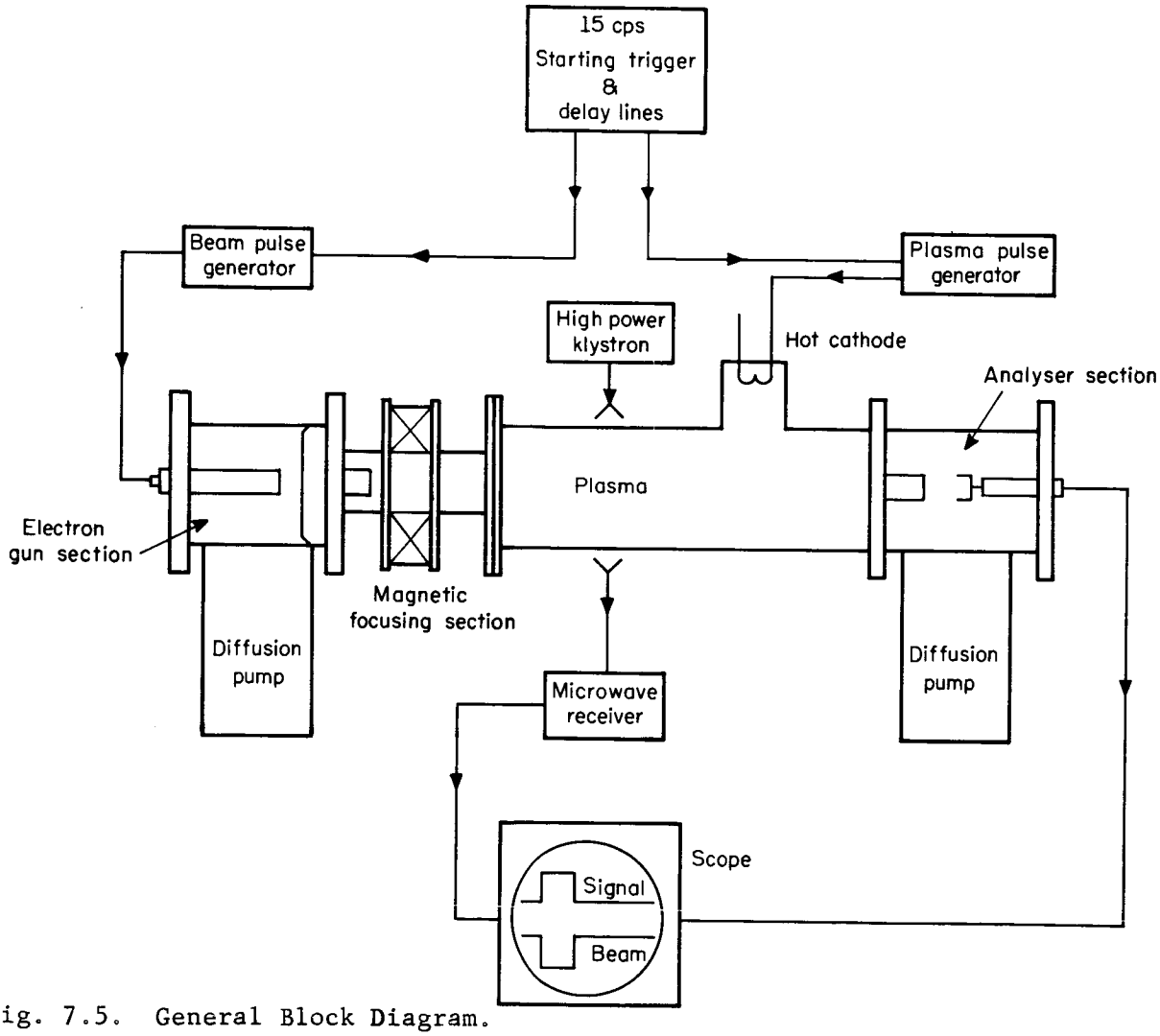

Fig. 7.5. General Block Diagram.

differential pumping. For example, with a neon pressure of 30 microns in the plasma section, the pressure around the electron gun stays below 10^{-4} Torr. This is essential because to both gun and analyzer sections, voltages up to 25 kV are applied. The focusing section consists of a 1-1/4" I.D. stainless steel tube 6" long, which simultaneously acts as the anode for the discharge. The Pyrex plasma tube is 15" long with an I.D. of 1-5/8". A neon discharge is being used because it is easy to fire and the decay time is reasonably long. In order to be able to work with low neon-pressures or to use hydrogen, a liquid-cooled hot cathode was installed. The amount of gas flowing into the system is controlled by an automatic pressure controller to ensure a constant pressure in the system.

A Pierce-type gun is used to produce a high-current electron beam. Although the dimensions of the device are very critical, it is relatively easy to build because there is no need for auxiliary focusing electrodes or magnets. Fig. 7.6 shows the cathode and anode assembly of the gun. The spherical shape of the cathode surface together with the focusing cylinder (cathode and focusing cylinder are on the same potential) and the conical shape of the anode aperture provide a strongly focusing effect. The focusing condition is fulfilled only for one acceleration voltage. But because in our construction the cathode-anode separation can be varied externally, the gun operates satisfactorily in a range from 5 to 25 kV. The electron-emitting surface of the cathode has to withstand ion bombardment and repeated

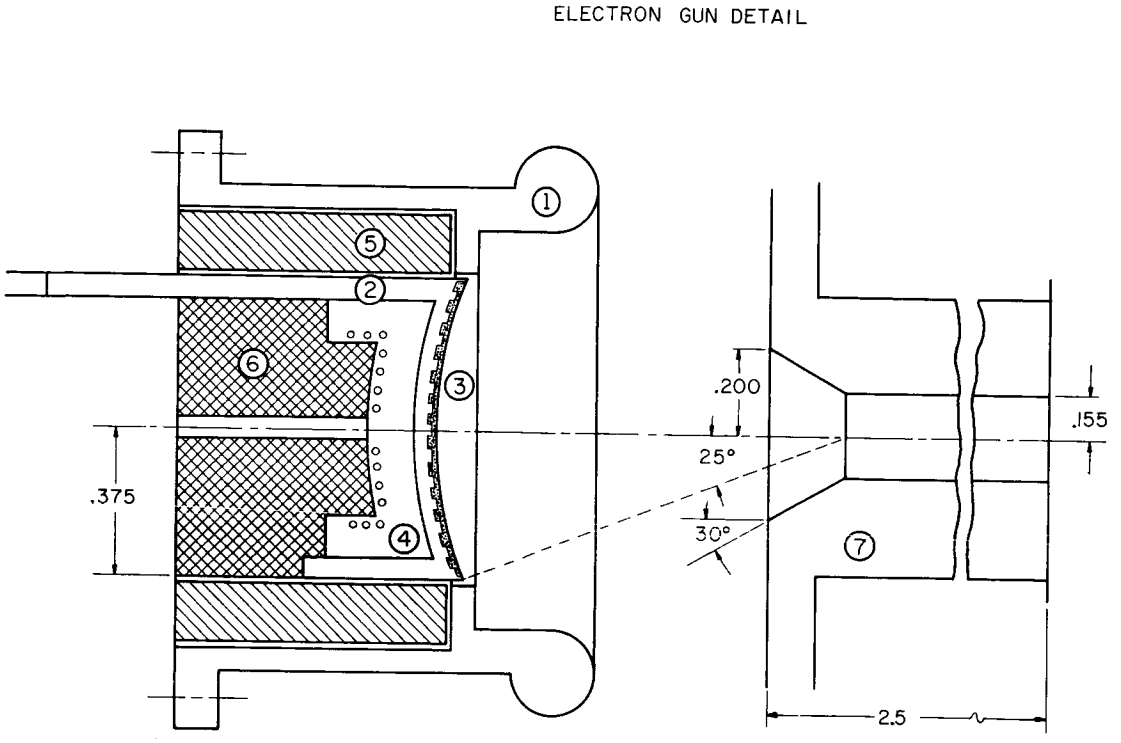

Fig. 7.6. Electron Gun Detail. 1) Molybdenum cylinder. 2) Titanium cathode cylinder. 3) Lanthanum boride. 4) Tungsten filament. 5) Alumina. 6) Boron nitrite. 7) Anode.

opening to air. We use pure Lanthanum hexa-boride because its emissivity is of the order of ampere/cm^3 at temperatures of 1200°C and it does not become poisoned by air. The cathode cylinder is made out of titanium, since the diffusion rate of boron into this material is small compared with other metals. Lanthanum hexa-boride sticks on no surface, but grooves in the surface of the cathode cup provide a mechanical hold. The heater is a flat spiral made out of 30 mil tungsten wire. The power necessary to heat the cathode to 1200°C is 250 watts. The magnetic field of the heater spiral has a strongly defocusing effect. This can be avoided by heating with ac and pulsing the gun at the time the heater current goes through zero. The duration of the beam is set on 2μ sec. During this time the plasma density changes about 5 per cent for the plasma densities we are interested in (10^{12} el./cm^3). The electron gun just described is capable of delivering an electron beam of 2 ampere at 24 kV.

The focusing magnet (Fig. 7.5) forces the electrons to traverse the plasma section in a parallel beam of approximately 3/8" diameter.

For the measurement of the beam energy distribution an electrostatic analyzer using a stopping potential was built. The accuracy turned out to be only $\pm$ 500 Volts. It will be necessary to use a different type of analyzer, probably an electrostatic deflection type.

Fig. 7.7 shows the microwave equipment and the pulse logic used in the experiment. The line-synchronized 15 c/sec square wave generator provides the reference signal for the lock-in amplifier and a starting trigger pulse for the pulsers. The trigger signal is passed through a 0 to 0.1 μsec delay line. With this delay the trigger phase can be changed with respect to the line phase and the beam current can be maximized. The second delay line (0 to 1000 μsec) is used to choose a certain plasma density for the experiment by changing the time elapsing between plasma and beam pulse.

For the scattering experiment a C.W. highpower microwave signal (2 Watt, 8.5 kmc) is propagated radially through the plasma tube. The scattered signal or the noise signal is picked up by a microwave horn and passed through a high-pass filter with a cutoff frequency of 9.0 kmc, which, for the scattering experiment, rejects stray signals of 8.5 kmc. These microwave signals are then mixed in a magic tee with another microwave signal from a local oscillator. The sum and difference frequencies are amplified in a preamplifier and a main amplifier of 100 mc center frequency and 4 mc bandwidth. The total gain of the amplifiers is 100 dB. The noise figure is 17 dB. The video signal of the main amplifier can either be monitored on an oscilloscope, or can be fed into a lock-in amplifier to integrate the signal. Stray signals from the plasma pulser are picked up by the receiver and, because of the high gain of the amplifiers, exceeds the signal of interest several times in amplitude. This does not disturb the visual observation on

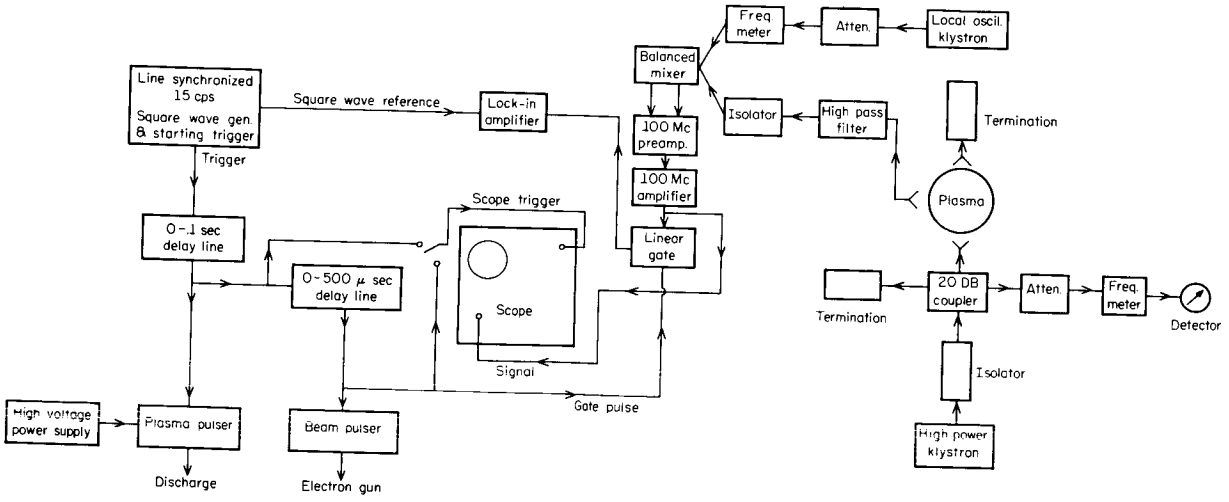

Fig. 7.7. Block Diagram of the Pulse Logic, the Microwave Equipment, and the Receiver Devices.

the scope since at least 100 μsec elapses between the plasma and beam pulse. On the other hand, for the repetition frequency of 15 c/sec this phase difference is so small that the stray signal is monitored by the lock-in amplifier. To get rid of this signal, a linear gate that opens only during the time the beam is switched on is inserted between the main amplifier and the lock-in amplifier.

The experimental setup described in this report is ready for use, and preliminary measurements are underway.

H. Bohmer

7.4 Ion Oscillations in a Weakly Turbulent Plasma

When a plasma is unstable for the electron-plasma oscillation, this growing oscillation will act to distort the velocity-distribution function in such a way that the system approaches to a weakly turbulent state. This feedback effect of the growing oscillation, however, may affect also the spatially inhomogeneous part of the distribution function which is varying on a longer time scale compared to the period of the electron-plasma oscillation. A typical example of such spatial inhomogeneity is the ion oscillation in an electron-ion plasma. Therefore, generalizing the quasilinear approximation to a spatially inhomogeneous system, we have undertaken to examine characteristics of the ion oscillation in an electron-ion plasma in the presence of the high-frequency turbulent fluctuation.

The kinetic behavior of a low density and high temperature electron-ion plasma can be described by the Vlasov equation

$$\frac{\partial F_\alpha}{\partial t} + \underset{\sim}{v}\cdot\underset{\sim}{\nabla} F_\alpha + \frac{e_\alpha}{m_\alpha}\underset{\sim}{E}\cdot\frac{\partial F_\alpha}{\partial \underset{\sim}{v}} = 0, \quad (\alpha = e,i) \tag{1a}$$

$$\underset{\sim}{\nabla}\cdot\underset{\sim}{E} = 4\pi\sum_\alpha e_\alpha \int F_\alpha d\underset{\sim}{v}, \tag{1b}$$

where the suffix α stands for the electrons and the ions. The function $F_\alpha(\underset{\sim}{x},\underset{\sim}{v};t)$ is a one-particle-distribution function of the α-th species of plasma particles.

It is assumed that the system is weakly unstable with respect to the electron-plasma oscillation, but stable for the ion oscillation. Assume a statistical ensemble of plasmas having a random distribution of phases of the electron-plasma oscillation. Then, the distribution functions of electron and ion may be decomposed into the following two parts:

$$F_\alpha(\underset{\sim}{x},\underset{\sim}{v};t) = F_\alpha^{\ell}(\underset{\sim}{x},\underset{\sim}{v};t) + f_\alpha^{h}(\underset{\sim}{x},\underset{\sim}{v};t) \ , \tag{2a}$$

where $f_\alpha^{h}(\underset{\sim}{x},\underset{\sim}{v};t)$ represents the high frequency component of the distribution function of the α-th particles. Since the ensemble average of $f_\alpha^{h}(\underset{\sim}{x},\underset{\sim}{v};t)$ vanishes identically, $F_\alpha^{\ell}(\underset{\sim}{x},\underset{\sim}{v};t)$ can be defined uniquely as

$$F_\alpha^{\ell}(\underset{\sim}{x},\underset{\sim}{v};t) = \langle F_\alpha(\underset{\sim}{x},\underset{\sim}{v};t)\rangle \ . \tag{2b}$$

The bracket represents the ensemble average. Corresponding to the

above decomposition of the distribution functions, the internal electric field can be separated as follows:

$$\underset{\sim}{E}(\underset{\sim}{x},t) = \underset{\sim}{E}^{\ell}(\underset{\sim}{x},t) + \underset{\sim}{E}^{h}(\underset{\sim}{x},t) \ , \tag{3a}$$

with the definition of

$$\underset{\sim}{E}^{\ell}(\underset{\sim}{x},t) = \langle \underset{\sim}{E}(\underset{\sim}{x},t) \rangle \ . \tag{3b}$$

Now, taking the ensemble average of Eqs. (1a) and (1b), we can decompose the Vlasov equation into the slowly varying part and the rapidly fluctuating part. In the equation of the rapidly fluctuating component, we may disregard the mode-mode coupling term. Since the system is assumed to be stable for the ion oscillation, the equation of the slowly varying component can be linearized by decomposing the distribution function $F_{\alpha}^{\ell}(\underset{\sim}{x},\underset{\sim}{v};t)$ into two parts as

$$F_{\alpha}^{\ell}(\underset{\sim}{x},\underset{\sim}{v};t) = F_{\alpha}(v;t) + f_{\alpha}^{\ell}(\underset{\sim}{x},\underset{\sim}{v};t) \ . \tag{4}$$

Thus, we obtain finally the following set of equations:

$$\frac{\partial f_{\alpha}^{h}}{\partial t} + \underset{\sim}{v}\cdot\nabla f_{\alpha}^{h} + \frac{e_{\alpha}}{m_{\alpha}} \underset{\sim}{E}^{h}\cdot\frac{\partial F_{\alpha}}{\partial \underset{\sim}{v}} + \frac{e_{\alpha}}{m_{\alpha}} \underset{\sim}{E}^{h}\cdot\frac{\partial F_{\alpha}^{\ell}}{\partial \underset{\sim}{v}} + \frac{e_{\alpha}}{m_{\alpha}} \underset{\sim}{E}^{\ell}\cdot\frac{\partial f_{\alpha}^{h}}{\partial \underset{\sim}{v}} = 0 \ , \tag{5a}$$

$$\nabla\cdot\underset{\sim}{E}^{h} = 4\pi \sum_{\alpha} e_{\alpha} \int f_{\alpha}^{h} d\underset{\sim}{v} \ , \tag{5b}$$

$$\frac{\partial f_{\alpha}^{\ell}}{\partial t} + \underset{\sim}{v}\cdot\nabla f_{\alpha}^{\ell} + \frac{e_{\alpha}}{m_{\alpha}} \underset{\sim}{E}^{\ell}\cdot\frac{\partial F_{\alpha}}{\partial \underset{\sim}{v}} = -\frac{e_{\alpha}}{m_{\alpha}} \left\langle \underset{\sim}{E}^{h}\cdot\frac{\partial f_{\alpha}^{h}}{\partial \underset{\sim}{v}} \right\rangle_{SI} \ , \tag{5c}$$

$$\nabla \cdot \underset{\sim}{E}^{\ell} = 4\pi \Sigma_{\alpha} e_{\alpha} \int f_{\alpha}^{\ell} d\underset{\sim}{v} \quad , \tag{5d}$$

and

$$\frac{\partial F_{\alpha}}{\partial t} = - \frac{e_{\alpha}}{m_{\alpha}} \langle \underset{\sim}{E}^{h} \cdot \frac{\partial f_{\alpha}^{h}}{\partial \underset{\sim}{v}} \rangle_{SH} \quad , \tag{5e}$$

where the suffixes SI and SH designate the spatially inhomogeneous part and the spatially homogeneous part of the assigned quantity. Eq. (5a) differs from the ordinary linearized Vlasov equation by the presence of the last two terms which represent the interaction between the high frequency electron plasma oscillation and the low frequency ion oscillation. These two terms can be treated as small perturbation terms in solving Eqs. (5a) and (5b). Solutions of Eqs. (5a) and (5b) are obtained by the method of the Fourier-Laplace transformation.

Then, it is straightforward to show that Eq. (5c) can be reduced to the quasilinear kinetic equation discussed by Drummond and Pines, and Vedenov and his collaborators. Therefore, the weakly turbulent stationary state of the present problem is essentially equivalent to that predicted by the quasilinear theory of the homogeneous electron plasma. On the other hand, the right hand side of Eq. (5c) is calculated as

$$C_{\alpha}(\underset{\sim}{k},\underset{\sim}{v};t) \equiv - \frac{e_{\alpha}}{m_{\alpha}} \langle \underset{\sim}{E}^{h} \cdot \frac{\partial f_{\alpha}^{h}}{\partial \underset{\sim}{v}} \rangle_{SI} \quad ,$$

which is

$$C_{\alpha} = (e_{\alpha}^2/m_{\alpha}^2 V) \Sigma_{\underset{\sim}{q}} G(\underset{\sim}{q},p_o(\underset{\sim}{q})) e^{2\gamma(q)t} (1/2\pi i) \int [Q_1+Q_2+i\varphi^{\ell}(\underset{\sim}{k},s)(Q_3+Q_4)] e^{st} ds \quad , \tag{6}$$

in which the Q quantities are

$$Q_1 = \underset{\sim}{q}\cdot\frac{\partial}{\partial \underset{\sim}{v}}\left(\frac{\underset{\sim}{q}}{d_1}\cdot\frac{\partial}{\partial \underset{\sim}{v}} f_\alpha^\ell\right) ,$$

$$Q_2 = \frac{i}{\epsilon}\sum_\beta \frac{4\pi e_\beta^2}{m_\beta |\underset{\sim}{k}-\underset{\sim}{q}|^2}\int \frac{\underset{\sim}{q}}{d_1}\cdot\frac{\partial f_\beta^\ell}{\partial \underset{\sim}{v}} h_\alpha d\underset{\sim}{v} ,$$

$$Q_3 = \frac{e_\alpha}{m_\alpha}\underset{\sim}{q}\cdot\frac{\partial}{\partial \underset{\sim}{v}}\left[\frac{\underset{\sim}{k}}{d_1}\cdot\frac{\partial}{\partial \underset{\sim}{v}}\left(\frac{\underset{\sim}{q}}{d_2}\cdot\frac{\partial F_\alpha}{\partial \underset{\sim}{v}}\right)\right] ,$$

$$Q_4 = \frac{i}{\epsilon}\sum_\beta \frac{4\pi e_\beta^3}{m_\beta^2 |\underset{\sim}{k}-\underset{\sim}{q}|^2}\int \frac{\underset{\sim}{k}}{d_1}\cdot\frac{\partial}{\partial \underset{\sim}{v}}\left(\frac{\underset{\sim}{q}}{d_2}\cdot\frac{\partial F_\beta}{\partial \underset{\sim}{v}}\right) h_\alpha d\underset{\sim}{v} ,$$

and the denominators are

$$d_1 = p_o(-\underset{\sim}{q})+s+i(\underset{\sim}{k}-\underset{\sim}{q})\cdot\underset{\sim}{v} ,$$

$$d_2 = p_o(-\underset{\sim}{q})-i\underset{\sim}{q}\cdot\underset{\sim}{v} ,$$

with the further abbreviations $f_\alpha^\ell = f_\alpha^\ell(\underset{\sim}{k},\underset{\sim}{v};s)$,

$$h_\alpha = h_\alpha(\underset{\sim}{q},\underset{\sim}{k}-\underset{\sim}{q},\underset{\sim}{v},s) \equiv \underset{\sim}{q}\cdot\frac{\partial}{\partial \underset{\sim}{v}}\left(\frac{\underset{\sim}{k}-\underset{\sim}{q}}{d_1}\cdot\frac{\partial F_\alpha}{\partial \underset{\sim}{v}}\right)+(\underset{\sim}{k}-\underset{\sim}{q})\cdot\frac{\partial}{\partial \underset{\sim}{v}}\left(\frac{\underset{\sim}{q}}{p_o(\underset{\sim}{q})+i\underset{\sim}{q}\cdot\underset{\sim}{v}}\cdot\frac{\partial F_\alpha}{\partial \underset{\sim}{v}}\right) , \quad (7)$$

and

$$G(\underset{\sim}{q},p_o(\underset{\sim}{q})) = \langle|\varphi^h(\underset{\sim}{q},p_o(\underset{\sim}{q}),t=0)|^2\rangle . \quad (8)$$

In Eq. (6), $\epsilon=\epsilon(\underset{\sim}{k}-\underset{\sim}{q},p_o(-\underset{\sim}{q})+s)$ is given as

$$\epsilon(\underset{\sim}{q},p) = 1-i\sum_\alpha \frac{4\pi e_\alpha^2}{m_\alpha q^2}\int \frac{\underset{\sim}{q}}{p+i\underset{\sim}{q}\cdot\underset{\sim}{v}}\cdot\frac{\partial F_\alpha}{\partial \underset{\sim}{v}} d\underset{\sim}{v} , \quad (9a)$$

and $p_o(q)$ is the root of

$$\epsilon(\underset{\sim}{q},p) = 0, \tag{9b}$$

corresponding to the high frequency branch. Since the contributions of ions to the high frequency oscillation can be disregarded, we may omit the terms referring to the ions in Eq. (6). Therefore, Eqs. (5c) and (5d) are reduced to the following set of equations:

$$(\frac{\partial}{\partial t} + i\underset{\sim}{k}\cdot\underset{\sim}{v})f_e^{\ell}(\underset{\sim}{k},\underset{\sim}{v};t) = i\frac{e}{m}\varphi^{\ell}(\underset{\sim}{k},t)\underset{\sim}{k}\cdot\frac{\partial F_e}{\partial \underset{\sim}{v}} = C_e(\underset{\sim}{k},\underset{\sim}{v};t) \ , \tag{10a}$$

$$(\frac{\partial}{\partial t} + i\underset{\sim}{k}\cdot\underset{\sim}{v})f_i^{\ell}(\underset{\sim}{k},\underset{\sim}{v};t) + i\frac{e}{m}\varphi^{\ell}(\underset{\sim}{k},t)\underset{\sim}{k}\cdot\frac{\partial F_i}{\partial \underset{\sim}{v}} = 0 \ , \tag{10b}$$

and

$$\varphi^{\ell}(\underset{\sim}{k},t) = \frac{4\pi e}{k^2}(n_e(\underset{\sim}{k},t) - n_i(\underset{\sim}{k},t)) \ , \tag{10c}$$

with the definition of

$$n_\alpha(\underset{\sim}{k};t) = \int f_\alpha(\underset{\sim}{k},\underset{\sim}{v};t)d\underset{\sim}{v} \ . \tag{10d}$$

Eq. (10a) is a kinetic equation of the spatially inhomogeneous system in which the quasilinear feedback effect of the high frequency fluctuation is taken into account.

Characteristic properties of the ion oscillation in the presence of the high frequency fluctuation can be examined by applying the moment approximation for Eqs. (10a), (10b), and (10c). Define the following quantities:

$$\underset{\sim}{j}^{\alpha} = \int \underset{\sim}{v} f_\alpha^{\ell}(\underset{\sim}{k},\underset{\sim}{v},t)d\underset{\sim}{v} \ , \tag{11a}$$

and

$$\langle v_i v_j \rangle^{\alpha} = \int v_i v_j f_{\alpha}^{\ell}(\underset{\sim}{k},\underset{\sim}{v},t)\, d\underset{\sim}{v} \ . \tag{11b}$$

Approximating Eq. (11b) as

$$\langle v_i v_j \rangle^{\alpha} = \delta_{ij} \frac{\varkappa T_{\alpha}}{m_{\alpha}} n_{\alpha} \ , \tag{12}$$

we obtain

$$\frac{\partial^2 n_e}{\partial t^2} + (\omega_e^2 + \frac{\varkappa T_e}{m} k^2) n_e - \omega_e^2 n_i + i\int \underset{\sim}{k}\cdot\underset{\sim}{v} C_e \, d\underset{\sim}{v} = 0 \tag{13a}$$

$$\frac{\partial^2 n_i}{\partial t^2} + (\omega_i^2 + \frac{\varkappa T_i}{M} k^2) n_i - \omega_i^2 n_e = 0 \ . \tag{13b}$$

The last term of Eq. (13a) is calculated as

$$i\int \underset{\sim}{k}\cdot\underset{\sim}{v} C_e(\underset{\sim}{k},\underset{\sim}{v};t)\, d\underset{\sim}{v} = (1/2\pi i)\int e^{st}\{\omega_e^2 \Delta[n_e - n_i] + \Gamma n_e\}\, ds \ , \tag{14}$$

in which $n_{\alpha} = n_{\alpha}(\underset{\sim}{k},s)$, and Δ and Γ are defined as

$$\Delta = \Delta(\underset{\sim}{k},s) = -(\frac{e}{m})^2 \frac{1}{V}\sum_{\underset{\sim}{q}} G_{\infty}(\underset{\sim}{q},p_o) I \frac{\underset{\sim}{k}\cdot(\underset{\sim}{q}-\underset{\sim}{k})}{k^2} [\frac{2\underset{\sim}{q}\cdot(\underset{\sim}{q}-\underset{\sim}{k})}{(\omega_e - is)^3 \omega_e} + \frac{q^2}{(\omega_e - is)^2 \omega_e^3}] \ , \tag{15a}$$

$$\Gamma = \Gamma(\underset{\sim}{k},s) = (\frac{e}{m})^2 \frac{1}{V}\sum_{\underset{\sim}{q}} G_{\infty}(\underset{\sim}{q},p_o) I \frac{\underset{\sim}{q}\cdot(\underset{\sim}{q}-\underset{\sim}{k})}{(\omega_e - is)^2} \ , \tag{15b}$$

in which

$$I = I(\underset{\sim}{q},\underset{\sim}{k};s) = \underset{\sim}{q}\cdot\underset{\sim}{k} - \frac{\omega_e^2}{\epsilon|\underset{\sim}{k}-\underset{\sim}{q}|^2} \{\frac{\underset{\sim}{q}\cdot\underset{\sim}{k}(\underset{\sim}{q}-\underset{\sim}{k})^2}{(\omega_e - is)^2} + \frac{\underset{\sim}{k}\cdot(\underset{\sim}{k}-\underset{\sim}{q})q^2}{\omega_e^2}\} \ , \tag{15c}$$

where $\omega_e = \omega_e(q)$ and $\epsilon = \epsilon(\underset{\sim}{k}-\underset{\sim}{q}, \omega_e(q) - is)$.

In Eqs. (15a) and (15b), $G_\infty(\underset{\sim}{q},p_o(q))$ is the stationary spectrum of the electrostatic potential.

The time behavior of the ion oscillation is determined from the characteristic equation of Eqs. (13a) and (13b),

$$D(\underset{\sim}{k},s) \equiv [s^2+(1+\Delta)\omega_e^2+u_e^2k^2+\Gamma][s^2+\omega_i^2+u_i^2k^2]-(1+\Delta)\omega_e^2 = 0 \ . \tag{16}$$

In order to obtain the roots s(k), Eq. (16) may be reduced to a quadratic in s^2 by disregarding the s-dependence in Δ and Γ. The solutions then are

$$s^{\pm}(k) = \pm i\sqrt{\frac{\omega_i^2(u_e^2k^2+\Gamma(k)+\omega_e^2(1+\Delta(k))u_i^2k^2}{\omega_e^2(1+\Delta(k))+u_e^2+\Gamma(k)}} \tag{17}$$

writing $u_e^2 = \varkappa T_e/m$ and $u_i^2 = \varkappa T_i/M$.

Finally, let us present some results for a special example. According to the recent work of Shapiro for the system composed of a plasma and a monoenergetic beam, the stationary spectrum of the fluctuation energy is determined from the quasilinear kinetic equation as follows:

$$|E_\infty(q)|^2 = 4\pi^3 n_b m(\omega_e^2/q^3)\frac{(\omega_e/q)-v_1}{u_o-v_1} \ , \tag{18}$$

where the range of the wave number q is restricted to

$$(\omega_e/v_2)<q\leq(\omega_e/v_1) = 2k_e\log(n_p/n_e)(u_o/v_T\sqrt{2\pi}) \ , \tag{19}$$

and n_b, n_p are the number density of electrons in the beam and the

plasma, respectively. u_o is the beam velocity directing the Z-axis. v_2 is defined as

$$v_2 = u_o(1+(n_b/n_p)^{1/3}) \ . \tag{20}$$

Since the turbulent spectrum $G_\infty(q,p_o(q))$ can be expressed by the stationary spectrum of the fluctuation energy $|E_\infty(q)|^2$ by a relation

$$G_\infty(q\cdot p_o(q)) = q^{-2}|E_\infty(q)|^2 \ , \tag{21}$$

substituting Eq. (18) into Eqs. (15a) and (15b), we can evaluate the quantities $\Delta(\underset{\sim}{k})$ and $\Gamma(\underset{\sim}{k})$ as follows:

$$\Delta(\underset{\sim}{k},\theta) = -(1/12)(n_b/n_p)(u_o k/\omega_e)^2$$

$$- i\pi(n_b/n_p)\frac{(2\omega_e/k)\cos\theta - v_1}{u_o - v_1}(k_e/k)^2\cos^3\theta \ , \tag{22a}$$

$$\Gamma(\underset{\sim}{k},\theta) = (1/3)(n_b/n_p)(u_o/v_T)^2(1-2\cos^2\theta)k^2V_T^2$$

$$+4\pi i(n_b/n_p)\frac{(2\omega_e/k)\cos\theta - v_1}{u_o - v_1}(k_e/k)^2(1-2\cos^2\theta)\omega_e^2 \ , \tag{22b}$$

where θ is the angle between the wave vector $\underset{\sim}{k}$ and the Z-axis. Substituting Eqs. (22a) and (22b) into Eq. (17), we obtain the following approximate expressions:

$$s^{\pm}(k) = \pm iV_a k \pm 2\pi(\omega_i^2/V_a k)(n_b/n_p)(1-2\cos^2\theta)\frac{(2\omega_e/k)\cos\theta - v_1}{u_o - v_1}(k_e/k)^2 \ , \tag{23}$$

where the phase velocity V_a is given as

$$V_a^2 = [1+(1/3)(n_b/n_p)(u_o/v_T)^2(1-2\cos^2\theta)]u_e^2+u_i^2 \quad . \qquad (24)$$

The terms proportional to (n_b/n_p) represent the effect of the high frequency turbulent fluctuation. Since the time behavior of the ion oscillation is determined to be varying as $\exp\{s^{\pm}t\}$, we can conclude that if $\theta < \pi/4$, the + mode grows in time while the - mode does so when $\theta > \pi/4$. This type of instability is different from the ordinary instability, because the system is always unstable for the low frequency acoustic oscillation regardless of the sign of the real part of Eq. (23). In Fig. 7.8 and Fig. 7.9 we illustrate some numerical examples for the given plasma-beam parameters.

As a conclusion, we emphasize that the present investigation has revealed remarkable aspects of the quasilinear feedback effect of the high frequency fluctuation. Namely, although the feedback effect of the high frequency fluctuation acts to stabilize the spatially uniform system, the same effect acting on the spatially inhomogeneous system gives rise to a parametric instability.

Y. H. Ichikawa

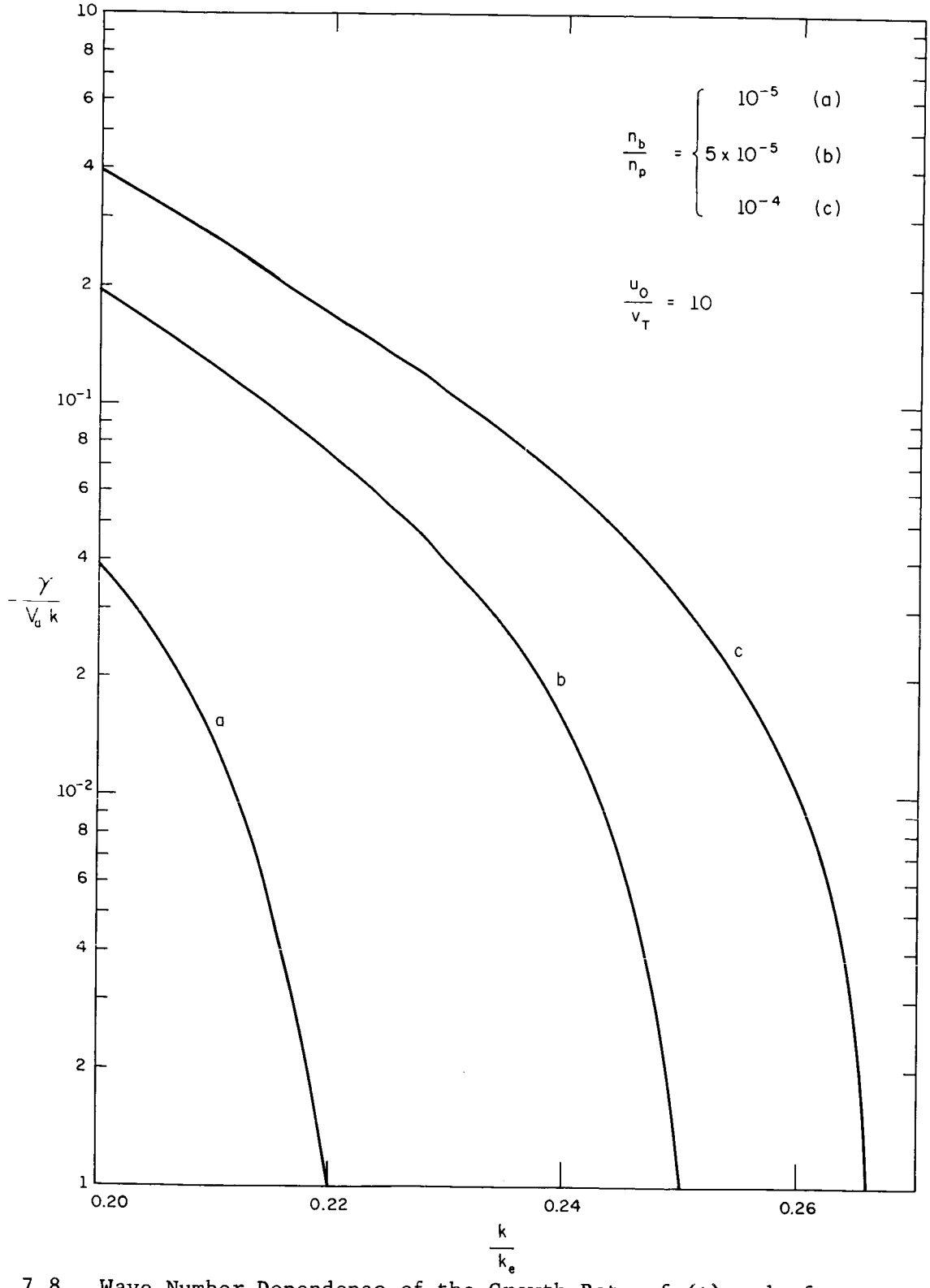

Fig. 7.8. Wave Number Dependence of the Growth Rate of (+)-mode for the Angle $\theta = 0$. The growth rate is equal to 0 for $k < 0.2\ k_e$.

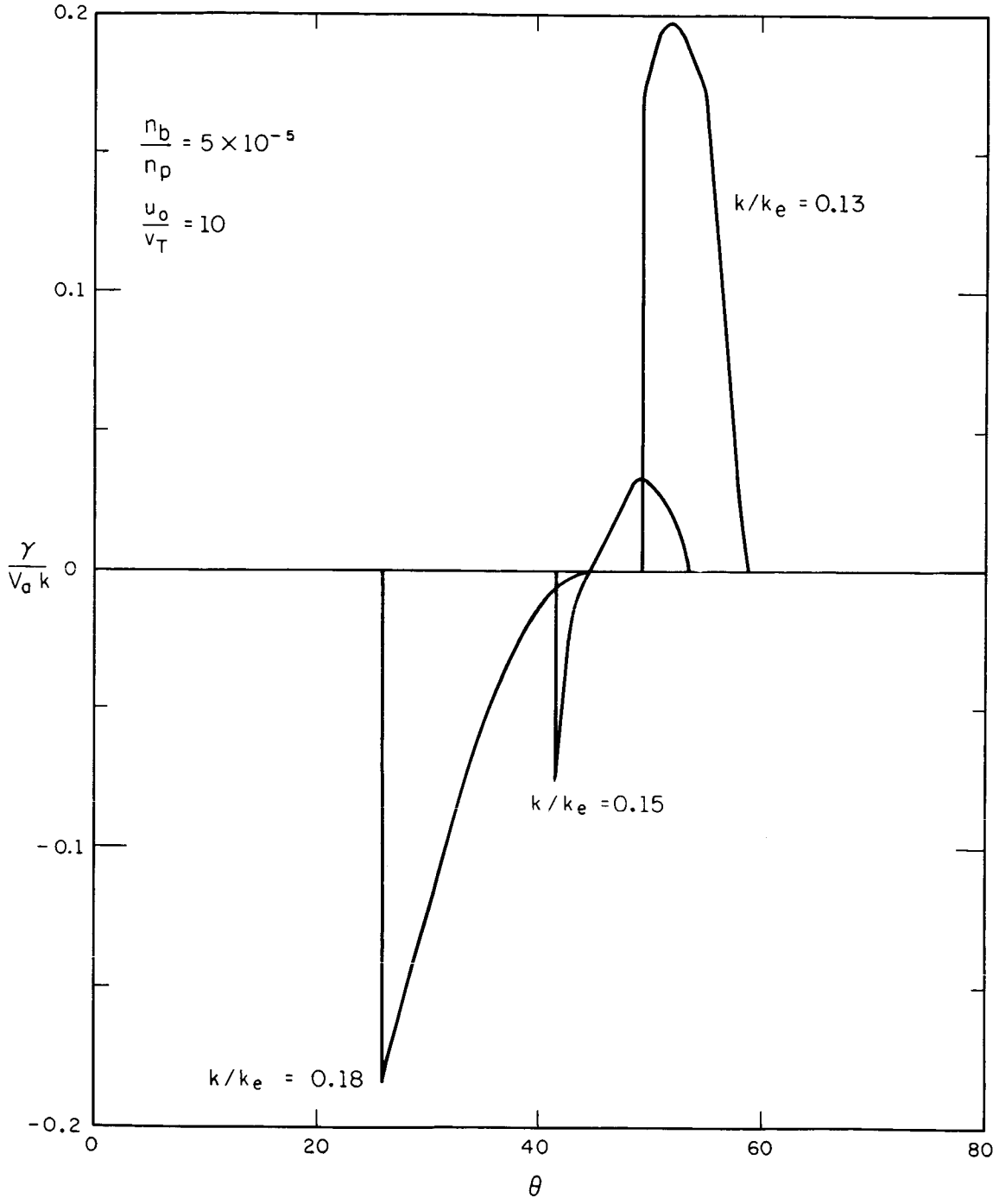

Fig. 7.9. Angular Dependence of the Growth Rate for Several Values of the Wave Number k.

8. SUPERCONDUCTIVITY STUDIES

C. B. Satterthwaite
J. O. Kopplin
M G. Craford*
J. R. Carlson
B. K. Moore
I. Toepke
C. Barnett**
R. P. Ries
D. Gutman

8.1 Introduction

The work of this group included (a) studies of thin-film superconductors and effects in superconductors observable by thin-film techniques (in collaboration with its Thin-Film Group), (b) studies of type-II superconductors, and (c) a device application of superconductors.

8.2 Thermal Conductivity of Vanadium

A study of the thermal conductivity of vanadium in the normal, mixed, and superconducting states has been started. Both axial and transverse magnetic fields will be used. A one kilogauss, liquid nitrogen cooled, long solenoid was designed and wound to provide the axial field. A power supply and controller were also designed and built. At the present time, construction of the actual apparatus is nearly complete, and work is being started on the associated systems--vacuum, temperature control, and thermometry. The work is to be conducted between 1° and $5^{\circ}K$; the low temperature will be obtained by pumping on a liquid He^4 pot. A promising single crystal of vanadium

*Also associated with the Thin Film Group.

**U. S. Navy. Assigned to group for thesis research.

has been obtained, and residual resistivity measurements have been made. Magnetization measurements are to be made, as well. The actual thermal conductivity sample will be about 2" long and 1/8" in diameter and will be cut from this crystal by spark erosion machining.

B. K. Moore

8.3 Microwaves from the ac Josephson Effect in Superconducting Shorts

Attempts have been made to detect microwave radiation from a number of superconducting shorts of various geometries, using a superheterodyne detector and the cryogenic apparatus described in the previous progress report. The sensitivity of the detector in the frequency range where radiation was expected was the order of 10^{-13} watts. No radiation was detected.

New techniques including photoetching are being used to make shorts of more ideal geometry. Hopefully, one would obtain shorts whose effective length (i.e., the length over which the voltage drop occurs) is equal to or less than the superconducting coherence length of about 10^{-4} cm. Also, shorts will be tested to see if their I-V characteristics show a coupling of an externally applied microwave field with the ac Josephson currents in the short as observed by Anderson and Dayem.[1]

J. R. Carlson

---

[1] P. W. Anderson and A. H. Dayem, Phys. Rev. Letters 13, 195 (1964).

8.4 Flux Flow in Type-II Superconductors

During the previous quarter an experimental investigation was started of flux flow in type-II superconductors. It has been postulated that the apparent resistive behavior of type-II superconductors in magnetic fields between He_1 and He_2 results from a viscous flow of magnetic flux transverse to the current.[2] The motion of quantized flux lines resulting from the Lorentz force due to the current is thought to be the source of the voltage drop.

An experiment was carried out to try to observe a voltage developed in a normal metal in close proximity to the superconductor, but electrically isolated from it. A thin foil of niobium (which is a type-II superconductor) and a foil of copper were separated by a thin insulating layer. These were immersed in liquid helium with a magnetic field applied perpendicular to the foils. Current through the niobium was increased and the voltage was monitored across both the Nb and the Cu.

A voltage was observed in the copper as the current in the niobium was increased which was proportional to the rate of change of current, indicating close inductive coupling. No voltage was observed in the copper with a steady current flowing in the niobium even at currents sufficiently large to render the niobium resistive.

---

[2] e.g., Kim, Hempstead, and Strand, Phys. Rev. 139A, 1163 (1965); Bardeen and Stephen (to be published).

One would conclude from this experiment that, if flux flow occurred in the Nb in the steady state, either it did not couple with the copper, or voltages were induced in the external measuring circuit that just canceled the voltage induced in the copper foil.

Other experiments of a different nature are anticipated to detect flux flow.

I. Toepke

8.5 Superconducting Parametric Amplifier (Picovoltmeter)

The second version of the picovoltmeter has been finished and is presently being tested. Spurious electrical and mechanical couplings between the ac drive circuits and the sensitive input circuitry are being measured, and reduced or eliminated where possible. Coupling via ac electromagnetic fields has been effectively eliminated by a set of magnetic and superconducting shields. A remaining source of noise, not yet identified, but apparently associated with vibration of the pickup coil is sufficiently large at present to limit sensitivity to about 1×10^{-11} V in 10^{-5} Ohm. Study of this noise source has been hampered somewhat by the irreproducible behavior of the miniature loudspeakers used to provide vibration of the input coil. The speakers do not cycle well over the range from room temperature to 4.2°K. Although the speakers usually have good properties for this purpose at 4.2°K, lack of reproducibility from one run to the next presents difficulties, and a good high-sensitivity run has yet to be accomplished.

The main source of difficulty appears to be the glues used to cement the cones into the speaker frame.

Analysis of the amplifier has continued. Stability of the amplifier when incorporated in various feedback circuits--in particular, those used for percise voltage or flux measurements--has been studied. Under proper conditions, sufficient feedback to provide accuracies of .01 per cent or better may be used without creating system instability in voltage measurements.

R. P. Ries

8.6 Penetration Depth of Magnetic Fields in Superconductors

The occurrence of ac Josephson tunneling current in Nb-NbO-In and Nb-NbO-Sn junctions has been reported in earlier progress reports. The present investigations are intended to obtain accurate measurements of the change in penetration depth as a function of temperature, magnetic field, and material using the ac Josephson current[3] on specimens of known and reproducible geometry.

An accurately-machined film-evaporation mask and switchable-sample holder were prepared such that eight identical junctions can be made and four tested on each run. Several supposedly identical junctions have been tested. Unfortunately, results are usually quite different for each of the eight junctions.

---

[3] It can be shown that the voltage at which an ac tunneling peak occurs in such a junction is proportional to $\sqrt{[\tau/(\lambda_1+\lambda_2+\tau)]}$, where τ is the oxide thickness and λ_1 and λ_2 penetration depth in the junction materials.

At the present time, only one junction has demostrated the desired structure well enough to provide data. The scatter in these data was large enough to prevent precise comparison with theoretical curves.

Further effort will be made to obtain and measure suitable junctions and reduce experimental scatter by statistical methods and/or reduction of thermal noise in the apparatus.

C. Barnett
D. Gutmann

8.7 Superconductive Tunneling in High Purity Single Crystal Niobium

We are attempting to measure the anisotropy of the superconducting energy gap in niobium using superconducting tunneling. The tunnel-junctions have been made on the 100, 110, and 111 crystalline faces of very high purity niobium single crystal (resistivity ratio, $R_{300}/R_{4.2} \approx 300$).

The junctions were made by orientating the crystal, using x-ray techniques, and cutting off 50 mil slabs parallel to the three crystalline planes. The surface of each slab was lapped, electropolished, and cleaned by outgassing in high vacuum. A thin oxide layer was then grown, and an indium film was evaporated on top of this oxide to form the other half of the tunneling junction.

The superconducting energy gap can be determined by measuring the dc-current-vs-voltage curve of the junction. The energy gap is expected to be anisotropic, giving rise to different niobium gaps for

junctions made on slabs of different orientation. Preliminary measurements indicate that the anisotropy, if detectable, will be less than 1 per cent.

There are specific heat data[4] which indicate that there are two superconducting energy gaps present in high-purity niobium. Preliminary attempts have also been made to detect this second gap, using tunneling. At this time, no indication of the second gap has been observed.

M. G. Craford

8.8 Crystallization of Nb_3SN

Work on this project during the past report period has been limited to the chemical analysis of the Nb-Sn solution from which Nb_3Sn crystals have been grown. The primary objective in this analysis has been the determination of the amount of niobium in solution with the tin in the crystal-growing temperature region of 1200°C. Several analytical methods have been investigated in this study, with recent attention being given to atomic absorption and flame-emission spectroscopy. Rather extensive work with flame-emission spectroscopy has shown the method to be accurate, with the data being reliable and reproducible, as far as the sample solutions are concerned. These sample solutions were prepared by dissolving the 0.2 to 0.5 gram solid

[4] Phys. Rev. Letters 14, 1025 (1965).

samples, withdrawn from the crystal-growing furnace, in 1:1 HF:HNO_3 and then diluting to 50 ml. Results indicate that the percentage of niobium in solution with the tin, in the temperature range of interest, is of the order of 1.5 per cent. Checks on the analysis procedure indicate accuracy of the order of $\pm$0.02 per cent with respect to the percentage of niobium; however, variation in the results of several tenths of a percent have been found. This seems to suggest the possibility of segregation in the sample, upon cooling and solidification at the time it is withdrawn from the furnace, or more extensive non-uniformity in the composition of the Nb-Sn solution in the furnace than was previously suspected. Attention is currently being given to the process of withdrawing the samples from the furnace to see if the above inconsistencies can be eliminated. The chemical analysis has been carried out by A. Karim Shallal, graduate student in chemistry and summer employee of the laboratory.

J. O. Kopplin

9. HIGH VOLTAGE BREAKDOWN

E. M. Lyman
D. A. Lee
T. Casale
J. Meyer
K. Brown

9.1 Effect of Gas in Conditioning Tungsten Electrodes: Current Suppression

The well-known phenomenon of current suppression and conditioning by means of low-pressure gas has been studied in the previously-described broad-area electrode system with single-crystal tungsten disks 3.5 cm in diameter spaced 0.7 mm apart. Two types of observations were made: 1) The voltage between the electrodes was held constant at about 75 per cent of the vacuum breakdown voltage while argon was rapidly admitted, raising the pressure from 4×10^{-10} to 10^{-3} Torr. The field emission current initially doubled, then during a period of half an hour dropped to about 1/30 of the initial high-vacuum value. 2) With argon in the system at a pressure of 10^{-3} Torr, the interelectrode voltage required to hold the emission at 100 μA was recorded. During a period of a few minutes to a few hours depending on the previous history, the voltage rose to 2 or 3 times the initial high-vacuum value. Both of these results are consistent with the picture of blunting the emitter tips at the cathode by sputtering.

Fowler-Nordheim plots of log i/V^2 vs. $1/V$ obtained at high vacuum, before and after the above conditioning, showed that the field enhancement factor β had been reduced by the sputtering. On the other hand, breakdown voltage measurements, before and after, showed that

the breakdown voltage had been increased by a factor of from 2 to 3. The product of the enhancement factor, β, with the average electric field, V/d, gives the critical field F_c for initiation of breakdown at the emitter tips. This was found to be a constant, $(6.5\pm1)\times10^7$ volts/cm, in agreement with previous observations.

9.2 Field-Emission Microscope Studies

The major effort has been in the development of single-crystal tungsten emitter tips and high-resolution screens. Tips with radii of 1000 Å have been fabricated by etching a 10 mil wire down to 1 mil in molten $NaNO_2$ then electropolishing it in 2N NaOH to remove the etch pits. When these tips were used in conjunction with a zinc orthosilicate screen, dusted on to a transparent stannic oxide coating on pyrex, a stable threshold voltage of 800 volts for a visible pattern was obtained. After flashing such a tip for a few seconds at 2100°C to drive off the adsorbed oxygen, a clean pattern corresponding to a single-crystal tungsten was obtained. Some qualitative observations of the patterns were made; the Fowler-Nordheim plots were straight lines, and reproducible.

E. M. Lyman

10. THIN FILMS

R. N. Peacock
M. G. Craford
J. T. Jacobs

K. G. Aubuchon
W. P. Bleha
T. A. O'Meara

10.1 Size Effects in Thin Films

Several vacuum leaks in the system to be used for preliminary experiments with size effects have made it impossible to obtain data during this quarter. Consideration of the theory and experimental background of the size-effect problem has occupied considerable time, as has work with the experiment. Many of the vacuum leaks have been in heli-arc welded joints. No piece has survived as much as one bake-out. While continuing to work with this apparatus, which did perform properly a year ago, another and more advanced arrangement is being built using components on hand or to be made in the Coordinated Science Laboratory shop. Less time will be lost should it not be possible to make the first vacuum system perform properly. The new system will use sorption roughing, ion pumping for normal running, and eventually cryo-pumping for maintaining a low pressure during the actual film depositions. The ion pumps can be small since they never handle a large load. A 15 ℓ/sec ion pump is used outside the baked portion. A bakeable 1-1/2 inch valve can be used to isolate it. Another 10 ℓ/sec ion pump inside the oven region maintains the vacuum after bakeout.

Initial tests of this system without the cryopump have given static pressures in the low 10^{-9} Torr range. And when the cryopump is complete, and in use, it is hoped that pressures of this sort can be maintained during an actual evaporation.

The cryopump, for which the drawings are now in the shop, has been designed for simple assembly. This is made possible by the use of modified Swage-Lok fittings in the support tubes for the liquid-nitrogen and liquid-helium reserviors. The value of this feature is evident when the large number of brazed and welded joints in the assembly is considered, with their corresponding possibilities of developing leaks.

Some form of film-thickness monitor useable in a baked ultra-high-vacuum system will be necessary for this program. The work on an ionization-gauge type of monitor described later in this section may prove useful.

J. T. Jacobs

10.2 Hall Effect Measurements on Films

During this quarter, a bakeable stainless-steel vacuum system has been constructed for the purpose of making Hall measurements on evaporated films. Contrary to those measurements reported previously, the deposition and subsequent Hall measurements will be done without

removing the film from the vacuum system. This will be made possible by the use of a magnetically coupled linear-motion feedthrough to move the sample into an appendage of the chamber situated between the poles of an electromagnet.

The equipment consists of a 4" NRC low-backstreaming diffusion pump, a 4" Granville-Phillips cold trap, and a chamber made from a section of 6" diameter stainless-steel tubing flanged at both ends and provided with eight 2-3/4" flanged ports for feedthroughs, gauges, and so on. In this condition, the system may be baked out at temperatures above 400°C. A stainless-steel gate valve using Viton gaskets has been obtained for use between the cold trap and chamber, when vacuum requirements are not so strict, and the bakeout temperature can be moderate. Using the valve, a pressure of 2×10^{-8} Torr was noted after the first bakeout at 190°C.

The commercial linear-motion feedthrough is expected to arrive shortly. A substrate holder, which must provide for temperature control and electrical connections, is under construction. When these are available the system will be completed and the experiments can start.

K. G. Aubuchon

10.3 Ionization Gauge Evaporation Rate Monitor

In the formation of thin films, the deposition rate is an important structure-determining parameter. For most applications it is necessary to know film thickness. Commonly used methods of

monitoring the deposition rate or total accumulated thickness of a film still in the vacuum include the quartz-crystal oscillator,[1] mechanical torsion systems,[2,3] and ionization gauges.[4,5] It is this latter method which is reported on here.

The ionization-gauge technique is useful for conditions where the operation of the quartz-crystal oscillator is not stable because of heat radiated from the vapor source. After deposition of a moderately thick film, the crystals may also stop oscillating completely. Since an ionization gauge can easily be made bakeable, the method is compatible with UHV. The greatest problem is distinguishing between the ion current resulting from the presence of residual gas in the system, and the ion current resulting from the desired ionization of the vapor stream. This situation results because the ambient gas pressure does not remain constant during a typical evaporation. Some of the theory of the ionization method, and especially the dependence of the

---

[1] Behrndt and Love in 1960 Seventh National Symposium on Vacuum Technology Transactions, C. R. Meissner, editor (Pergamon Press, 1961), p. 87.

[2] Mayer, Schroen and Stünkel, op. cit., p. 280.

[3] C. A. Neugebauer, J. Appl. Phys. 35, 3599 (1964).

[4] H. Schwarz, Rev. Sci. Instr. 32, 194 (1961).

[5] M. Perkins in 1961 Eighth National Symposium on Vacuum Technology Transactions, vol. 2, L. E. Preuss, editor (Pergamon Press, 1962), p. 1025.

ionization-gauge reading on the temperature of the "molecular beam" is given by Schwarz in Ref. 4. The ion current at constant deposition rate is proportional to $T^{-\frac{1}{2}}$.

Schwarz used a single gauge with a beam chopper to obtain both the background and beam values. Since a self-contained mechanical shutter system, bakeable at 450°C under vacuum, was not considered practical, it was chosen here to use two similar gauges, with one shielded from the evaporant beam. By placing the shielded gauge near the unshielded one, the outgassing effects of the evaporation source were assumed to cause equal effects in both. It was found that the gauges helped to decide when the charge had outgassed sufficiently to permit deposition of a pure film, since in their location they responded much better to outgassing than does a gauge located at a distant point.

For the usual deposition rates of 1 to 100 Å/sec, the equivalent pressure of the beam at the substrate is of the order of 10^{-6} to 10^{-4} Torr. Standard Alpert-type gauges may be used in this range, and were by Perkins[5] and by Brownell, et al.[6] For compactness, and for use with high beam densities where the normal gauges are nonlinear, a new gauge design shown in Fig. 10.1 was used. This design also has the advantage of shielding both filaments from the evaporant for greater stability of emission, and longer filament life. The gauge constant for air was about 10 Torr^{-1}.

---

[6] Brownell, et al., Rev. Sci. Instr. 35, 1147 (1964).

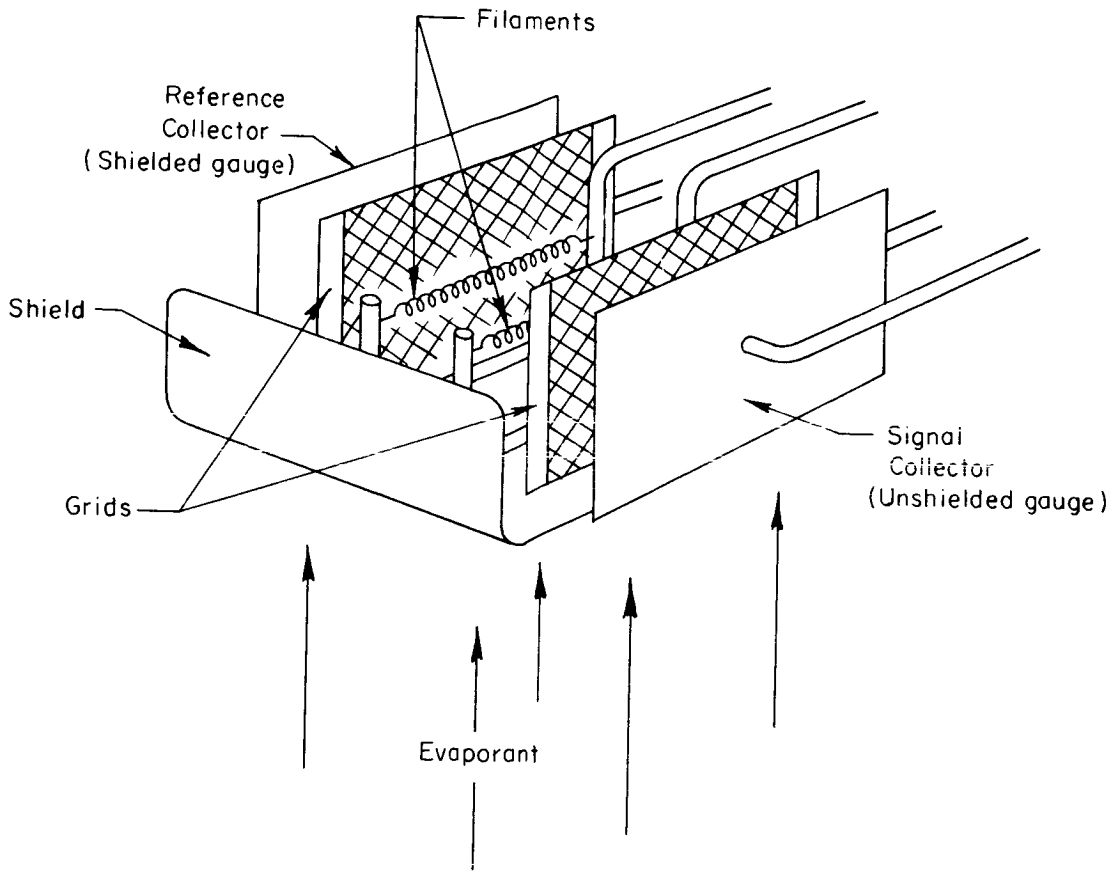

Fig. 10.1. Evaporation Rate Monitor.

In operation, an emission current of 2 mA was convenient. When used in a vacuum system having a residual pressure of 10^{-6} Torr, evaporation rates as low as 0.5 Å/sec could be determined for gold. The detection of small evaporation rates for more reactive metals such as copper and titanium was disturbed by the gettering action of films of these materials which caused sudden changes in pressure. It was also found necessary to calibrate the gauge for each evaporant. For the above work two Varian model 971-0003 ionization-gauge supplies were used to operate the monitor, and the difference of the output signals was plotted on a strip-chart recorder.

Presently a circuit is being prepared which will use the output signals to control the source temperature and thus maintain a constant evaporation rate.

W. P. Bleha

11. COMPUTER OPERATIONS

H. G. Slottow
C. Arnold
G. Crawford
L. Hedges
J. Knoke
V. Metze
R. Nash
E. Neff
J. Stifle

11.1 Introduction

This group is responsible for the development and maintenance of the CSL computing facility.

11.2 CSX-1 Computer

11.2.1 Operations.

Period: 22 June 1965 to 1 September 1965

Total Running Time:		1699.3 hours
Average Per Day (7 day week):		23.9 hours
Operational Time:	100%	1699.3 hours
Scheduled Maintenance Time:	0%	0.0 hours
Emergency Maintenance Time:	0%	0.0 hours

L. Hedges

11.3 CDC 1604 Computer

11.3.1 Operations.

Period: June 1 to August 31, 1965

Total Running Time:		1210.60 hours
Average Per Day (7 day week):		13.16 hours
Operational Time:	94.61%	1145.35 hours
Preventive Maintenance Time:	3.37%	40.75 hours

Engineering Time: 2.02% 24.50 hours

Emergency Maintenance Time: 0.00% 0.00 hours

E. Neff

11.3.2 Systems Programming. A systems-output subroutine for graph and alphanumeric output to oscilloscope is near completion. Alphanumeric output will be controlled by FORTRAN-format statements. Graphs will be plotted from coordinated lists, and the program features include automatic scaling, options for axis and hash-mark plotting, and fixed- or floating-point data. Maximum flexibility is maintained by a calling sequence capable of changing any of the more than twelve basic parameters and operating modes.

The new assembler for the 1604 system has been completed and has performed properly on a series of short test programs. It will now be made available to the laboratory staff for extensive tests on actual research programs.

C. Arnold
R. Nash

12. SWITCHING SYSTEMS

S. Seshu
E. Manning
A. McKellar
G. Metze

R. Marlett
S. C. Chang
G. Martens
D. Crockett
W. J. Bouknight

12.1 Computer Compiler†

The preliminary investigation of the theoretical feasibility has been completed. A report on the preliminary investigation has been issued as R-264. The implementation of these concepts as a pair of compilers is in progress.

S. Seshu
G. Metze

12.2 Switching Circuits†

It was shown that there does not exist a non-trivial sequential machine with a speed-independent asynchronous linear realization. It was further shown that any sequential machine has a quasi-linear asynchronous realization. These results have been issued as R-258.

A. McKellar

12.3 Self-Diagnosis†

The experimental investigation of the self-diagnosis of the CSX-1 computer has been completed and has been issued as R-259.

E. Manning

†Portions of this work were supported by the National Science Foundation under Grant NSF GK-36.

12.4 Active Realizations of State Models‡

A procedure has been developed for realizing the state equations

$$\dot{\underset{\sim}{x}} = A\underset{\sim}{x} + B\underset{\sim}{u}$$

$$\underset{\sim}{y} = C\underset{\sim}{x} + D\underset{\sim}{u}$$

as an RC network plus voltage-dependent current sources.

Alternatively a realization as an RLC network plus voltage-dependent current and voltage sources plus current-dependent current and voltage sources can be obtained.

G. Martens

12.5 Behavior of Sequential Machines under Failure†

Two-stage "AND-OR" realizations are currently being studied from the point of view of failure. Strong connectedness, totally sequential behavior and oscillations are topics of interest in this study.

S. C. Chang

12.6 Computer Self-Diagnosis†

Procedures for finding checkout sequences for computers are being considered whose validity can be determined without simulation

†Portions of this work were supported by the National Science Foundation under Grant NSF GK-36.

‡Portions of this work were supported by the Air Force Office of Scientific Research under Grant No. AFOSR 931.65.

or even a detailed knowledge of the computer to be tested. The fundamental notion involved is that all nonredundant failures must manifest themselves in some observable way. The problem is to be able to enumerate the effects of all failures. The ultimate goal is to obtain computer design principles which allow checkout sequences for the entire computer to be obtained algorithmically.

R. Marlett

12.7 Synthesis†

A new investigation has been started on an extension of A. McKellar's synthesis procedure for switching circuits.

D. Crockett

12.8 System Evaluation†

A study has been started to evaluate computer system designs, with respect to timing, blocking, and saturation, by simulation techniques.

W. J. Bouknight

†Portions of this work were supported by the National Science Foundation under Grant NSF GK-36.

13. NETWORKS AND COMMUNICATION NETS

M. E. Van Valkenburg
W. Mayeda
T. Kamae
G. Kishi**
J. Numata
K. Onaga
J. A. Resh
R. A. Rohrer*
G. A. Stumpff
M. Takagi**
T. M. Trick
N. Wax

13.1 Multiparameter Sensitivity Considerations in Network Synthesis†

A new definition of multiparameter sensitivity has been found which simplifies comparison of networks with respect to multiparameter sensitivity (the change in transmission due to incremental changes in all network elements). New non-series-parallel structures have been studied in comparison to latter networks, and it has been shown that the new network structures always have smaller values of multiparameter sensitivity than two classes of equivalent ladder networks. Synthesis procedures have been outlined for the determination of the non-series-parallel networks.

S. C. Lee
M. E. Van Valkenburg

13.2 Relatively Optimum Flow†

Suppose flow $\psi_{ij}(G)$ is a maximum flow from vertex i to vertex j in a communication net G. Let $\psi_{ij}(e)$ be a flow which is

---

*On leave.

**Visiting.

†Portions of this work were supported by the Air Force Office of Scientific Research under Grant No. AFOSR 931.65.

assigned to edge e when flow $\psi_{ij}(G)$ is assigned to G. Then we say that $\psi_{ij}(G)$ is a relatively optimum flow if there exists no maximum flow $\psi'_{ij}(G)$ from i to j such that every edge flow $\psi'_{ij}(e)$ satisfies

$$\psi'_{ij}(e) \leq \psi_{ij}(e)$$

and for at least one edge in G, inequality in the above equation holds.

We have discovered an interesting property concerning relatively optimum flows; that is, if $\psi_{ij}(G)$ is a relatively optimum flow, then there exists a set of v-1 independent cutsets of G (where v is the number of vertices in G) called a set of M cutsets such that path P^r_{ij} of every path flow $\psi(P^r_{ij})$, where $\Sigma_r \psi(P^r_{ij}) = \psi_{ij}(G)$, passes through each cutset in the set exactly once. This property permits us to assign a relatively optimum flow $\psi_{ij}(G)$ by knowing a set of M cutsets. A method of obtaining a set of M cutsets is also found.

Among these relatively optimum flows $\psi_{ij}(G)$, there exists at least one flow such that the summation of every edge flow is minimum. Such a flow is called an absolutely optimum flow. To obtain such a flow for a communication net is an important problem for future study. Details concerning relatively optimum flows will be published as a report soon.

W. Mayeda
M. E. Van Valkenburg

13.3 Frequency of Edge Occurrence in a Set of Paths of a Complete Graph

Given a complete, non-orientated graph G with n nodes and two specified distinct nodes, i and j, the question is asked, "How many times does a given edge appear in the formation of all paths between i and j?"

By decomposing G into two subgraphs, G_1 containing nodes i and j, and G_2 containing the remaining nodes, by symmetry it is clear that the answer involves three cases:

1. the edge directly connecting i and j is used just once;
2. any edge a connecting G_1 and G_2 is used a fixed number, say P_a times;
3. any edge b contained wholly in G_2 is used a fixed number, say P_b times.

The task of obtaining expressions for P_a and P_b is essentially a counting problem which can be handled by use of combinatorial analysis.[1] Using Feller's notation (e.g., $(n-2)_k = (n-2)(n-3)\cdots(n-k-1)$ for k a positive integer and $n > 2$; and for $k = 0$, $(n-2)_k \equiv 0$), the total number of paths from i to j is

$$P = \sum_{k=1}^{n-1} (n-2)_{k-1}$$

for $n > 2$, and where k = path length.

---

[1] William Feller, An Introduction to Probability Theory and Its Applications, vol. 1 (John Wiley & Sons, Inc., 1957), pp. 26-61.

Subtracting the expression for the total number of paths from i to j which do not contain edge a yields after simplifying

$$P_a = \frac{P-1}{n-2} , \quad n > 2 .$$

The expression

$$P_b = 2\left[\sum_{k=4}^{n-1} (k-2)(n-4)_{k-3}+1\right] , \quad n > 4 ,$$

is clearly not quite so simple and involves more calculation.

Since k in the above expression represents path length, each term of the summation represents the number of times the given edge is used to form paths from i to j of length k.

G. Stumpff

13.4 Stochastic Flow and its Efficient Transmission Through Communication Nets

As demonstrated by such applications as service for telephone calls, telephone messages, and customers at a supermarket, the generation of information or service demands, and the time required for services are, in general, of a stochastic nature. Stochastic flow of such messages or service demands "through" nets. So far, the study of communication nets has been mainly focused on steady (or nonstochastic) flow. In the study of stochastic systems, average properties are first considered. By considering average flow, we can reduce the properties of stochastic (or unsteady) flow to these of steady flow; there are

many differences that are evident at a closer look. As a concrete example, we take digital transmission of information through store-and-forward communication nets.

The inter-arrival times of messages (or symbols) at a station are exponentially distributed with an average rate of λ messages per second, customarily referred to as a Poisson input. The message (or symbol) lengths are also exponentially distributed with average length of $1/\mu$ bits per message (or symbol) exponential service time. The channel capacity is measured in bits per second. Since arrivals of messages at each station are not steady without storage, there is a positive probability with which the station is overflooded by incoming messages. With provision of storage at each station, the message can wait for transmission as long as necessary. (A waiting line or queue is formed in front of each channel.) We assume that transmission is performed by a first-come first-served basis and that storage capacity is unlimited. At each station a message is received in a form of perforated tapes; it is checked for possible errors, and is joined to a proper queue for retransmission if there is no error. The message (or symbol) is coded in such a way that error can be detected. Whenever errors are detected, retransmission is requested from the sending station immediately after message reception. It is clear why such a system is called a store-and-forward net.

Properties of waiting lines of stochastic service systems have been extensively investigated in the case of single-channel systems and important results are readily available, but little has been done

for multi-channel systems because of mathematical complexity. Difficulty arises from a fact that inter-arrival time statistics and service time statistics are no longer independent for intermediate (relay) stations while the queuing theory customarily assumes their independence.

We have studied the nature of information flow from a certain station to another station through the net. We adapt the independent assumption of said statistics for every station. The independent assumption coupled with Burke's Theorem that the output of a queue is also Poisson if the input is Poisson, enable us to consider each channel separately. The quality of a given flow ψ or performance of the net with given flow ψ is measured by average time delay per message $D(\psi)$, operation cost per message $K(\psi)$, and utility of channels $E(\psi)$ in case of noisy nets. In general, the performance index $P(\psi)$ of flow ψ is given by

$$P(\psi) = \alpha \cdot D(\psi) + \beta \cdot K(\psi) + \lambda \cdot E(\psi)$$

$$\alpha + \beta + \lambda = 1$$

$$\alpha, \beta, \lambda \geq 0 \ .$$

An efficient way of information transmission through net is to minimize $P(\psi)$ over all possible flows with the fixed average receiving flow value. It turns out that average behavior of stochastic flow through store-and-forward communication nets is equivalent to behavior of steady flow through lossy communication nets. According to study of lossy nets,

a minimization technique of $E(\psi)$ is a minimum-path type and so are those for $D(\psi)$ and $K(\psi)$. Hence, the performance index $P(\psi)$ can be minimized by a composite technique of minimum-path types.

K. Onaga

13.5 Analysis of Lossy Communication Nets by Modified Incidence Matrices†

A paper of this title has been accepted for presentation at the Third Allerton Conference on Circuit and System Theory, October 20-22, 1965, and for publication in the Conference Proceedings. This paper introduces two incidence matrices for a lossy net. One of the new incidence matrices A_α differs from the usual incidence matrix A of a directed graph only in that all -1 entries are replaced by $-\alpha_j$'s; the other, $A_{1/\alpha}$ differs from A only in that all +1 entries are replaced by $+1/\alpha_j$'s, where α_j is the branch flow efficiency of branch j and is defined by the relation

$$f_j = \alpha_j f^j$$

where f_j and f^j are the receiving and sending flows of branch j, respectively. Obviously, the new incidence matrices A_α and $A_{1/\alpha}$ contain the usual incidence matrix A as a special case ($\alpha_j = 1$). The use of A_α or $A_{1/\alpha}$ has made it possible to describe a lossy net in matrix

†Portions of this work were supported by the Air Force Office of Scientific Research under Grant No. AFOSR 931.65.

form and to obtain the approximate maximum flows between two vertices of a lossy communication net. Details will appear in a CSL report.

T. Murata

13.6 Modified Unistor Graph

Modified unistors have been defined. For example, the transconductance of a vacuum tube is expressed by one modified unistor. A M.U. graph (modified unistor graph) is a linear graph consisting of modified unistors and can represent a linear electrical network. An example of the evaluation of vertex potentials by M.U. graph is offered in the report. Also, the report includes the proof of Mason's formula for signal flow graphs using M.U. graphs.

J. Numata

13.7 On Cascaded Symmetric LC Ladder Networks with Resistive Termination†

In his recent paper, Kawakami[2] of Tokyo Institute of Technology attempted to obtain the necessary and sufficient condition that a given rational function of s be the inverse voltage-transfer function of a cascaded symmetric or anti-symmetric LC ladder network with resistive termination. It appears that his proof may not give the correct sufficiency conditions.

†Portions of this work were supported by the Air Force Office of Scientific Research under Grant No. AFOSR 931.65.

[2]M. Kawakami, "The Necessary and Sufficient Condition for a Network to be Composed of Symmetric or Anti-Symmetric Sub-Networks," Reports of IECEJ, December, 1964 (published in Japanese).

The inverse voltage-transfer function of a resistively terminated LC ladder network can be expressed as

$$S(s) = \frac{\prod_j (s+\mu_j) \prod_k (s^2+2\nu_k s+\nu_k{}^2+\tau_k{}^2)}{\prod_i (s^2+\lambda_i{}^2)} , \qquad (1)$$

where λ_i corresponds to a transmission zero of the network.

Suppose that

$$F_{2k+1} = \begin{bmatrix} A^{2k+1} & B^{2k+1} \\ C^{2k+1} & D^{2k+1} \end{bmatrix}$$

is the ABCD-matrix of a section of a simple ladder network of 2k+1 elements. Then one has

$$C^{2k+1} = C^{2k-1}(1+Z_{2k}Y_{2k+1}) + D^{2k-1}Y_{2k+1} ,$$

$$D^{2k+1} = C^{2k-1}Z_{2k} + D^{2k-1} .$$

Let R_1 and R_2 be the resistive termination of the network. A symmetric network is composed of two networks in cascade described by ABCD matrices of

$$\begin{bmatrix} A(s) & f_1(s)R_1 \\ f_2(s)/R_1 & D(s) \end{bmatrix} \quad \text{and} \quad \begin{bmatrix} D(s) & f_1(s)R_2 \\ f_2(s)/R_2 & A(s) \end{bmatrix} .$$

Then, S(s) in Equation (1) is

$$S(s) = R_1 \frac{I_1}{V_2} = (1 + \frac{R_1}{R_2}) f_2(s) D(s)$$

$$= (1 + \frac{R_1}{R_2}) R_1 C^{2k+1}(s) D^{2k+1}(s) \ . \qquad (2)$$

Equating Eqs. (1) and (2) and using induction on k, we can prove that Y and Z must have the form a, the form sa, or the form

$$\Sigma \frac{sa}{s^2+b^2} \ ; \ a,b \text{ constants} \ ,$$

and that the numerator of S(s) is of odd degree.

Therefore, if a function of the form of Eq. (1) is given, we can determine the necessary length of ladder from the degree of its numerator and the number of LC resonance circuits from the degree of its denominator. As proved above, all Y's are capacitive or the parallel combination of a series LC and all Z's are inductive or the series combination of a parallel LC.

Let 2n+1 be the degree of the numerator, then the number of L, C, parallel LC or series LC in the network is also 2n+1. Hence, we have the n equations as a condition of symmetry. These are necessary and sufficient for symmetry.

T. Kamae

14. INFORMATION SCIENCE

R. T. Chien
R. B. Ash
J. T. Barrows
D. Chow
H. T. Hsu
V. Lum
R. J. Tracey

14.1 Introduction

The main effort in this area is to develop information-theoretic methods for the design and optimalization of digital systems for data-transmission and data-processing. During the past quarter several problems in algebraic coding theory have been investigated. Particularly significant results are obtained in (1) decoding of cyclic codes, (2) construction of codes for compound channels, (3) theory of linear residue codes for multiple-error correction. Methods of algebraic coding theory are also applied with success to the design of information-retrieval systems.

14.2 Algebraic Theory of Bose-Chaudhuri-Hocquenghem Codes

As a class, the Bose-Chaudhuri-Hocquenghem codes[1] (from here on abbreviated as BCH codes) is probably the most powerful and the most important class of error-correcting codes known today. In the binary case, the BCH codes can be as long as 2^m-1 bits, correct any combination of t independent errors within the boundaries of the codeword,

[1] Bose, R. C. and D. K. Ray-Chaudhuri, "On a Class of Error Correcting Binary Group Codes," Inf. and Control 3, 68-79 (1960).

and require at most mt check bits. When used properly, a BHC code is capable of ensuring a very high degree of accuracy in data transmission and storage.

Recently a great deal of progress has been made in the art of decoding which has reduced the theory of BCH codes to engineering practice. In fact, the decoding circuitry of many BCH codes of limited length are so simple that they are commercially produced.[2,3,4]

To fully utilize the high potential of coding and error-correction, however, one must consider codes of longer duration. It is generally believed that the accuracy of the present method of determining the minimum distance of BCH codes (known as the BCH bound) decreases as n (code length) and t (number of errors corrected) increase. Hence, for large n and t there is a strong possibility that one could do much better than what is known now.[5] To realize such plausible

---

[2]Chien, R. T., "Cyclic Decoding Procedure for Bose-Chaudhuri-Hocquenghem Codes," IEEE Trans. IT-10, 357-363 (1964).

[3]Rudolph, L. D. and M. E. Mitchell, "Implementation of Decoders for Cyclic Codes," IEEE Trans. IT-10, p. 259 (1964).

[4]It is most interesting to observe that the theory and implementation of BCH codes are possible only with the extensive use of theory of Galois fields, a most fundamental part of modern algebra that has so far defied any application to science and engineering.

[5]Peterson, W.W., and J. L. Massey, "Coding Theory," URSI Report of Progress in Information Theory in the United States, 1960-63, IEEE Trans. IT-9, No. 4, pp. 223-229 (October, 1963).

expectations into engineering usage we must solve two important problems:

(1) To find a systematic procedure for the accurate determination of minimum distances of BCH codes of large n and t.

(2) To find simple decoding algorithms for implementation that does not depend on the BCH bound.

Results connected with (1) are reported in 14.2.1. Results on decoding of cyclic codes, in the direction of (2), are reported in 14.2.2.

14.2.1 Determination of Minimum Distance of Bose-Chaudhuri-Hocquenghem Codes.

As an extension of Mattson and Solomon,[6] the problem of determining the minimum distance of a generalized BCH code has been reduced to that of finding the roots of polynomials over a finite field.

Let $f(x)$ be the recursion polynomial of the BCH code, α be a primitive n-th root of unity and m_o any integer. We define

$$E(\alpha) = \{e \mid 0 \leq e < n,\ f(\alpha^{m_o+e}) = 0\} .$$

In other words, $E(\alpha)$ is the set of integers e within the range $0 \leq e < n$ such that α^{m_o+e} is a root of $f(x)$. The following theorem has been proved.

Theorem 1: For each $a=(a_{n-1},a_{n-2},a_{n-3},\cdots a_0)$ in the BCH code V there exists a polynomial $p_a(x)$ with coefficients in $GF(2^m)$, an extension field of GF(2), such that

---

[6] Mattson, H. F., and G. Solomon, "A New Treatment of Bose-Chaudhuri Codes," SIAM Journal 9, No. 4, pp. 654-670 (December, 1961).

$$P_a(x) = c_1 x^{e_1} + c_2 x^{e_2} + \cdots + c_k x^{e_k}$$

and

$$a_i = \alpha^{m_o i} P_a(\alpha^i) \qquad i = 0,1,2,\cdots,n-1$$

where $e_1, e_2, \cdots, e_k$ are elements of $E(\alpha)$.

It follows readily from Theorem 1 that the number of zeros in the code vector is equal to the degree of $P_a(x)$. ($f(x)$ has no repeated factors.) The following theorem concerning the BCH bound of a generalized BCH code has been established.

Theorem 2: Let $f(x)$ be the recursion polynomial of a generalized BCH code such that

$$f(\alpha^{m_o+e}) = 0 \qquad e = m_o+(d_o-1), m_o+d_o, \cdots, m_o-1$$

then the minimum distance of the code is $d \geq d_o$.

V. Lum

14.2.2 Decoding of Cyclic Codes.

In two recent papers,[7,8] it was shown that error-correction may be achieved in a step-by-step way by

(1) shifting the syndrome in a shift register with feedback,

(2) attempting a trial correction at the leading position, and

(3) evaluating a determinant $|M_t|$ to detect whether a valid correction has been made.

---

[7] Chien, R. T., "Cyclic Decoding Procedures for Bose-Chaudhuri-Hocquenghem Codes," IEEE Trans. IT-10, pp. 357-363 (1964).

[8] Massey, J. L., "Step-by-step Decoding of the Bose-Chaudhuri-Hocquenghem Codes," IEEE Trans. IT-11 (to appear).

Peterson[9] has shown that the determinant

$$|M_t| = \begin{vmatrix} S_1 & 1 & 0 & 0 & \cdots & 0 \\ S_3 & S_2 & S_1 & 1 & \cdots & 0 \\ \vdots & \vdots & \vdots & \vdots & & \vdots \\ S_{2t-1} & S_{2t-2} & S_{2t-3} & S_{2t-4} & & S_t \end{vmatrix}$$

is zero if the S_i's are functions of t-1 or fewer distinct variables, and that it is non-zero if the S_i's are functions of t or t+1 distinct variables. Hence, whether $|M_t|$ equals zero or not can be used to decide whether t-1 or t+1 errors are present.

We have observed that if the code in question satisfied the condition $|M_{t-1}| \neq 0$ when the S_i's are functions of t+1 or t+2 distinct variables, then the amount of computation required in decoding digits can be greatly reduced. In fact, it would only be necessary to compute $|M_{t-1}|$ rather than $|M_t|$. One class of codes that satisfies this condition is the perfect codes, the class of codes that meets the Hamming bound.

For a perfect code of minimum distance $d \geq 2t+1$ each coset leader is of weight $w \leq t$. Furthermore, a vector of weight t+1 will have a coset leader of weight $w \geq 2t+1-(t+1)=t$. Similarly, a vector of weight t+2 will have a coset leader of weight $w \geq 2t+1-(t+2)=t-1$. Consequently, $|M_{t-1}| \neq 0$ in either case.

---

[9] Peterson, W. W., Error Correcting Codes, MIT Press (1961).

This type of simplification is also applicable to non-binary cases where the matrix N_t suggested by Gorenstein and Zieler[10] is used.

The search for a more general class of codes that satisfies the condition on $|M_{t-1}|$ is in progress.

V. Lum
R. T. Chien

14.3 Coding Methods for Information Retrieval

The information retrieval problem considered here may be defined as follows. A collection of documents is given. The documents are characterized by a set of attributes with some restrictions on the maximum number of attributes allowed for a specific document. A query is defined also by a given set of attributes. By retrieval we mean the process of obtaining a list of documents, each of which has all the attributes of the query, or, in other words, to obtain a list of documents that "covers" the query.[11]

For a typical situation the number of documents in the system will certainly be in the millions, with each document characterized by around ten attributes while the total number of attributes may be over 10,000. In any mechanized system it is also important to remember that whatever addressing scheme is used it is always desirable to minimize the storage requirements of the system.

---

[10] Zieler, N., A Class of Cyclic Linear Error-Correcting Codes in p^m Symbols, MIT Lincoln Laboratory Group Report 55-19 (Lexington, Mass., 1961).

[11] Kautz, W. H., and R. C. Singleton, "Nonrandom Binary Superimposed Codes," IEEE Trans. IT-10, 363-378 (1964).

14.3.1 Retrieval by Algebraic Coding.

With a proper formulation a solution of the problem just outlined was obtained by applying algebraic coding theory. We first recognize that each document (including the query) can be represented by a binary vector of n bits where n is the total number of attributes. We then consider a t-error-correcting code of length n, with t sufficiently large to cover all documents in the system. The syndrome of each document vector, which is at most mt bits long with $2^m-1=n$, is now a unique address for the document. The following fundamental theorem has been proved.

Theorem 1: Let $s_d, s_q, s_{d+q}=s_d+s_q$ be the syndromes of the document, the query, and the comparison vector (document plus query); and f_d, f_q, f_{d+q} be their coset weights, respectively. Then the document vector covers the query vector if and only if

$$f_{d+q} = f_d - f_q \ .$$

By Theorem 1 the retrieval problem has been reduced to the problem of computing coset weights. A number of methods for this has been constructed and the results are summarized in a forthcoming paper.

The problem of computing f_{d+q} can be treated as an algebraic decoding problem as follows. From s_{d+q} we compute the rank r_s of the matrix M_t as defined by Peterson. If r_s is not equal to f_d-f_q+1, then we immediately conclude that the document does not cover the query. If $r_s = f_d-f_q+1$, then we proceed to solve for the r_s elementary

symmetric functions σ_k. If either the set of equations are inconsistent or the polynomial $\sigma(x) = \sum_{k=o}^{r_s} \sigma_k z^{r_s-k}$ contains irreduceable factors, the document does not cover the query.

We note that with this procedure we only have to compute the rank of M_t for the majority of situations. Only very rarely do we have to complete the decoding procedure. In that case, the efficient method of extracting the roots of $\sigma(x)$ should be used.[7]

R. T. Chien

14.3.2 Retrieval by the Theory of Group Representations.

We are investigating the application of the theory of group representations and the theory of group characters to the retrieval problem.[12] With the theory of group characters we can compute a function f(v) for every vector of n-tuples which is the coset weight of v. It is clear that such a method can be readily adopted to the computing of f_{d+q}. At the moment, the difficulty of this method of attack lies in the fact that such computations tend to be lengthy for long codes. However, there are many indications that, with some additional restrictions on the code, the complexity of the computing job can be greatly reduced.

Also being investigated are questions related to using multiple copies of identical codes to simplify the computation process. It has been observed that if two codes are used the average length of

[12] Peterson, W. W., Error-Correcting Codes, MIT Press (1961).

computation is reduced by 75 per cent. This is accomplished with the use of a longer address for each document. Exact formulas for trade-off are being studied.

D. Chow

14.4 Coding for Compound Channels

14.4.1 General Theory.

Due to various sources of disturbances most channels for data-transmission and storage are perturbed by both burst-type and random noise. These situations are best modeled by compound channels where both burst errors and independent errors are allowed with suitable proportion but not simultaneously. Codes for error-correction in compound channels require a reasonable amount of redundancy and are simple to implement. There are definite advantages on the practical side.

We have shown that a set of necessary and sufficient conditions for a code V to correct, in superimposed manner, t independent errors and burst errors of length b is the following:

(1) V is capable of correcting t independent errors,

(2) V is capable of correcting all bursts of length b or less,

and (3) Let E_t be a t-tuple error and E_b be a burst of length b, then

$$\text{Syndrome } (E_t) \neq \text{Syndrome } (E_b) .$$

It is clear that whenever the syndromes of E_t and E_b are equal these two error patterns add up to a code vector. Denote by L_t the

length of the longest sequence with t non-zero digits then

$$b = n-L_t-1 \ .$$

Methods of computing L_t are being investigated with some success. Progress to date is reported in the following section.

R. T. Chien

14.4.2 Computation of Maximum Length Sequences of Weight t.

To compute L_t we must find S_t, the longest sequence with weight t that is contained in any codeword. The recursion polynomial h(x) of the code V plays an important role with regard to this. We recall that each code vector a(x) satisfies the linear recurrence equation:

$$\sum_{j=0}^{k} h_j a_{i+j} = 0 \ ,$$

where

$$h(x) = \sum_{j=0}^{k} h_j x^j \ , \qquad h_0=h_k=1 \ ,$$

$$a(x) = \sum_{i=0}^{n-1} a_i x^{n-i-1} \ .$$

Each code vector can thus be completely determined once k consecutive bits are given. The following propositions have been established with regard to L_t.

Proposition 1: The length L_1 of the sequence S_1 is given by

$$L_1 = k+g$$

where g is the length of the longest gap in the recursion polynomial h(x).

Proposition 2: The length L_2 of the sequence S_2 is given by

$$L_2 = \max(k+w, k+g_1+w_{g_1}, \cdots, k+g_\delta+w_{g_\delta})$$

where w is the maximum number of consecutive coincidences obtainable by comparing h(x) with a non-zero shift of itself, g_δ is the length of δ-th gap in h(x), and w_{g_δ} is the number of consecutive coincidences obtained by comparing h(x) with a version of itself shifted according to the δ-th gap.

H. T. Hsu

14.5 Linear Residue Codes for Multiple Error Correction

Linear residue codes are based on ordinary arithmetic rather than modular arithmetic. As a result, it is capable of correcting arithmetic errors as well as transmission errors, a fact that makes it very useful as multiple purpose codes.[13] When used for improving the reliability of data-transmission, a general-purpose computer can be used efficiently for decoding and no special-purpose hardware is required.

Linear residue codes for single errors and burst errors have been investigated with success, and methods of implementing these codes are well known.[14] However, despite the striking similarity between

---

[13] Goldberg, E. I., and W. E. Webb, Application of BN Modulo-A Codes to Aerospace Vehicle Control Systems, Tech. Rept. ASD-TDR-62-169, Cont. AF 33(616)-8053. Telecomputing Corp., N. Hollywood, California.

[14] Chien, R. T., "Linear Residue Codes for Burst-Error Correction," IEEE Trans. IT-10, 127-133 (1964).

cyclic codes and linear residue codes no general multiple-error-correcting linear residue codes analogous to the Bose-Chaudhuri-Hocquenghem codes are known. The purpose of this research effort is to develop classes of such linear residue codes that are also amenable to simple implementation.

Our preliminary investigation is quite successful. With the use of properties of a number representation called the Non-Adjacent Form we are able to construct four general classes of codes, namely

I. $A_d=2^{k(d-1)}-2^{k(d-2)}+\cdots+(-1)^{d-2}2^k+(-1)^{d-1}$

II. $A_d=2^{k(d-1)}+2^{k(d-2)}-\cdots+(-1)^{d-1}2^k+(-1)^d$

III. $A_d=2^{k(d-1)}+2^{k(d-2)}+\cdots+2^{k(d-m)}-2^{k(d-m-1)}-\cdots-2^k-1, \quad 1 \leq m \leq d,$

IV. $A_d=2^{k(d-1)}-2^{k(d-2)}-\cdots-2^{k(d-m)}+2^{k(d-m-1)}+\cdots+2^k+1, \quad 1 \leq m \leq d,$

where A_d is the generator for the code and d is the minimum distance.

These codes are very general and use a moderate amount of redundancy. We are presently engaged in an intensive search for methods of constructing new classes of linear residue codes for multiple-error-correction that require even less redundancy.

J. Barrows

Security Classification

DOCUMENT CONTROL DATA R&D

(Security classification of title, body of abstract and indexing annotation must be entered when the overall report is classified)

1. ORIGINATING ACTIVITY (Corporate author)
University of Illinois
Coordinated Science Laboratory
Urbana, Illinois 61803

2a. REPORT SECURITY CLASSIFICATION
Unclassified

2b. GROUP

3. REPORT TITLE
PROGRESS REPORT FOR JUNE, JULY, & AUGUST, 1965

4. DESCRIPTIVE NOTES (Type of report and inclusive dates)
Quarterly progress report for period June 1, 1965, through August 31, 1965.

5. AUTHOR(S) (Last name, first name, initial)

6. REPORT DATE
October 11, 1965

7a TOTAL NO. OF PAGES
130

7b. NO. OF REFS.

8a. CONTRACT OR GRANT NO.
DA 28 043 AMC 00073(E)

b. PROJECT NO.
20014501B31F

c.

d.

9a. ORIGINATOR'S REPORT NUMBER(S)

9b. OTHER REPORT NO(S) (Any other numbers that may be assigned this report)

10. AVAILABILITY/LIMITATION NOTICES
Qualified requesters may obtain copies of this report from DDC.
May be released to OTS.

11. SUPPLEMENTARY NOTES

12. SPONSORING MILITARY ACTIVITY
U. S. Army Electronics Command
Fort Monmouth, New Jersey 07703

13. ABSTRACT

Work in data reduction for the ionospheric program is described. Analyses of spurious torques for the orbiting relativity gyro are presented. Variations in photographic observability are noted. The effect of micrometeorite cratering of the orbiting gyro has been studied.

Some preliminary data obtained with the high-resolution secondary emission spectrometer are discussed. Additions and modifications to this apparatus and those for the study of the angular distributions of secondary particles and for the study of adsorption-desorption kinetics are described.

A new measuring technique for bubble-chamber data processing, a new assembler for the CSX-1, and a new method of sequencing the control unit of a digital machine, tending to minimize the complexity of diagnostic procedures and of hardware, are described.

The project on optimization methods for time-lag systems was completed. Also completed was the project on pulse-width modulated control systems. The results for these two projects are described in R-254 and R-255. Several results were obtained in the continuing projects on the parameter variation problem, synthesis of interconnected linear time-varying systems, stability of nonlinear systems, suboptimal linear time-invariant control, and computer-oriented formulation and solution of the optimal control problem.

DD FORM 1 JAN 64 1473

Security Classification

Security Classification

KEY WORDS	LINK A		LINK B		LINK C	
	ROLE	WT	ROLE	WT	ROLE	WT
Aerospace Surface physics Computer research Control systems Automatic teaching device Vacuum instrumentation Plasma physics Superconductivity High voltage breakdown Thin films Computer operations Switching systems						
Networks & communication nets Information science						

INSTRUCTIONS

1. ORIGINATING ACTIVITY: Enter the name and address of the contractor, subcontractor, grantee, Department of Defense activity or other organization (corporate author) issuing the report.

2a. REPORT SECURITY CLASSIFICATION: Enter the overall security classification of the report. Indicate whether "Restricted Data" is included. Marking is to be in accordance with appropriate security regulations.

2b. GROUP: Automatic downgrading is specified in DoD Directive 5200.10 and Armed Forces Industrial Manual. Enter the group number. Also, when applicable, show that optional markings have been used for Group 3 and Group 4 as authorized.

3. REPORT TITLE: Enter the complete report title in all capital letters. Titles in all cases should be unclassified. If a meaningful title cannot be selected without classification, show title classification in all capitals in parenthesis immediately following the title.

4. DESCRIPTIVE NOTES: If appropriate, enter the type of report, e.g., interim, progress, summary, annual, or final. Give the inclusive dates when a specific reporting period is covered.

5. AUTHOR(S): Enter the name(s) of author(s) as shown on or in the report. Enter last name, first name, middle initial. If military, show rank and branch of service. The name of the principal author is an absolute minimum requirement.

6. REPORT DATE: Enter the date of the report as day, month, year; or month, year. If more than one date appears on the report, use date of publication.

7a. TOTAL NUMBER OF PAGES: The total page count should follow normal pagination procedures, i.e., enter the number of pages containing information.

7b. NUMBER OF REFERENCES: Enter the total number of references cited in the report.

8a. CONTRACT OR GRANT NUMBER: If appropriate, enter the applicable number of the contract or grant under which the report was written.

8b, 8c, & 8d. PROJECT NUMBER: Enter the appropriate military department identification, such as project number, subproject number, system numbers, task number, etc.

9a. ORIGINATOR'S REPORT NUMBER(S): Enter the official report number by which the document will be identified and controlled by the originating activity. This number must be unique to this report.

9b. OTHER REPORT NUMBER(S): If the report has been assigned any other report numbers (either by the originator or by the sponsor), also enter this number(s).

10. AVAILABILITY/LIMITATION NOTICES: Enter any limitations on further dissemination of the report, other than those imposed by security classification, using standard statements such as:

(1) "Qualified requesters may obtain copies of this report from DDC."

(2) "Foreign announcement and dissemination of this report by DDC is not authorized."

(3) "U. S. Government agencies may obtain copies of this report directly from DDC. Other qualified DDC users shall request through

_____."

(4) "U. S. military agencies may obtain copies of this report directly from DDC. Other qualified users shall request through

_____."

(5) "All distribution of this report is controlled. Qualified DDC users shall request through

_____."

If the report has been furnished to the Office of Technical Services, Department of Commerce, for sale to the public, indicate this fact and enter the price, if known.

11. SUPPLEMENTARY NOTES: Use for additional explanatory notes.

12. SPONSORING MILITARY ACTIVITY: Enter the name of the departmental project office or laboratory sponsoring (paying for) the research and development. Include address.

13. ABSTRACT: Enter an abstract giving a brief and factual summary of the document indicative of the report, even though it may also appear elsewhere in the body of the technical report. If additional space is required, a continuation sheet shall be attached.

It is highly desirable that the abstract of classified reports be unclassified. Each paragraph of the abstract shall end with an indication of the military security classification of the information in the paragraph, represented as (TS), (S), (C), or (U).

There is no limitation on the length of the abstract. However, the suggested length is from 150 to 225 words.

14. KEY WORDS: Key words are technically meaningful terms or short phrases that characterize a report and may be used as index entries for cataloging the report. Key words must be selected so that no security classification is required. Identifiers, such as equipment model designation, trade name, military project code name, geographic location, may be used as key words but will be followed by an indication of technical context. The assignment of links, roles, and weights is optional.

DD FORM 1 JAN 64 1473

Security Classification

13. ABSTRACT (continued)

Progress continues in circuitry development toward the goal of a 20 student station classroom. Plasma discharge display tube research this quarter has included experiments with tubes of varying widths and hole diameters, and trials with different gas additives. Modifications to the new PLATO Tutorial Logic were made to increase its flexibility and applicability to several courses; namely: 1) a revision of Electrical Engineering 322; 2) Library Science 195; and 3) FORTRAN Programming for Business Students. Revisions and modifications of TEXT-TESTER, ARITHDRILL, and PROOF have continued. Sixty students were used in the "retention of conceptual materials" experiment this quarter. A PLATO program, VERBOSE, using the CONNECT feature of the PLATO compiler was written as a starting point toward the development of more general PLATO programs useful in studying the structure of concepts.

The program of study of the pumping speed of ion-getter pumps at low pressures has continued. A pressure controller has been added to the system to improve the reproducibility of the data. This change and some recent data are discussed.

A careful evaluation of the errors in the Monte Carlo Method has been made for the hot side of the shock. Extensive measurements have been carried out in the Linear Plasma Betatron for various pressures and electric fields. It has been shown that the runaway current is associated with the buildup of ion-acoustic oscillations. A new experiment on electron-beam-plasma interactions has been started, in which the scattering of microwaves by instability-stimulated density fluctuation is used as the primary diagnostic tool. Theoretical studies of the influence of high-frequency turbulence can give rise to a parametric growth of the ion-acoustic mode.

Work is reported on a superconducting parametric amplifier (picovoltmeter), a study of the anisotropy of the energy gap in superconducting niobium, an attempt to observe microwave radiation from the ac Josephson effect in a superconducting bridge, studies of flux flow in type-II superconductors, a determination of the temperature dependence of the penetration depth using the ac Josephson effect, the thermal conductivity of a type-II superconductor in the mixed state, and the crystallization of Nb_3Sn from a solution of Nb in molten Sn.

During gas conditioning, the electron-emitting protrusions on a tungsten cathode are blunted resulting in current suppression and breakdown voltage elevation, but the critical breakdown field at the emitter tips remains unchanged. Development of single-crystal emitter tips and high-resolution fluorescent screens is described.

Additional equipment is under construction for the work on size effects, and for that on Hall measurements on thin films. Results are reported for an ionization-gauge type of deposition rate monitor.

Operation statistics for the CDC 1604 and CSX-1 systems are reported. The development of plotting routines for the cathode-ray output and a new assembler for the CDC 1604 are noted.

The experimental study of self-diagnosis using the CSX-1 computer as a vehicle has been completed. New results are reported on the realization of sequential machines as linear and quasi-linear switching circuits. Further progress is reported on the computer compiler, state-model realizations, and computer diagnosis.

13. ABSTRACT (continued)

The relationship of multiparameter sensitivity to synthesis procedures in networks has been studied, and the results of Kawakami relating to symmetric LC ladder networks have been extended. The problems of optimum flow in a communication net have received further attention. The concept of "relatively optimum flow" is introduced, and stochastic flow through a communication net is considered. Other studies relate to fundamentals of graph theory having application to the theory of communication nets.

Work in information-theoretic methods for the design and optimalization of digital transmission and processing systems, particularly in algebraic coding theory, are described. Results are given in decoding cyclic codes, construction of codes for compound channels, and in the theory of linear residue codes for multiple-error correction. Applications of the coding theory are given for information-retrieval systems.